A new role for LRP2 in forebrain development

DISSERTATION

zur Erlangung des akademischen Grades
doctor rerum naturalium
(Dr. rer. nat.)
im Fach Biologie

eingereicht an der
Mathematisch-Naturwissenschaftlichen Fakultät I
Humboldt-Universität zu Berlin

von
Herr Dipl.-Biol. (technisch orientiert) Uwe Anzenberger
geboren am 22.03.1976 in Singen a. Htwl.

Präsident der Humboldt-Universität zu Berlin:
Prof. Dr. Christoph Markschies

Dekan der Mathematisch-Naturwissenschaftlichen Fakultät I:
Prof. Thomas Buckhout, Phd

Gutachter:

1. Prof. Dr. Thomas Willnow
2. Prof. Dr. Michael Bader
3. Prof. Dr. Wolfgang Lockau

Tag der mündlichen Prüfung: 22. September 2006

Abstract

LRP2 is a member of the low-density lipoprotein receptor gene family that is mainly expressed in the yolk sac and in the neuroepithelium of the early embryo. Deficiency for this 600 kDa protein in mice results in holoprosencephaly, indicating an important yet unknown role for LRP2 in forebrain development.

In this study, mice with a complete or a conditional loss of *lrp2* function were used to further elucidate the consequences of the lack of LRP2 expression. This study shows that the presence of LRP2 in the neuroepithelium but not in the yolk sac is crucial for early forebrain development. Lack of the receptor resulted in an increase of Bone morphogenic protein (Bmp) 4 signaling in the rostral telencephalon at E9.5. As a consequence, *sonic hedgehog* (*shh*) expression at E10.5 was lost completely in a ventral region of the telencephalon termed anterior entopeduncular area (AEP). The absence of Shh activity in this area subsequently led to the loss of ventrally induced oligodendroglial and interneuronal cell populations in *lrp2* deficient mice. Similar dorsalizing effects have also been observed in mice with increased Bmp4 signaling. Taking into account that Bmp4 was found to bind to LRP2 *in vitro* and *in vivo* in this study, these results suggest a previously unknown role for LRP2 in patterning the rostral ventral neural tube, possibly by acting as a clearance receptor for Bmp4.

The underlying molecular mechanisms by which LRP2 patterns the ventral forebrain were then further analyzed in the zebrafish, a model organism that is amenable for various experimental manipulations. The cytoplasmic tail, the transmembrane domain and a short extracellular part of the zebrafish LRP2 were identified by searching the Sanger Zebrafish Zv4.0 genomic database. LRP2-deficient animals were generated by injecting Morpholino oligonucleotides that interfered with the splicing of the *lrp2*-pre-mRNA leading to a deletion of the transmembrane-exon. Injected animals suffered from impaired renal clearance processes, demonstrating the functional conservation of LRP2 in the larval zebrafish pronephros and in the mammalian kidney.

Brain structures were not affected in these animals and the expression patterns of marker genes for early forebrain development that were changed in the mouse were not changed in the zebrafish.

Apparently, Morpholino mediated interfering with the splicing of the *lrp2*-pre-mRNA did not affect the early forebrain formation because properly processed

lrp2-mRNA was supplied maternally and sufficient for proper brain formation.

Keywords:
LRP2, Megalin, Holoprosencephaly, Shh

Abstract

LRP2 gehört zu einer Gruppe funktionell und strukturell eng verwandter Proteine, die in der *Low Density* Lipoprotein Rezeptor (LDLR) Genfamilie zusammengefasst werden. LRP2 wird während der frühen Embryonalentwicklung hauptsächlich im Dottersack und im Neuroepithel exprimiert. Der funktionelle Verlust dieses 600 kDa großen Proteins in Mäusen führt zu schweren Fehlbildungen bei der Vorderhirnentwicklung, die als Holoprosenzephalie bezeichnet werden. LRP2 scheint daher eine wichtige, aber bisher unbekannte Funktion während der Vorderhirnentwicklung auszuüben.

Um die zu Grunde liegenden Mechanismen dieser Fehlbildungen zu analysieren, wurden für diese Arbeit Mäuse verwendet, bei denen *lrp2* im gesamten Tier oder nur in bestimmten Geweben inaktiviert war. Es konnte gezeigt werden, dass die Expression von LRP2 im Neuroepithel, nicht aber im Dottersack wichtig für die korrekte Vorderhirnentwicklung ist. Das Fehlen des Proteins führte am Tag 9.5 der Embryonalentwicklung zu einer Überaktivierung des *Bone morphogenic protein* (Bmp) 4 Signalweges im rostralen Telencephalon. Am Tag 10.5 war ein Verlust der *sonic hedgehog* (*shh*) Expression in einem begrenzten Bereich des ventralen, rostralen Telencephalons zu sehen, der als anteriore entopedunculare Zone (AEP) bezeichnet wird. Das Fehlen von Shh in der AEP führte zum Verlust von ventralen Oligodendrozyten und Interneuronen, deren Bildung normalerweise in diesem Bereich von Shh induziert wird. Ähnliche Defekte wurden ebenfalls in Mäusen beschrieben, bei denen der Bmp4 Signalweg verstärkt ist. Es konnte in dieser Arbeit gezeigt werden, dass Bmp4 sowohl *in vitro* als auch *in vivo* an LRP2 bindet und dem lysosomalen Abbau zugeführt wird. Diese Ergebnisse deuten darauf hin, dass LRP2 maßgeblich an der Entwicklung des ventralen Telencephalons beteiligt ist - möglicherweise indem es die verfügbare Menge an Bmp4 durch Endozytose reguliert.

Die Signalwege, in die LRP2 eingebunden ist, sollten im Zebrafisch weiter untersucht werden, da dieser Organismus leichter als die Maus experimentell manipuliert werden kann. Durch Datenbankanalysen (Sanger Zebrafish Zv 4.0) konnte die codierende Sequenz des zytoplasmatischen Bereiches, der Transmembran-Region, sowie eines kurzen extrazellulären Bereiches von LRP2 im Zebrafisch identifiziert werden. Tiere, denen funktionelles LRP2 fehlte, wurden durch die Injektion von Morpholino-Oligonukleotiden generiert. Die Morpholino-Oligonukleotide

interferierten selektiv mit der Prozessierung der *lrp2*-prä-mRNA und führten zur Deletion des Transmembran-Exons von LRP2. Injizierte Tiere zeigten Störungen bei Resorptionsvorgängen im Pronephros, ein Phänotyp der bereits für die Niere von *lrp2* defizienten Mäusen beschrieben wurde. Diese Ergebnisse zeigen, dass die Funktion von LRP2 im Zebrafisch Pronephros und in der Niere der Säugetiere konserviert ist.
Die Gehirnstrukturen waren bei diesen Tieren allerdings normal entwickelt und auch die Expressionsmuster von Markergenen für die Vorderhirnentwicklung waren normal.
Vermutlich war die Störung der *lrp2*-prä-mRNA Prozessierung nicht ausreichend, um hier einen Effekt hervorzurufen, da bereits im 1-Zell Stadium genügend komplett prozessierte maternale *lrp2*-mRNA für die Translation von LRP2 vorhanden war.

Schlagwörter:
LRP2, Megalin, Holoprosenzephalie, Shh

This document was created using LaTeX

Contents

List of Figures

1 Introduction

1.1 The low-density lipoprotein receptor gene family

The low-density lipoprotein receptor (LDLR) gene family is composed of ten members of structurally closely related cell-surface proteins (Figure 1). In addition to humans, members of this family have been identified in different taxa including invertebrates like the fruitfly (Wehrli et al., 2000), and vertebrates like the african clawfrog (Houston, 2002), the house mouse (Gafvels et al., 1994; Brown et al., 1998) and the rat (Lee et al., 1989). So far, no members of the LDLR gene family have been identified in eukaryotic unicellular organisms such as baker's yeast.
The receptors are homologous among species, even receptors of two evolutionary distant organisms display a high grade of conservation at the amino acid level (Houston, 2002). This high degree of evolutionary conservation suggests that the LDLR gene family early developed roles that are critical for the functional integrity of multicellular organisms.
The core of the gene family (Figure 1) in mammals consists of the low-density lipoprotein receptor (**LDLR**), the LDLR related proteins 1, 1B and 2 (**LRP1, LRP1B, LRP2**), the very low-density lipoprotein receptor (**VLDLR**), the apolipoprotein E receptor-2 (**ApoER2**) and the multiple epidermal growth factor repeat containing protein 7 (**MEGF7**). Members of the family that are not included in the core because of their differing domain structure (Figure 1) are the low-density lipoprotein receptor related protein 5, 6 (**LRP5/LRP6**) and the sorting protein related receptor containing LDLR class A repeats (**SorLA**). A table summarizing important ligands, functions and sites of expression for the gene family members can be found at the end of this section on page 17.
All of these receptors belong to the superfamily of type I cell-surface receptors, featuring a large amino-terminal extracellular domain, a single transmembrane segment and a short carboxy-terminal cytoplasmic tail region. The extracellular part is mainly composed of motifs responsible for binding ligands and of motifs important for releasing ligands (Brown et al., 1997) upon internalization in the endosomes in a pH-dependent manner (Rudenko et al., 2002).

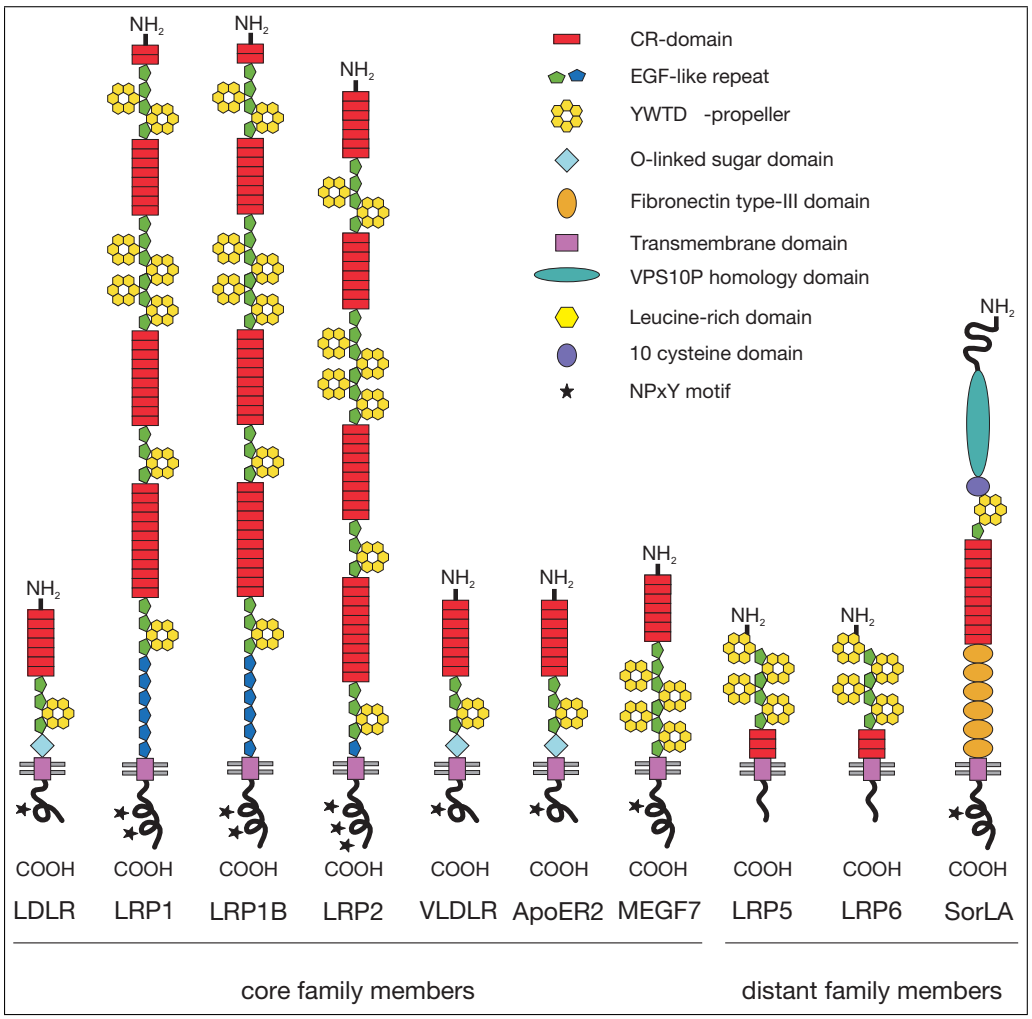

Figure 1: Depicted are the seven core family members of the LDL receptor gene family and the three more distantly related family members. All share common motifs, including a single transmembrane segment, complement-type repeats and epidermal growth factor (EGF) precursor homology domains. The NPxY-motif(s)in the cytoplasmic tail of the receptor mediate the clustering into clathrin-coated pits. O-linked sugar domains are found in the LDLR, VLDLR and ApoER2 only. Abbreviations: LDLR, low-density lipoprotein receptor; LRP1, 1B, 2, low-density lipoprotein receptor related protein 1, 1B, 2; VLDLR, very low-density lipoprotein receptor; ApoER2, apolipoprotein E receptor 2; MEGF7, multiple EGF-repeat-containing protein 7; LRP5, 6, low-density lipoprotein receptor related protein 5, 6; SorLA, sorting protein related receptor containing LDLR class A repeats.

The motifs responsible for binding ligands are termed complement-type repeat (CR)-domains and consist of 40 amino acids containing six cysteine residues that are disulphide linked in the pattern one to three, two to five, and four to six. Each CR-domain harbors a Ca^{2+} binding site that is important for the correct folding and stabilization of this protein module. Typically, an acidic motif (asp-any amino acid-ser-asp-glx) is located between cysteine residues five and six (Bieri et al., 1995; Fass et al., 1997). The difference in ligand binding-specificity is mainly due to the variability of amino acid sequences linking the CR-domains.
The motif responsible for releasing ligands is termed epidermal growth factor precursor homology (EGFP) domain and is composed of three epidermal growth factor (EGF)-like repeats with a stretch of 260 amino acids intersected between EGF-like repeat two and three. This additional stretch of amino acids contains six repeats of the amino acids tyr-trp-thr-asp (YWTD) and folds into a structure called ß-propeller. At low pH in the endosmes the ß-propeller undergoes conformational changes and becomes an alternate ligand for the CR-domains, thereby triggering the release of lipoprotein ligands (Rudenko et al., 2002).
The LDLR, VLDLR and ApoER2 contain an O-linked sugar domain that immediately preceeds the membrane-spanning segment (Iijima et al., 1998). Carbohydrate chains of variable length are linked to this domain preventing the proteolytic cleavage of the extracellular part of the receptor (Kozarsky et al., 1988). The VLDL and ApoER2 receptors can be synthesized with or without this sugar domain in a tissue specific manner. A single trans-membrane domain anchors the receptors in the plasma membrane of the cell. The cytoplasmic tail is highly variable in the different receptors and contains one or more asn-pro-any amino acid-tyr (NPxY) motifs (Figure 1). The NPxY motifs localize the receptor to specialized regions (clathrin coated pits) of the cell surface for endocytosis (Chen et al., 1990; Bansal and Gierasch, 1991) and bind phosphotyrosine binding (PTB) domain containing adaptor proteins.
Although a plethora of different ligands has been identified for the various members of the LDLR gene family, one ligand that is common to all members of the LDLR gene family is the receptor associated protein (RAP). RAP binds to the nascent amino acid chain in the endoplasmatic reticulum helping the protein to fold correctly. Furthermore it prevents the premature binding of ligands that are often synthesized in the same cell type (Willnow, 1998). RAP binds all members of the LDL receptor gene family except LDLR with high affinity and is commonly used in binding studies as a specific receptor antagonist.

LDLR

The low-density lipoprotein receptor was the first member of the family to be identified by Brown and Goldstein 20 years ago. They could show that the physiological role of the receptor is to take up cholesterol-carrying lipoproteins into target cells (Brown and Goldstein, 1986). Cholesterol serves many important functions within the organism: it is an important component of the cell membrane and the major precursor for the synthesis of vitamin D and steroid hormones, including cortisol and aldosterone in the adrenal glands, the sex hormones progesterone, estrogen, and testosterone.
Cholesterol is a steroid-derived lipid and not soluble in water. Because of its hydrophobic nature cholesterol is transported in the bloodstream surrounded by a monolayered phospholipid shell. The shell also contains protein molecules that mediate binding to the receptor, leading eventually to endocytosis of the package. There are two known ligands for the LDLR. The main ligand is the low-density lipoprotein (LDL) that binds to the receptor by apolipoprotein B-100 (apoB). The second ligand is the very low-density lipoprotein (VLDL) that also binds to the receptor with its protein part, apolipoprotein E (apoE) (Havel, 1989).
Basically every cell type in the adult organism expresses the LDLR at variable levels, suggesting an important function of this receptor. Heterozygous carriers of mutations in the gene encoding the LDLR that disable the receptor's function have a disturbed lipid metabolism. The cholesterol level in these individuals is elevated due to the inability of the cells to clear LDL respectively VLDL particles from the bloodstream. As a consequence, patients suffer from premature atherosclerosis and coronary artery disease. Individuals carrying a homozygous mutation for LDLR have dramatically elevated cholesterol levels and usually suffer fatal heart attacks within the first two decades of life (Havel, 1989), a condition referred to as familial hypercholesterolemia.
Although the LDL receptor is expressed in the embryonic and adult nervous system, LDLR-knockout mice surprisingly do not show defects in embryonic neuronal development (Ishibashi et al., 1993).

LRP1

The LDLR related protein 1 was the second member of the family to be discovered (Herz et al., 1988). Its main site of expression are hepatocytes and neurons, but it is expressed at low levels in many other cell types (Moestrup et al., 1992).

Because LRP1 is expressed in hepatocytes and binds ApoE (Beisiegel et al., 1989, 1991; Willnow et al., 1994), it was initially thought to be mainly involved in lipid metabolism. Subsequent studies revealed that LRP1 binds to proteases and their inhibitors, coagulation factors, lipases and the amyloid precursor protein (APP) (Gliemann, 1998; Kounnas et al., 1995), implying a much broader biological function for this receptor.
A unique feature of LRP1 is the fact that this receptor is cleaved by the protease furin in an 85 kDa and a 515 kDa fragment in the late secretory compartment. The 85 kDa fragment comprises the transmembrane domain and the cytoplasmic tail, whereas the 515 kDa fragment encompasses the extracellular region that remains noncovalently linked to the smaller fragment.
Mice homozygous for a disruption in the LRP1 gene die around day 12.5 of embryonic development (Herz et al., 1993), indicating a critical role for the receptor in embryogenesis. Convincing evidence that LRP1 is involved in signal transduction came from Boucher et al. (2003). By generating a smooth muscle cell (SMC) specific LRP1 conditional knockout mouse, they were able to show that LRP1 forms a complex with the platelet derived growth factor receptor (PDGFR) thereby inhibiting PDGF signaling. Inactivation of LRP1 in vascular SMCs of mice causes abnormal activation of PDGFR signaling, resulting in a marked susceptibility to cholesterol-induced atherosclerosis. Importantly, atherosclerosis was not caused by an abnormal lipid metabolism since cholesterol levels were not elevated in the knockout animals compared to the wildtype animals.
Further proof that LRP is part of the PDGF signaling pathway was obtained by treating conditional knockout mice with a synthetic inhibitor (Gleevec) of the PDGF signaling pathway. Animals receiving the inhibitor were rescued and did not develop atherosclerosis (Boucher et al., 2003) because Gleevec was mimicking the inhibitory function of the missing LRP1 protein.

LRP1B

The LDLR related protein 1B was the last of the LDL receptor gene family to be discovered by Liu et al. (2001). In their study the authors found homozygous deletions or abnormal transcripts of the LDLR related protein 1B (LRP1B) gene in nearly 50% of the non-small cell lung cancer cell lines they analyzed. Similarly, alterations of the LRP1B gene have been described in high-grade urothelial cancer (Langbein et al., 2002). LRP1B, originally termed LRP-DIT (LRP-deleted in tumors) is therefore considered a candidate tumor suppressor gene.

On the amino acid level, LRP1B is 60% identical to LRP1 and has an overall structure nearly identical to LRP1, with the exception of two additional exons. One (exon 68) codes for an additional repeat in the fourth ligand-binding repeat cluster and another (exon 90) encodes a 33 amino acid sequence within the cytoplasmic tail that shows no homology to other known proteins (Marschang et al., 2004).
Animals lacking functional LRP1B show no obvious phenotype, probably due to functional compensation by other family members. Unexpectedly, knockout animals are not prone to develop tumors suggesting that the role of LRP1B as a tumor suppressor gene is depending on preceding events to malignant transformation and that loss of LRP1B alone is not sufficient to induce the formation of tumors (Marschang et al., 2004).

VLDLR

The very low-density lipoprotein receptor was identified by Takahashi et al. (1992) in a screen for novel LDL receptor-like cDNAs. The newly discovered receptor displays a close structural similarity to the LDLR (Figure 1) and binds, like every core member of the LDL receptor gene family, apoE, mediating its endocytosis. Therefore, the receptor has been proposed to function in the VLDL metabolism. However, VLDLR is not expressed in the liver, the main site of VLDL catabolism. The highest level of expression of VLDLR in adults is found in heart and skeletal muscle and in the endothelial cells lining the major blood vessels (Willnow et al., 1996b; Wyne et al., 1996).
Additional proof that the receptor only plays a minor role in the VLDL metabolism came from the analysis of VLDLR-deficient mice in which the lipoprotein profile is completely normal compared to wildtypes (Frykman et al., 1995). However, these mice tend to be leaner because they are partially resistant to diet-induced obesity (Goudriaan et al., 2001). The mechanism by which the VLDLR protects from obesity remains to be elucidated.

ApoER2

The human homologue of the apolipoprotein E receptor-2 was identified in a genome-wide search for receptors that are homologuous to the LDLR by Kim et al. (1996). Like VLDLR, ApoER2 binds to ApoE and is also not expressed in the liver. Instead, expression is restricted to the brain and testes in adults (Novak et al., 1996; Stockinger et al., 1998). Mice lacking the receptor do not show any

major disturbance in lipid homeostasis (Trommsdorff et al., 1999), but the males are virtually infertile, implying a role for ApoER2 in the production or survival of sperm (Andersen et al., 2003).
A major step in understanding the function of the VLDLR, respectively the ApoER2 was the generation of the compound knockout by Trommsdorff et al. (1999). Mice that are deficient for both receptors are characterized by the inability to properly coordinate limb movement. Further analysis of these animals showed that the order of neuronal layering of the cerebellum was reversed, leading to the coordination defects mentioned above (Trommsdorff et al., 1999; Hiesberger et al., 1999).
Interestingly, the phenotype of the compound knockout animals strikingly resembled that of a naturally occuring mutation (termed *reeler*) in the gene for the protein Reelin, described by Falconer (1951). Reelin is a secreted protein produced by a specialized population of neurons on the surface of the developing neocortex. The protein confers positional information to neurons that are migrating from their birthplace in the ventricular zone along the radial glial guidance fibers to their final positions in the cortex. Mice lacking functional Reelin protein display the same layering defect seen in the VLDLR/ApoER2 compound knockout. Another naturally occuring mutation in the gene for *disabled1* (*dab1*) causes the same neurological disorders as in *reeler* mice (Sweet et al., 1996). This phenotype was not compounded in mice lacking both Reelin and Dab1 (Howell et al., 1999), suggesting that the two proteins function in a linear pathway that controls cortical development. Since Reelin is an extracellular signaling molecule and Dab1 is a cytoplasmic adaptor protein, these studies imply that specific receptors for Reelin are present on the cell surface of migrating neurons.
The finding that VLDLR/ApoER2 compound knockout animals mimick the phenotype of mice lacking Reelin or Dab1 and that both receptors bind Dab1 on their cytoplasmic tails suggested a function as receptors for Reelin (Trommsdorff et al., 1999). Hiesberger et al. (1999) and D'Arcangelo et al. (1999) showed that both receptors indeed bind Reelin with high affinity. Together, these findings suggest that VLDLR and ApoER2 participate in transmitting the extracellular Reelin signal to intracellular signaling processes initiated by Dab1.

MEGF7

The multiple epidermal growth factor repeat containing protein 7 was found during a screen for cDNAs that are expressed in the central nervous system and contain multiple EGF-, respectively CR-domains (Nakayama et al., 1998). The biolog-

ical role of the receptor is not completely understood so far, but homozygous MEGF7-deficient mice are growth-retarded and display abnormalities in the fore- and hindlimb development (Johnson et al., 2005; Simon-Chazottes et al., 2006). These findings may reflect a possible involvement of MEGF7 in cellular signaling similar to what has been reported for other family members.

LRP5 and LRP6

The low-density receptor related proteins 5 and 6 are closely related to each other in structure and in amino acid sequence. The extracellular part of these receptors contains CR- as well as EGF-domains but they are arranged in a different manner than in the core members of the LDLR gene family (Figure 1). The cytoplasmic tail region does not contain an NPxY-motif, which is present in all other core family members. Both receptors are expressed in a variety of tissues, the main sites of expression being heart and skeletal muscle, liver and kidney (Brown et al., 1998; Hey et al., 1998; Dong et al., 1998). The loss of LRP5 function in humans leads to decreased bone mineral density and skeletal fragility, a disorder termed Osteoporosis-Pseudoglioma syndrome (OPPG) (Gong et al., 2001). Mouse embryos lacking functional LRP6 die at birth and exhibit a variety of severe developmental abnormalities including a truncation of the axial skeleton, limb defects, malformation of the urogenital tract and small eyes (microphtalmia) (Tamai et al., 2000; Pinson et al., 2000). The observed phenotypes in LRP6-deficient animals strongly resemble phenotypes seen in animals with defects in the wingless-type protein (Wnt) signaling pathway that is important during embryogenesis. It was shown by Pinson et al. (2000) and Tamai et al. (2000) that LRP5 and LRP6 act as co-receptors for signaling proteins of the Wnt-family. Without these co-receptors the Wnt proteins can not bind to their authentic receptor, the signal is not relayed and target genes are not activated. Lack of functional LRP6 mimicks the defects observed in mice that are devoid of a functional Wnt signaling pathway, emphasizing again the importance of members of the LDL gene receptor family in signal transduction pathways.

SorLA

The sorting protein related receptor containing LDLR class A repeats was identified independently by biochemical purification of RAP binding proteins (Jacobsen et al., 1996) and by a genetic screen for novel LDL receptor family members (Yamazaki

et al., 1996; Morwald et al., 1997). The extracellular domain consists of motifs that are shared with other members of the family, e.g. CR-domains and a ß-propeller (Jeon et al., 2001), whereas other motifs are only present in sorLA. For example, a unique motif with homology to proteins involved in vacuolar protein sorting (VPS) is present at the amino-terminus of the receptor suggesting a role for SorLA in intracellular sorting mechanisms. Indeed, the receptor has been shown to interact with the amyloid precursor protein (APP) and to regulate its intracellular trafficking (Andersen et al., 2006; Offe et al., 2006).

LRP2

The low-density receptor related protein 2 was identified by Kerjaschki and Farquhar in 1982. In their original work they purified a large glycoprotein (gp) with a molecular weight of 330 kDa from brush border membranes of the rat kidney. Rats immunized with this purified protein (gp330) developed anti-brush border antibodies and displayed inflamed glomeruli in the kidney leading eventually to renal failure (Kerjaschki and Farquhar, 1982). The disease pattern seen in these rats strikingly resembled a specific kind of kidney inflammation in humans termed Heymann nephritis (HN).
In the initial study, Kerjaschki and Farquhar isolated a degradation product of LRP2, further studies showed that the molecular weight of the intact protein was 600 kDa and the protein was renamed to gp600 (Hjalm et al., 1996; Saito et al., 1994). Since gp600 it is the biggest member of the LDLR gene family, a widely used designation is Megalin.
Like the other receptors of the gene family, LRP2 is a multi-ligand endocytic receptor expressed in a variety of tissues. In the adult organism, LRP2 is expressed mainly in the proximal tubules of the kidney, in type II pneumocytes and in the Clara cells of the lung, minor expression sites are the ependyma of the brain, endometrium of the uterus, principal cells of the epididymis, inner ear and lining cells of the ileum (Zheng et al., 1994; Kounnas et al., 1994; Hermo et al., 1999). In the mouse embryo it is expressed in the neuroepithelium as well as in the visceral endoderm of the yolk sac at midgestation. At later stages it can be found most prominently in the choroid plexus, ependyma, metanephric tubules, ear, thyroid, pericardium, and intestine (Kounnas et al., 1994). In all these tissues LRP2 is expressed on the apical surface of the epithelial cell layer. A large number of ligands for LRP2 has been identified *in vitro* including proteases, protease inhibitor complexes, plasminogen, aminoglycosides, vitamin carrier proteins, lactoferrin, lipoprotein-lipase and apolipoprotein B (Stefansson et al., 1995b,a; Willnow et al., 1992; Kounnas et al., 1993)
Basic insight into the receptors function *in vivo* was gained when Willnow et al. (1996a) generated mice that lacked functional LRP2 protein by targeted gene disruption. Mice that are heterozygous for the defective gene are phenotypically indistinguishable from their littermates whereas animals homozygous for the defective gene show a variety of abnormalities. The knockout animals are characterized by fused brain hemispheres, lacking olfactory bulbs and facial abnormalities such as a shortened snout (Figure 2). Most animals are blind or have abnormally developed

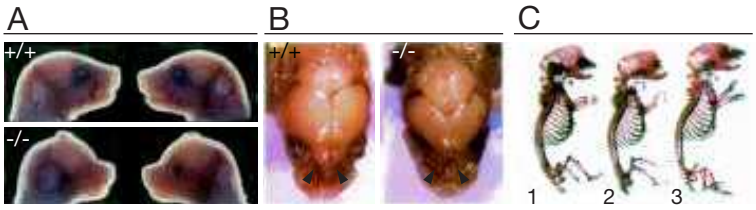

Figure 2: Cranofacial and brain malformations in *lrp2*-deficient newborn mice. (A) Head profiles of wildype (+/+) and *lrp2*-deficient (-/-) newborn mouse. (B) brains of +/+ and -/- mice after removal of the skin and bone. Arrowheads indicate olfactory bulbs. (C) Alizarin Red S/Alcain Blue staining of bone (red) and cartilage (blue) of a wild type (specimen 3) and two variably affected *lrp2* $^{-/-}$ mouse fetuses at day 18.5 (specimens 1 and 2). Modified from Willnow et al. (1996a)

eyes (Willnow et al., 1996a). Because of the severity of these defects most of the embryos homozygous for the gene defect die shortly after birth due to respiratory insufficiency (Willnow et al., 1996a).
Little is known about the exact mechanism by which LRP2 contributes to forebrain formation in the developing embryo. The various defects mentioned above are the typical hallmarks of a disease termed holoprosencephaly (HPE) in humans and indicate an essential function of the protein in establishing normal forebrain structures. The first defects in forebrain morphology are visible at day 8.5 of embryonic development (Figure 3). Embryos that were obtained from matings of *lrp2* $^{+/-}$ animals were analyzed by scanning electron microscopy. One fourth of these embryos showed distinct dysplastic abnormalities primarily around the region of the forebrain neural folds (fnf). The telencephalic vesicles were found to be reduced in size and in some cases the epithelial cohesion was impaired (Willnow et al., 1996a).
First evidence that the forebrain defect is probably a consequence of a reduction of proliferation in a specific area of the rostral neural tube came from Spoelgen et al. (2005). He showed that the neuroepithelium wall thickness in the rostral forebrain is reduced in *lrp2* $^{-/-}$ animals compared to wildtype animals. This reduction in wall thickness was found to be most pronounced in a region termed anterior entopeduncular area (AEP) and in the medial ganglionic eminece (MGE) (Figure 4 F, G, H). He could also observe a decrease of proliferation in this restricted area of the forebrain (Figure 4 D, I), whereas the number of apoptotic cells in that region was not changed (Figure 4E, K).
In adults, LRP2 is heavily expressed in the renal proximal tubule cells of the kidney

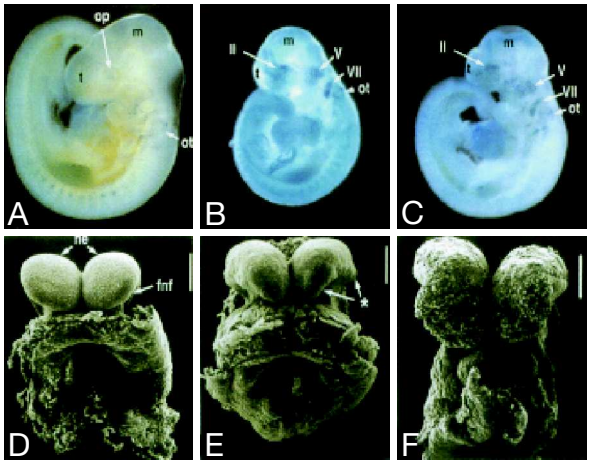

Figure 3: Analysis of E8.5 and E9.5 *lrp2* mutant mouse embryos. (A-C) Nile blue staining of E9.5 wild-type (A) and *lrp2* $^{-/-}$ mouse embryos (B and C). op, Optic vesicle; ot, otic vesicle; m, midbrain; t, telencephalon; II, perioptic neural crest and mesoderm; V, trigeminal ganglion; VII, facio-acoustic ganglion. (D-F) Scanning electron microscopy of forebrain development in E8.5 embryos. The asterisk (E) indicates dysplastic forebrain neural folds (fnf); ne, neuroepithelium (Bars in D-F = 200 um). Modified from Willnow et al. (1996a).

where low molecular weight metabolites (<70 kDa) that have passed glomerular filtration are reabsorbed. The urine of *lrp2* knockout mice is abundant in these low molecular weight metabolites (small plasma proteins, plasma vitamin carrier proteins, peptide hormones like insulin or parathyroid hormone and lysozyme) because they are apparently not resorbed by the proximal tubules of the kidney (Leheste et al., 1999; Willnow and Herz, 1995). This condition is called low molecular weight proteinuria. Because vitamins are lost together with their carrier proteins in the urine, these animals also suffer from a disturbed vitamin homeostasis (Leheste et al., 2003; Nykjaer et al., 1999; Moestrup et al., 1996). These findings show that LRP2 plays an important role in reuptake of metabolites from the glomerular filtrate in the renal proximal tubules.

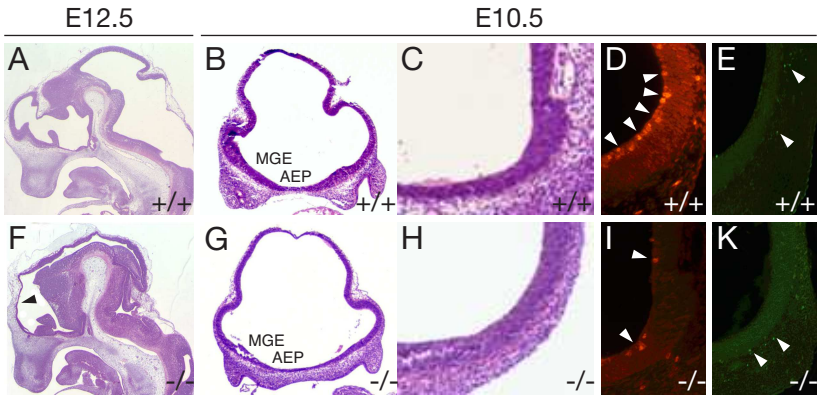

Figure 4: Neuroanatomy and analysis of cell proliferation and apoptosis of *lrp2*-deficient embryos. (A, F) Sagittal (B-E, G-K) coronal forebrain sections from wild-type (A-E) and *lrp2* $^{-/-}$ (F-K) embryos subjected to H+E staining (A-C, F-H), or detection of cell proliferation (D, I) (anti-phosphohistone H3 immunofluorescence), or detection of apoptosis (E, K) (TUNEL assay). *Lrp2* $^{-/-}$ animals suffer from a reduction in neuroepithelial wall thickness (F, arrowhead) compared with controls (A). (B, G) Coronal forebrain sections , indicating a decrease in thickness of the ventral neuroepithelium that is most pronounced in the AEP and the MGE of *lrp2* $^{-/-}$ embryos (G) compared with wild-types. (D, I) Coronal sections through the rostroventral neural tube analyzed for cell proliferation, indicating a reduction of mitotic cells in the *lrp2* $^{-/-}$ embryos (I, arrowheads) compared with wild-types (D, arrowheads). No difference is seen in the number of apoptotic nuclei in both genotypes (E, K, arrowheads). Abbreviations: AEP, anterior entopeduncular area; MGE, medial ganglionic eminence. Modified from Spoelgen et al. (2005).

1.2 Holoprosencephaly

The failure of the forebrain (prosencephalon) to divide into bilateral cerebral hemispheres is a defect known as holoprosencephaly (HPE). As a consequence the development of facial as well as of brain structures is affected. In humans, the disease manifests itself in a spectrum of defects (Matsunaga and Shiota, 1977). The most severe cases involve malformations of the brain that lead to perinatal death. Mildly affected individuals display facial defects where the eyes, nose or upper lip are affected, but where the brain is developed almost normally. The least severe of the facial anomalies is the median cleft lip (premaxillary agenesis). The most severe is cyclopia, an abnormality characterized by a single eye located in the area normally occupied by the root of the nose, and a missing or tubular-shaped

Receptor	Expression	Biological functions	Ligands
LDLR	ubiquitous, e.g. hepatocytes, macrophages, central nervous system	cholesterol homeostasis	apoE, apoB
LRP1	almost all cell types, e.g. hepatocytes, neurons, vascular smooth muscle cells, macrophage, trophoblast, embryonic tissues	endocytosis of a broad range of ligands, regulation of calcium currents, phagocytosis of apoptotic cells, embryonic development	apoE, amyloid precursor protein, lipoprotein lipase, alpha2-macroglobulin, protease/protease inhibitor complexes, platelet derived growth factor
LRP1B	central nervous system	unknown	synaptotagmin, laminin receptor precursors, apoE
LRP2	apical plasma membrane of absorptive and secretory epithelia, thyroid and parathyroid gland, trophectoderm, visceral yolk sac, neuroectoderm	vitamin/nutrient supply, calcium homeostasis, recovery of filtered low-molecular weight proteins, uptake and transcytosis of thyroglobulin	apoB, apoE, apoJ, apoH, albumin, cubilin, retinol-binding protein, vitamin D binding protein, sonic hedgehog, bone morphogenic protein 4
VLDLR	developing and adult brain, heart and endothelial cells, adipose tissue	neuronal migration, synaptic transmission	apoE, Reelin, lipoprotein lipase, tissue factor pathway inhibitor
ApoER2	developing and adult brain, testis	neuronal migration, synaptic transmission, male fertility	apoE, Reelin
MEGF7	restricted expression pattern in the embryo, adult central nervous system	limb development, body growth	apoE
LRP5	macrophages, smooth muscle cells, CNS neurons, developing lung, osteoblasts, osteoclasts	Regulation of bone formation, Wnt signal transduction	Wnt proteins
LRP6	smooth muscle cells, eye primordium, osteoblasts, osteoclasts	limb development, mid- and hindbrain development	Wnt proteins
SorLA	neurons, hepatocytes, spleen, lung	intracellular sorting of proteins	APP, ApoE, lipoprotein lipase, head activator protein

Figure 5: Ligands and functions of the mammalian LDL receptor gene family members. The table highlights a selection of biological functions and ligands of the listed receptors.

nose located above the eye. Based on the severity of the defects, three forms of holoprosencephaly are distinguished in humans:

1. Alobar holoprosencephaly is the most severe form. The brain fails to separate and affected individuals display facial abnormalities.

2. Semilobar holoprosencephaly is an intermediate form of the disease. The brain hemispheres display a slight tendency to separate.

3. Lobar holoprosencephaly is the least severe form. The hemispheres are almost completely separated, the brain appears physiologically nearly normal.

In humans, holoprosencephaly is the most common brain abnormality, affecting 1 in 16,000 live-born children (Roach et al., 1975) and 1 in 250 miscarried foetuses (Matsunaga and Shiota, 1977). Holoprosencephaly can have many reasons. Genetic disorders can lead to HPE, but also exposure of the embryo to teratogenic chemicals like ethyl alcohol or retinoic acid during pregnancy can result in HPE (Cohen and Shiota, 2002). The molecular mechanisms leading to HPE are not completely understood at present. Studies in the mouse show that the defect is likely a result of defective patterning during the development of the area giving rise to the forebrain.

1.3 Forebrain development

The forebrain (prosencephalon) is the rostral-most portion of the brain. Together with the midbrain (mesencephalon) and the hindbrain (rhombencephalon) these three primary portions of the brain are formed during early development. Later in development, the forebrain separates into the diencephalon and the telencephalon. The diencephalon can be further subdivided into the epithalamus, thalamus and hypothalamus. Functionally, the diencephalon is responsible for linking the nervous to the endocrine system and for relaying sensory information to the cerebral cortex. The telencephalon can also be divided into subregions: limbic system, cerebral cortex, basal ganglia, corpus striatum and olfactory bulbs.
In humans, the telencephalon serves the following major functions: attributing motor function to the body, sensing of smell, formation of memory and emotional sensation. In the mouse, the structures giving rise to the central nervous system start forming approximately at day 8.5 of embryonic development. At this time a specialized region of the ectoderm on the dorsal surface of the embryo termed

neural plate starts folding in upon itself to form the neural tube. The process of the flat neural plate forming into the cylindrical neural tube is termed neurulation (Sadler, 2003). The rostral part of the neural tube is giving rise to brain structures, whereas the caudal part develops into the spinal chord. Pathways that are involved in neural tube patterning have also been implicated in the etiology of HPE.
In particular, alterations in the pathways that specify the dorsoventral axis of the rostral neural tube may cause this syndrome. For example, increased dorsal signaling through bone morphogenic proteins (Bmps) or through wingless type proteins (Wnts) results in HPE (Golden et al., 1999). Also, loss of sonic hedgehog (Shh) expression, a factor that specifies ventral cell fates in the neural tube (Rubenstein et al., 1998; Inoue et al., 2000) leads to holoprosencephalic syndrome in humans and mice (Chiang et al., 1996; Roessler et al., 1996). Recent findings suggest a likely involvement of LRP2 in the Shh pathway in forebrain development, e. g. McCarthy et al. (2002) showed that LRP2 binds Shh with high affinity and mediates endocytosis of the morphogen. Internalized Shh was able to bypass lysosomal degradation, implicating LRP2 as a new regulatory component of the Shh signaling pathway (McCarthy et al., 2002).

1.3.1 The sonic hedgehog pathway

Sonic hedgehog is a secreted protein expressed in the notochord and in the floorplate that undergoes autocatalytic cleavage into a 19 kDa amino terminal (Shh-N) and a 25 kDa carboxy terminal (Shh-C) domain. During cleavage, a cholesterol moiety becomes covalently attached to Shh-N (Porter et al., 1996), the active fragment that binds the receptor Patched (Ptch) (Ingham and McMahon, 2001). This cholesterol modification is crucial for the proper activity of Shh-N (Porter et al., 1996).
In the absence of sonic hedgehog, Ptch constitutively inhibits activity of the pathway by binding to another transmembrane protein termed Smoothened (Smo). Binding of Shh-N to Ptch results in the release of Smo and activation of downstream Shh target genes through glioma-associated oncogene (Gli) proteins (Ingham and McMahon, 2001).
Expression of LRP2 in the yolk sac and in the neuroepithelium of the developing embryo and its ability to take up lipoproteins suggest a possible function for the receptor in delivery of cholesterol-rich lipoproteins from the maternal circulation to the embryo for Shh activation (Farese and Herz, 1998). The idea that a lack of cholesterol can lead to forebrain malformations is supported by experiments

where pregnant rats received an inhibitor for cholesterol biosynthesis and were fed a cholesterol free chow. Embryos, where the mother was subjected to this treatment and that were depleted of cholesterol indeed displayed HPE (Lanoue et al., 1997). A known genetic disorder in humans (Smith-Lemli-Opitz syndrome) that affects cholesterol synthesis also leads to HPE (Kelley et al., 1996). Alternatively, expression of LRP2 in the neuroepithelium and its ability to bind Shh indicates a more direct effect as a co-receptor in Shh signaling (McCarthy et al., 2002).

2 Aim of this study

During the last years, our understanding of the members of the low-density lipoprotein receptor gene family has changed substantially. It was initially assumed that the family members act mainly in the lipid metabolism but now it has become clear that most members of this protein family are playing essential roles in more biological processes than merely endocytosis.
Especially the generation of mouse models lacking specific receptors has proved that most family members are part of important signaling cascades. The generation of LRP2-deficient mice by Willnow *et al.* in 1996 provided insights into this receptor's physiological function. Whereas the receptor's function in the kidney has been well characterized, the forebrain defects have only been described histologically so far, the underlying mechanism remaining to be elucidated.
The aim of this study was to determine the role of LRP2 during early forebrain development. The receptor is heavily expressed in the visceral endoderm of the yolk sac and in the neuroepithelium of the developing embryo. In the yolk sac it is considered to be important for the supply of the early embryo with lipids and vitamins from the maternal circulation.
A role for the receptor in the neuroepithelium besides the described proliferative defects seen in the AEP and MGE of *lrp2* $^{-/-}$ embryos has not been established yet. Theoretically, both sites of expression could be important for forebrain development. To answer the question to what extent LRP2 in the embryo proper respectively in the yolk sac contributes to the observed forebrain malformations, the receptor's function in these tissues should be dissected. This should be achieved by conditional *lrp2* gene inactivation in the embryo proper.
In addition to that, different signaling pathways important for forebrain development should be analyzed by comparing the expression patterns of marker genes in *lrp2* knockout and wildtype embryos.
This study should provide new insights on how LRP2 contributes to the proper formation of forebrain structures in the developing embryo.

3 Material and Methods

3.1 Animal Experiments

3.1.1 Mouse husbandry

Mice were kept at standard conditions according to the German animal protection act. The used wildtype mice were of mixed genetic background (129SvEmcTer and C57BL/6N). The generation of mice with a targeted disruption of the *lrp2* gene has been described (Willnow et al., 1996a). The *lrp2* gene defect was analyzed in receptor-deficient and somite-matched wildtype littermates on a hybrid (129SvEmcTer x C57BL/6N) background.
For conditional inactivation of the *lrp2* gene in the epiblast, animals homozygous for a *loxP*-modified allele of the *lrp2* gene ($lrp2^{lox/lox}$) (Leheste et al., 2003) were crossed with mice carrying a knock-in of the *Cre* transgene into the *mesenchyme homeobox 2* gene locus $Meox2^{tm1(cre)Sor}$ obtained from Jackson Laboratories (www.JAX.org) (Tallquist and Soriano, 2000). Embryos from breeding of $lrp2^{lox/wt}/Meox2^{tm1(cre)Sor}$ mice with $lrp2^{lox/lox}$ animals were used for phenotypic analysis following genotyping of embryo- or yolk sac-derived tissues.
Timed matings were set up in the evening to obtain embryos at different stages of development. The presence of a vaginal plug in the morning was considered as day 0.5 post coitum (dpc). The embryos were harvested by sacrificing pregnant mice according to the German animal protection act, staged by counting the somites and further processed.

3.1.2 Zebrafish husbandry

Zebrafish were kept at standard conditions according to the German animal protection act. The used wildtype line was of the AB background. Embryos were kept in egg water (60 μg/ml Instant Ocean Sea Salts, Aquarium Systems Inc, USA) with or without 0,003% PTU (1-Phenyl-2-thiourea, Sigma, USA) to suppress pigmentation and were staged by hours post fertilization (hpf) at 28.5°C or by counting somites (Kimmel et al., 1995).

3.1.3 Morpholino Injections

Morpholino antisense oligonucleotides were purchased from GENE TOOLS, LLC, USA. Sequences were chosen to target an exon splice donor site resp. the ATG region of the corresponding mRNA. This resulted in aberrant splicing of the mRNA, resp. blocking of the translation initiation site. The Morpholinos were injected at a concentration of 100 mM in sterile ddH_2O using glass micropipettes and a microinjector/micromanipulator setup (MPPI-2 Pressure Injector/ BP15 Back Pressure Unit, Applied Scientific Instrumentation, USA; MM33 Micromanipulator, Maerzhaeuser, Germany). One- to two-cell stage embryos were used for the injection of approximately 4 nl Morpholino-solution. The effect of the splice-variant-Morpholinos was verified by RT-PCR on total embryo RNA. MO sequences (5'→3'):

*lrp2*MO1	AATCAGTGCTTGTGGTTTACCTGGG
*lrp2*MO2	GTACGAGTGTGTTCACCTGTGCCAG
dab2MO	TTCTGCTTCAGGTGACTGTGACATG

3.1.4 Dye filtration experiments

1 mg/ml solutions of lysine-fixable 10 kDa dextran labeled with rhodamine (10 kDa-RD; Molecular Probes, USA) and lysine-fixable 70 respectively 500 kDa dextran labeled with fluoresceine (70 resp. 500 kDa-FD; Molecular Probes, USA) were prepared in phosphate buffered saline (PBS; 137 mM NaCl, 2.7 mM KCl, 12.5 mM Na_2HPO_4, 1.7 mM KH_2PO_4, pH 7.4). Recombinant His-tagged RAP (39 kDa) was custom-labeled with the Cy2™ bisfunctional reactive dye kit (Cy2-RAP; Amersham, UK) according to manufacturer's instructions.
The tracers were injected into the common cardinal vein (CCV) of embryos anaesthetized with 0.2 mg/ml tricaine (3-amino benzoic acid ethyl ester, Sigma, USA) solution in egg water using the same setup as for injecting morpholinos. Uptake of filtered tracer was evaluated 1 to 1.5 hrs after injection on whole mounts using a fluorescent dissecting stereomicroscope (Leica MZ16F, Leica, Germany). Embryos were then fixed in 4% paraformaldehyde (PFA), embedded in either Technovit 7100 (Heraeus Kulzer, Germany) or Tissue-Tek® (Sakura, Japan) and sectioned at 5 μm on a Leica RM 2155 or Leica Cryocut 3000 rotary microtome (Leica, Germany).

3.1.5 Acridine orange staining

Acridine orange (AO) is a vital dye that stains apoptotic cells, but not necrotic cells (Barrallo-Gimeno et al., 2004). Zebrafish embryos were incubated in 5 μg/ml AO solution for 1 hr in the dark at RT. The embryos were then washed three times for 10 min with egg water at RT and analyzed using a fluorescence dissecting stereomicroscope (Leica MZ16F, Leica, Germany).

3.2 Microbiological Methods

3.2.1 Culture media

Medium	Composition
LB	10 g/l bacto-tryptone, 5 g/l bacto-yeast extract,10 g/l NaCl; pH 7.2
SOC	20 g/l bacto-peptone, 5 g/l bacto-yeast extract, 0.5 g/l NaCl, 0.17 g/l KCl, 0.95 g/l $MgCl_2$, 3.6 g/l glucose; pH 7.0
LB-Agar	LB-medium containing 15 g/l agar

3.2.2 Preparation of electrocompetent bacteria

A single colony of *E. coli* HB101 picked from a LB agar plate was used to inoculate 20 ml of LB medium in a 250 ml sterile flask. The cells were grown overnight with vigorous aeration at 37°C. The next day 10 ml of the cell suspension was diluted into 1 l of LB medium and grown at 37°C until the OD_{600} reached 0.5. The cell suspension was then incubated on ice for 20 min and the cells were harvested by centrifugation (4000xg; 15 min; 4°C). The pellet was resuspended in 1 l of icecold sterile 10% glycerol. Cells were again collected by centrifugation (4000xg; 15 min; 4°C) and the pellet was resuspended in 500 ml of icecold sterile 10% glycerol. The suspension was pelleted again (4000xg; 15 min; 4°C) and resuspended in 20 ml icecold sterile 10% glycerol. After collecting (4000xg; 15 min; 4°C) and resuspending in 2 ml of 10% icecold sterile glycerol once more, the cells were stored at -80°C in 100 μl aliquots.

3.2.3 Cryopreservation of bacteria

1 ml of an overnight culture of *E. coli* HB101 was mixed with 1 ml of 50% glycerol and immediately frozen at -80°C.

3.2.4 Transformation of bacteria with DNA

Electrocompetent *E. coli* HB101 cells were transformed with purified plasmid DNA or directly with DNA-ligation reactions. An aliquot of electrocompetent HB101 cells was thawed on ice. 10 ng of plasmid DNA (or 1/3 of the ligation reaction) were mixed with 40 μl of electrocompetent HB101 cell suspension and electroporated at 1.8 kV.
The cell suspension was transferred from the cuvette to a 2.0 ml tube, mixed with 1 ml of SOC medium and incubated at 37°C for 30 min. Cells were then collected (2500xg; 5 min; RT) and resuspended in 100 μl of LB medium and plated on a LB agar plate containing the appropriate selective agent.

3.3 Molecular biology methods

3.3.1 Isolation of plasmid DNA from bacteria

5 ml of LB medium were inoculated with a single colony of *E. coli* HB101 picked from a LB agar plate containing the appropriate selection marker. The LB culture was grown overnight at 37°C with vigorous shaking.
The next day the cells were collected by centrifugation (14000xg; 5 min; RT). The pellet was resuspended in resuspension buffer (50 mM Tris-HCl, 10 mM EDTA, 100 μg/ml RNase A; pH 8.0) and subsequently lysed by adding an equal volume of lysisbuffer (200 mM NaOH, 1% SDS (w/v)). The solution was mixed cautiously with an equal volume of neutralization buffer (3.0 M K-acetate; pH 5.5) and incubated on ice for 15 min. Cellular debris and genomic DNA were removed by centrifugation of the solution (14000xg; 20 min; 4°C). Remaining proteins were removed by extracting the supernatant with an equal volume of phenol/chloroform/isoamylalcohol (25:24:1) followed by centrifugation (14000xg; 5 min; RT) to separate the phases. The upper, aqueous DNA containing phase was mixed with 2.5 volumes of 100% ethanol and the DNA was precipitated by centrifugation (14000xg; 20 min; 4°C). The pellet was washed once with 70% ethanol and resuspended in 50 μl of TE-buffer (10 mM Tris-HCl, 1 mM EDTA; pH 8.0). The purified plasmid DNA was stored at -20°C.

3.3.2 Isolation of genomic DNA from tissue samples

Tissue for isolating genomic DNA was obtained by subjecting adult mice to a tail biopsy, respectively adult zebrafish to a tailfin biopsy. Yolk sac tissue was used to isolate DNA for genotyping mouse embryos. DNA was isolated by incubating the tissue with Protease K in tail buffer (10 mM Tris-HCl, 0.3 M Na-Acetate, 0.1 mM EDTA, 1% SDS (w/v); pH 7.0) at a final concentration of 0.5 mg/ml for several hours to overnight at 52°C. Proteins were removed by extracting with an equal volume of phenol/chloroform/isoamylalcohol (25:24:1) followed by centrifugation (14000xg; 5 min; RT) to separate the phases. The upper, aqueous DNA containing phase was mixed with 2.5 volumes of 100% ethanol. The precipitate was collected by centrifugation (14000xg, 10 min, 4°C) washed once with 70% ethanol and redissolved in TE-buffer (10 mM Tris-HCl, 1 mM EDTA; pH 8.0). Isolated genomic DNA was stored at 4°C.

3.3.3 Isolation of total RNA from tissue samples

Total RNA was isolated with the TRIZOL® reagent from Invitrogen, USA. Tissue samples were homogenized in 1 ml of TRIZOL® reagent per 50-100 mg of tissue and incubated for 5 min at RT. 0.2 ml of chloroform were added to the homogenate per 1 ml of TRIZOL® reagent. Samples were shaken vigorously by hand for 15 seconds and incubated at RT for 3 min. The phases were separated by centrifugation (12000xg; 15 min; RT). Following centrifugation, the upper aqueous phase was transferred to a fresh tube and precipitated by adding 0.5 ml of isopropyl alcohol per 1 ml of TRIZOL®. The RNA was collected by centrifugation (12000xg, 10 min, 4°C) and washed once with 1 ml of 70% ethanol per 1 ml TRIZOL®. The pellet was air-dried for 10 min redissolved in RNase-free water and stored at -80°C.

3.3.4 DNA and RNA concentration determination

The concentration of DNA and RNA samples was determined spectrophotometrically at a wavelength of 260 nm (OD_{260}) since the concentration of DNA and RNA is a direct function of the optical density at this wavelength. For DNA, an OD_{260} of 1.0 equals a concentration of 50 μg/ml of double stranded DNA, for RNA an OD_{260} of 1.0 equals a concentration of 40 μg/ml of RNA.
DNA quality measurement was done by measuring the OD_{280} because proteins absorb UV-light maximally at this wavelength. Pure DNA solutions have an OD_{260}:

OD_{280} ratio of 1.8. A lower ratio indicated contamination of the sample with proteins.

3.3.5 Enzymatic digest of DNA

The appropriate amount of DNA was incubated with the corresponding restriction enzyme(s) and buffer at a ratio of 0.5 U emzyme/μg DNA. The digest was incubated at 37°C for 2 hrs to overnight. All restriction enzymes were obtained from New England Biolabs, USA. After incubation, the digest was either column purified or subjected to gel electrophoresis to isolate the fragment of interest.

3.3.6 Agarose gel electrophoresis of DNA and RNA

DNA and RNA fragments were separated according to their molecular weight on 0.8-2.0% agarose gels. Ethidium bromide was added to the gel at a final concentration 0.5 μg/ml to facilitate visualization of the DNA resp. RNA fragments after electrophoresis.

3.3.7 Isolation of DNA from agarose gels

Polymerase chain reaction (PCR) products or DNA digests were resolved on 0.8-1.2% agarose gels containing ethidium bromide. By exposing the agarose gel to UV-light, the DNA was visualized and bands of interest were cut from the gel. The DNA was extracted using the High Pure PCR Product Purification Kit from Roche, Switzerland. The gel slice was incubated with binding buffer (3 M guanidine-thiocyanate, 10 mM Tris-HCl, 5% ethanol (v/v); pH 6.6) at a ratio of 300 μl buffer/100 mg agarose at 52°C until the gel slice was completely dissolved. The sample was transferred to a filter column and subjected to centrifugation (14000xg, 1 min, RT). The filter column was washed two times with 500 μl washing buffer (2 mM Tris-HCl, 20 mM NaCl, 80% ethanol (v/v); pH 7.5) and the DNA was eluted with 50 μl elution buffer (10 mM Tris-HCl; pH 8.5) and stored at -20°C.

3.3.8 Ligation of PCR-products in the pGEM-T Easy Vector

The PCR-reaction-mix was separated electrophoretically on a 0.8-1.2% agarose-gel, and the band of interest cut from the gel and column purified. Ligation of PCR-Products with the pGEM-T® Easy Vector (Promega, USA) was done according to

the manufacturers instructions: 5-10 ng of the PCR-product were incubated with 5 μl 2X Rapid Ligation Buffer®, 30 ng of pGEM-T Easy Vector and 3 U of T4 DNA-Ligase. The volume of the reaction setup was adjusted to 10 μl with H_2O and incubated at 16°C overnight. The next day 1/3 of the ligation reaction was used to transform electrocompetent *E. coli* HB101.

3.3.9 Polymerase chain reaction

If not stated otherwise PCR was carried out according to the following parameters: 50 ng of template DNA were incubated in the presence of 250 μM dNTPs, 300 nM forward primer, 300 nM reverse primer, 2 units AmpliTaq Gold DNA-Polymerase (Perkin-Elmer, USA), 0.01% Triton X-100 (v/v), 50 mM KCl, 10 mM Tris-HCl, 1.5 mM $MgCl_2$ and 0.001% (w/v) gelatin; pH 8.3 in a thermocycler. During the first cycle the reaction mix was denatured at 95°C for 10 min, primers were allowed to anneal at 60°C for 1 min and DNA synthesis was carried out at 72°C for 1 min. For the following 35 cycles the reaction mix was denatured at 95°C for 45 sec, annealed at 60°C for 45 sec and elongated at 72°C for 45 sec. This was followed by a final elongation step at 72°C for 10 min. The reaction mix was then cooled down to 4°C and further processed.

3.3.10 Primer sequences

Mouse specific primer

Primer identifier	Sequence (5'→3')
BPA	GATTGGGAAGACAATAGCAGGCATGC
g15	CTGAGGTACCCAGTCTCCTGTCAG
g20	GACCATTTGGCCAGCCAAGG
g21	CATATCTTGGAAATAAAGCGAC
LAKA	ACCTTGCGTGAATTCTGGG
morecre	CCAGATCCTCCTCACAAATCAGC
morefor	GGGACCACCTTCTTTTGGCTT
morerev	AAGATGTGGAGAGTTCGG
TKP2	TGAAAACCACACTGCTCGATCCGGAAC

Zebrafish specific primer

Primer identifier	Sequence (5'→3')
Dab2 For	CCCCCTCCCACACTTTTTCTTTCA
Dab2 Rev	TGCCATTTCCTTCACCCTTTTGTC
LRP2 For1.1	GCAGATGCATGAATGGAGGAACG
LRP2 For	AATGGGCAAGTCTAGAGGAGC
LRP2 Rev2	TTTGGGAGGAACAAACGGA
LRP2 Rev3	TCCACTGCCTGCTGATATGT
LRP2seq For	GGATGGATGGATGGATGGATA
LRP2seq Rev	ATTGGTGACTATACAAGGGCG
Nkx2.1 For	GACCTGCCGGCCTATCAAGACG
Nkx2.1 Rev	CGGAGCGCCACCCCAGTT
Olig2 For	TGAACGCCATGGACTCTGACACGA
Olig2 Rev	CCTGGCACATGCTACACGGACAAG

3.3.11 Reverse transcription

Generation of cDNA from RNA was done using the Sensiscript® Reverse Transcription Kit (Qiagen, Germany). 50 ng of total RNA were incubated with 2.0 μl 10x Buffer RT, 2.0 μl dNTP Mix (5 mM each dNTP), 1 μM Oligo-dT primer, 10 U RNase inhibitor and 1.0 μl Sensiscript® Reverse Transcriptase. The volume of the reaction setup was adjusted to 20 μl with H_2O and incubated at 37°C for 60 min. The reaction mix was then stored at -20°C.

3.3.12 In vitro transcription of digoxigenin labeled RNA

Digoxigenin (DIG)-labeled Probes for *in situ* hybridization (ISH) were generated using the DIG labeling kit (Roche, Switzerland). 1μg of linearized template plasmid-DNA was incubated with transcription buffer(40 mM Tris-HCl, 6 mM $MgCl_2$, 10 mM dithiothreitol, 2 mM spermidine; pH 8.0), 1 mM ATP, 1 mM GTP, 1 mM CTP 0.65 mM UTP, 0.65 mM DIG-11-UTP, 40 U RNA Polymerase and 20 U RNase Inhibitor. The volume of the reaction was adjusted to 20 μl and incubated for 2 hrs at 37°C. Template DNA was removed by incubating the reaction setup with 20 U DNase I at 37°C for 15 min. The RNA was purified using the RNeasy Mini Cleanup Kit (Qiagen, Germany).

3.3.13 In situ probes

The source of the probes is given in brackets after the gene name. Probes where the source was cDNA were obtained by amplifying a 500-600 bp fragment of the corresponding cDNA using the primers listed in section 3.3.10 Mouse specific primer", resp. "Zebrafish specific primer". The obtained PCR product was subcloned into the pGEM-T® Easy Vector and sequenced to verify the orientation and identity of the insert as described. The source for probes that were not generated from cDNA but obtained from other workgroups is listed along with the gene name in the following tables.

Mouse specific probes

Gene name	Probe	Restr.-site	Promotor
bone morphogenic protein 4 (J. Huelsken, ISREC, Epalinges)	*bmp4*	*Eco*RV	Sp6
distal-less homeobox 2 (J. Rubenstein, UCSF, San Francisco)	*dlx2*	*Eco*RI	T3
fibroblast growth factor 8 (W. Birchmeier, MDC, Berlin)	*fgf8*	*Bam*HI	T7
glioma-associated oncogene homolog 1 (A. Joyner, MSRI, Toronto)	*gli1*	*Not*I	T3
glioma-associated oncogene homolog 2 (J. Huelsken, ISREC, Epalinges)	*gli2*	*Hind*III	T7
glioma-associated oncogene homolog 3 (J. Huelsken, ISREC, Epalinges)	*gli3*	*Hind*III	T7
hepatocyte nuclear factor 3ß (B. Hogan, VUMS, Nashville)	*hnf3ß*	*Xmn*I	T7
muscle segment homeobox 1 (W. Birchmeier, MDC, Berlin)	*msx1*	*Eco*RI	T7
oligodendrocyte lineage transcription factor 2 (W. Birchmeier, MDC, Berlin)	*olig2*	*Eco*RI	T7
paired box DNA binding protein 6 (C. Bönsch, MDC, Berlin)	*pax6*	*Eco*RI	Sp6
patched protein homolog 1 (J. Huelsken, ISREC, Epalinges)	*ptc1*	*Sal*I	T3
sonic hedgehog (A. McMahon, Harvard University, Cambridge)	*shh*	*Hind*III	T3
thyroid transcription factor 1 (W. Birchmeier, MDC, Berlin)	*nkx2.1*	*Sal*I	T3
wingless-type integration site family member 1 (W. Birchmeier, MDC, Berlin)	*wnt1*	*Sal*I	T7

Zebrafish specific probes

Gene	Probe	Restr.-site	Promotor
cubilin (S. Seyfried, MDC, Berlin)	*cub*	*Not*I	T3
disabled homolog 2 (cDNA)	*dab2*	*Sac*II	Sp6
low density lipoprotein receptor related protein 2 (cDNA)	*lrp2*	*Sal*I	T7
oligodendrocyte lineage transcription factor 2 (cDNA)	*olig2*	*Sac*II	Sp6
paired box DNA binding protein 2.1 (N. Hastie, HGMPRC, Edinburgh)	*pax2.1*	*Bam*HI	T7
sonic hedgehog (S. Seyfried, MDC, Berlin)	*shh*	*Hind*III	T7
thyroid transcription factor 1 (cDNA)	*nkx2.1*	*Sal*I	T3
wilms tumor gene 1 (N. Hastie, HGMPRC, Edinburgh)	*wt1*	*Apa*I	T7

3.3.14 ISH on whole-mount mouse embryos

Mouse embryos were dissected in PBS and fixed overnight in 4% (PFA) in PBS. After fixation the embryos were dehydrated through a series of graded methanol solutions: 25%, 50%, 75% and 100% methanol in PBS, containing 0.1% Triton X-100 (PBT) for 10 min each and stored at -20°C until use. For ISH, embryos were rehydrated through a series of graded methanol solutions (reverse of above) and punctured (eyes, hindbrain, heartsac) to facilitate penetration of solutions. Specimens were washed two times for 10 min in PBT and bleached in PBT containing 6% H_2O_2 for 1 hr. After washing with PBT for 5 min the embryos were permeabilized with 10 μg/ml Proteinase K in PBT for 20 min at RT. The proteinase K digest was stopped by washing with 2 mg/ml glycine in PBT for 5 min, followed by two additional washes in PBT. Next, the embryos were refixed with 4% PFA containing 0.2% glutaraldehyde for 20 min at RT, and washed twice with PBT for 5 min. The embryos were then incubated with prehybridization solution (750 mM NaCl, 75 mM Na_3Citrate, 50% formamide, 50 μg/ml heparin, 100 μg/ml torula yeast RNA, 0.1% Triton X-100; pH 4.5) for 3 hrs at 65°C. After prehybridization

the embryos were incubated overnight at 65°C with the DIG-labeled RNA probe in fresh prehybridization buffer at a final concentration of 1 μg/ml.
The next day, the embryos were washed extensively in a series of buffers of increasing stringency: 2 times for 30 min at 65°C with wash-solution I (600 mM NaCl, 60 mM Na_3Citrate, 50% formamide, 1 %SDS; pH 4.5), 2 times for 30 min at 65°C with wash-solution II (300 mM NaCl, 30 mM Na_3Citrate, 50% formamide; pH 4.5) and 3 times for 10 min at RT with Tris buffered saline, containing 1% Tween (TBST; 140 mM NaCl, 2.7 mM KCl, 2.5 M Tris-HCl, 1% Tween; pH 7.5). After washing, the embryos were blocked with TBST containing 10% sheep serum for 3 hrs at RT, and incubated with an anti-digoxigenin-alkaline-phosphatase (anti-DIG-AP) conjugate at a dilution of 1:2000 overnight. The anti-DIG-AP was preabsorbed with embryopowder (3 mg/ml) in TBST at a dilution of 1:400 for 3 hrs at 4°C before use. Unspecifically bound antibody was removed the next day by three brief washes for 5 min, 5 washes for 1 hr at RT and a single wash overnight at 4°C, all in TBST.
The next day, embryos were washed 3 times for 10 min in staining buffer (NTMT, 100 mM NaCl, 100 mM Tris-HCl, 50 mM $MgCl_2$, 0,1% Triton X-100; pH 9.5) before they were incubated with NTMT containing 1.88 mg/ml nitro blue tetrazolium chloride (NBT) and 0.94 mg/ml 5-Bromo-4-chloro-3-indolyl phosphate (BCIP). BCIP is the AP-substrate which reacts further after the dephosphorylation to give a dark-blue indigo dye as an oxidation product. NBT serves herein as the oxidant and gives also a dark-blue dye. The staining reaction was stopped by washing the embryos 3 times for 10 min at RT in NTMT, followed by a 4 hrs incubation in PBT pH 5.3 at RT. The embryos were refixed in 4% PFA containing 0.1% Glutaraldehyde (GTA) for 20 min at RT and cleared by incubating in 25%, 50%, 70% and 80% glycerol in PBS for 5 min each at RT. The embryos were stored at 4°C in the dark.

3.3.15 ISH on whole-mount zebrafish embryos

Zebrafish embryos were dechorionated and fixed overnight in 4% PFA in PBS. After fixation the embryos were dehydrated through a series of graded methanol solutions: 25%, 50%, 75% and 100% methanol in PBS, containing 0,1% Triton X-100 (PBT) for 5 min each and stored at -20°C until use.
For ISH, embryos were rehydrated through a series of graded methanol solutions (reverse of above) and washed 4 times 5 min at RT in PBT. This was followed by a digest with proteinase K (10 μg/ml) in PBT for 30 min at RT. The digest

was stopped by washing 3 times with PBT for 1 min at RT. The embryos were refixed in 4% PFA in PBS for 20 min at RT and washed 5 times for 5 min at RT. Specimens were then incubated for at least 2 hrs in prehybridization buffer (750 mM NaCl, 75 mM Na_3Citrate, 50% formamide, 50 μg/ml heparin, 500 μg/ml torula yeast RNA, 0.1% Triton X-100; pH 4.5). After prehybridization the embryos were incubated overnight at 67°C with the DIG-labeled RNA probe in fresh prehybridization buffer at a final concentration of 1 μg/ml.
The next day, the embryos were washed extensively with a series of buffers of increasing stringency: 1 time for 20 min at 67°C with prehybridization buffer, 3 times 20 min at 67°C with wash-solution I (150 mM NaCl, 15 mM Na_3Citrate; pH 4.5, 50 % formamide), 1 time for 20 min at 67 °C with wash-solution II (150 mM NaCl, 15 mM Na_3Citrate; pH 4.5, 25% formamide), 2 times 20 min at 67°C with wash-solution III (150 mM NaCl, 15 mM Na_3Citrate; pH 4.5), 4 times 30 min at 67°C with wash-solution IV (30 mM NaCl, 3 mM Na_3Citrate; pH 4.5) and 1 time for 5 min with PBT at RT. After washing the embryos were blocked in PBT containing 5% sheep serum and 10 mg/ml bovine serum albumin (BSA) for 2 hrs at RT and incubated with an anti-digoxigenin-alkaline-phosphatase (anti-DIG-AP) conjugate at a dilution of 1:2000 overnight in PBT containing 2 mg/ml BSA. The anti-DIG-AP was preabsorbed with smashed zebrafish embryos in PBT containing 2 mg/ml BSA at a dilution of 1:400 for 3 hrs at 4°C before use. Unbound anti-DIG-AP was washed off the next day by incubating the embryos 8 times for 30 min at RT in PBT. The embryos were then incubated 3 times 5 min in staining buffer (NTMT, 100 mM NaCl, 100 mM Tris-HCl, 50 mM $MgCl_2$, 0,1% Triton X-100; pH 9,5) and then in NTMT containing 1.88 mg/ml nitro blue tetrazolium chloride (NBT) and 0.94 mg/ml 5-Bromo-4-chloro-3-indolyl phosphate (BCIP). The staining raction was stopped by washing the embryos 3 times 5 min in Stop-solution (50 mM NaH_2PO_4/Na_2HPO_4, 1 mM EDTA, 0.1% Tween; pH 5.8). Embryos were stored in 80% glycerol in Stop-solution at 4°C.

3.3.16 Genotyping of mice

Polymerase chain reaction (PCR) was used to genotype the *lrp2* $^{-/-}$ as well as the *lrp2* $^{lox/lox}$ and the *Meox2* $^{tm1(cre)Sor}$ animals.
The primerpair BPA/g21 amplified a 300 bp fragment that was specific for the knockout allele of *lrp2*, primerpair g20/g21 amplified a 200 bp fragment specific for the wildtype allele of *lrp2*. The tissue specific *lrp2*$^{lox/lox}$ animals had to be screened using the primerpair morefor/moreref that amplified a 400 bp fragment specific

for the wildtype *lrp2* allele, whereas the primerpair morefor/morecre amplified a 300 bp fragment specific for the *loxP* modified *lrp2* allele. These animals had to be screened additionally for the the *Meox2*$^{\text{tm1(cre)Sor}}$ gene locus. Primerpair TKP2/G15 amplified 500 bp of the *cre* modified *Meox2* allele and primerpair LAKA/G15 amplified a 500 bp fragment that was specific for the wildtype *Meox2* allele.

3.3.17 Membrane extracts

To specifically enrich membrane or membrane-associated proteins, the sample tissue was smashed using a micropestel or a homogenizer in a minimal volume of solution A (20 mM Tris-HCl, 2 mM $MgCl_2$, 0.25 mM Sucrose, 250 μM PMSF; pH 7.5). The cellular debris was removed by a centrifugation step at a low g-force (1000xg, 10 min, 4°C). Nuclei were removed by an additional centrifugation step at a medium g-force (10000xg, 10 min, 4°C). Finally, the supernatant was ultracentrifuged at a high g-force (100000xg, 45 min, 4°C) to pellet the membrane fraction. The pellet was resuspended in 40 μl of solution B (50 mM Tris-HCl, 2 mM $MgCl_2$, 80 mM NaCl, 1 mM PMSF; pH 8.0) and stored at -80°C until use. For western blotting, 50 μg of membrane extract were applied to a 8-12% SDS-polyacrylamide-gel.

3.3.18 Protein concentration determination

Protein concentration was determined spectrophotometrically at a wavelength of 595 nm (OD_{595}) as described by Bradford (1976). The procedure is based on the formation of a complex between the dye Brilliant Blue G, and proteins in solution. The protein-dye complex causes a shift in the absorption maximum of the dye from 465 to 595 nm. The extent of absorption is proportional to the amount of protein present. Samples containing known concentrations of bovine serum albumin (BSA) were used as standard.

3.3.19 SDS polyacrylamide gel electrophoresis of proteins

Proteins were separated depending on their molecular weight on continuous or gradient gels (for separation of proteins of high and low molecular weight at the same time) containing 8-12% polyacrylamide (PA). If not stated otherwise, 50 μg of protein were mixed with sample buffer, incubated for 5 min at 95 °C and resolved

at 20-100 V (2-10 V/cm)in SDS-PAGE running buffer (196 mM glycine, 0.1% SDS, 50 mM Tris-HCl pH 8.4) After electrophoresis the gels were either subjected to western blotting or to coomassie brilliant blue staining.

3.3.20 Western blotting

Western blotting was used to transfer proteins electrophoretically from a damageable polyacrylamide gel to a more robust support. The setup in the transfer case was as follows: Scotch Brite Pad (3M, USA), then Whatman paper (3M, USA), PA-gel, Hybond-C nitrocellulose membrane (GE Healthcare, USA), Whatman paper and Scotch Brite Pad. The assembled case was inserted in the case holder and put into the transfer chamber filled with transfer buffer (25 mM Tris-HCl, 192 mM Glycine; pH 8.4). The transfer was run at 100 V for 2 hrs or at 20 V overnight. The efficiency of the transfer was evaluated by staining the membrane with Ponceau S staining solution (0.1%(w/v) Ponceau S in 5%(v/v) acetic acid) to visualize the protein bands.
The membrane was then incubated with blocking solution (133 mM NaCl, 1.7 mM KCl, 4.3 mM Na_2HPO_4, 1.4 mM KH_2PO_4, 0.08% Tween 20, 5% FCS, 5% dry milk powder; pH 7.4) for 1 hr at RT.
The primary antibody was applied in binding buffer (133 mM NaCl, 1.7 mM KCl, 4.3 mM Na_2HPO_4, 1.4 mM KH_2PO_4, 0.08% Tween 20, 5% dry milk powder; pH 7.4) at a dilution of 1:100-1:1000, depending on the antibody. Incubation with the primary antibody was carried out at 4°C overnight with rocking. Unspecifically bound antibody was removed the next day by washing the membrane 2 times 15 min in wash-buffer I (133 mM NaCl, 1.7 mM KCl, 4.3 mM Na_2HPO_4, 1.4 mM KH_2PO_4, 0.08% Tween 20, 0.1%SDS, 1% NP-40; pH 7.4) and two times in wash-buffer II (133 mM NaCl, 1.7 mM KCl, 4.3 mM Na_2HPO_4, 1.4 mM KH_2PO_4, 0.08% Tween 20; pH 7.4). The membrane was then incubated with the peroxidase-conjugated secondary antibody at a dilution of 1:1000 in binding buffer for 1 hr at RT. After washing 2 times 15 min with wash-buffer I and 2 times 15 min with wash-buffer II, the membrane was incubated with detection solution (Super Signal West PicoStable Peroxide/Luminol Enhancer solution, Pierce, USA). Bands were detected using a CCD-camera (Fujifilm LAS-1000/ Intelligent Dark Box, Fujifilm, Japan).

3.3.21 Coomassie brilliant blue staining of SDS-PAGE-gels

Coomassie brilliant blue staining is based on the binding of the dye coomassie brilliant blue R250, which binds nonspecifically to proteins. For staining, the gel was incubated with coomassie blue staining solution (0.025% coomassie brilliant blue R250, 40% (v/v) methanol, 7% (v/v) acetic acid) for 4 hrs to overnight. The next day, the gel was transferred to destaining solution I (40% (v/v) methanol, 7% (v/v) acetic acid), incubated for 30 min and transferrred to destaining solution II (7% (v/v) acetic acid, 5% (v/v) methanol). Destaining solution II was changed several times until the background was clear. The stained gel was imaged and dried to preserve.

3.3.22 In vitro analysis of protein-protein binding

Binding of Bmp4, Bmp5, and Wnt1 to LRP2 was quantified by BIAcore (Biosensor, Sweden) as described previously (Moestrup et al., 1998). A continuous flow of HBS buffer (10 mM HEPES, 3.4 mM EDTA, 150 mM NaCL, 0.005% surfactant P20; pH 7.4) passing over the sensor surface was maintained at 5 μl/min. The carboxylated dextran matrix of the sensor chip flow cell was activated by injection of 60 μl of a solution containing 0.2 M n-ethyl-N'-(3dimethylaminopropyl)carbodiimide and 0.5 M N-hydroxysuccimide in water. Then 120 μl of 10 mM sodium acetate (pH 4.5) containing 0.33 μg/μl purified rabbit LRP2 (Hannelore Schulz, MDC, Berlin) were injected. The remaining binding sites were blocked by subsequent injection of 35 μl 1 M ethanolamine (pH 8.5). The surface plasmon response signal from immobilized LRP2 generated 15,167 BIAcore response units (RU) equivalent to 23.45 fmol/mm^2 immobilized LRP2. To test binding, immobilized rabbit LRP2 on the sensor chip was incubated with 0.5 μmol/l recombinant human Bmp4 or Bmp5 (Research and Development, USA) or with 20-fold concentrated Wnt1 medium (Olav Andersen, MDC, Berlin) in 10 mM HEPES, 150 mM NaCl, 1.5 mM $CaCl_2$, 1 mM EGTA; pH 7.4, and the relative increase in response between LRP2 and control flow channels was determined. Kinetic parameters were determined by using the BIAevaluation 3.0 software.

3.3.23 In vivo uptake and degradation studies

Bmp4 was radiolabeled with ^{125}I using the IODO-GEN® iodination reagent (1,3,4,6-tetrachloro-3α-6α-diphenylglycouril, Pierce, USA). This method labels exposed tyrosine residues of the protein (Fraker and Speck, 1978) with ^{125}I. 100 μg of

recombinant Bmp4 (Research and Development, USA) in PBS were incubated with 500 μCi of $Na^{125}I$ in pre-coated iodination tubes (Pierce, USA) for 10 min at RT. The reaction was stopped by removing from the tube and unincorporated $Na^{125}I$ was removed subsquently by column-purification (PD-10 desalting columns, Amersham, USA). The specific activity of the iodinated Bmp4 was $3.1x10^8$ cpm/μg.
For cell uptake studies, replicate monolayers of rat choriocarcinoma (BN16) cells were incubated for 2 hrs with 1.6 ng/ml of ^{125}I-Bmp4 in the presence of buffer, 200 μmol/l chloroquine or 100 μg/ml RAP. The amount of excreted lysosomal degradation products of ^{125}I-Bmp4 protein was determined to measure the rate of endocytosis. After 2 hrs, the medium was removed and mixed with trichloraceticacid to precipitate the not endocytosed ^{125}I-Bmp4 in solution. Short peptides that were generated by lysosomal degradation cannot be precipitated by this treatment. After precipitation of the proteins the specific activity of the supernatant was measured and expressed as picogram ligand per mg of total cell protein (Hilpert et al., 1999).

3.4 Histology

3.4.1 Paraffin sections

For paraffin sections tissue samples were fixed overnight in 4% PFA in PBS at 4°C. After fixation the samples were dehydrated through a series of graded ethanol/PBS solutions for 2 hrs each step: 70%, 80%, 90%, 96% and 100% ethanol. Following dehydration, the samples were incubated 2 times for 2 hrs in Roti-Histol® (Roth, Gemany). The samples were preinfiltrated with paraffin for 2 hrs at 67°C and finally infiltrated with fresh paraffin overnight at 67°C. The next day, the samples were embedded in molds and stored at 4°C until use. If not otherwise stated, sectioning was done at 5 μm on a rotary microtome (Leica, Germany). Slides were stored at 4°C until further processing.

3.4.2 Plasticsections

Samples were embedded in Technovit 7100 (Heraeus Kulzer, Germany) according to the manufacturer's instructions: specimens were fixed and dehydrated as described for "Paraffin sections", followed by a pre-infiltration with 50% ethanol/50% Technovit 7100 (v/v) for 2 hrs at RT. Next, samples were infiltrated with Technovit 7100 containing 1% (w/v) hardener I for 2 hrs at RT. Finally specimens were

embedded in Technovit 7100 containing 1% hardener I and 6% (v/v) hardener II. After polymerisation, samples were cut at 5 μm on a rotary microtome (Leica, Germany). Slides were stored at 4°C until further processing.

3.4.3 Cryosections

Specimens were fixed for 1 hr at RT in 4% PFA and incubated in 30% sucrose/PBS overnight. The next day, embryos were transferred to Tissue-Tek® OCT (Sakura, Japan) and slowly cooled down in ethanol containing dry ice. The samples were then dissected at 5 μm on a rotary cryotome (Leica, Germany). Slides were stored at -80°C until further processing.

3.4.4 Counterstaining of sections

Paraffin sections were counterstained using hematoxilin and eosin. Hematoxylin specifically stains nuclei whereas eosin stains the cytoplasms of cells. The sections were deparaffinized by two incubations in Roti-Histol® (Roth, Germany), rehydrated by subsequent washes in 100%, 80%, 50%, 30% ethanol and H_2O. The slides were incubated for 4 min with Mayer's hematoxylin solution (5% (w/v) aluminum potassium sulphate, 0.1% (w/v) hematoxylin, 0.02% (w/v) sodium iodate, 2% (v/v) glacial acetic acid; Roth, Germany) and rinsed for 5 min with tap water. Incubating in acid alcohol (70% (v/v) ethanol, 0.25% (v/v) concentrated hydrogen chloride acid) for 45 sec was followed by a second rinse with tap water for 5 min. After two dips in 96% ethanol, the sections were incubated with eosin staining solution (90% ethanol, 0.1% eosin; Roth, Germany) for 45 sec and washed immediately 5 times with isopropanol. The slides were dipped 2 times in Roti-Histol®, dried and mounted with Histo-clear® (Roth, Germany).
Plastic sections were counterstained using Orange G (Sigma-Aldrich, USA), staining the cytoplasms of tissues. The sections were incubated for 30 sec with Orange G staining solution (0.5% (w/v) Orange G in ethanol), rinsed with tap water for 2 min, dried and mounted with Histo-clear® (Roth, Germany).

3.4.5 Immunohistchemistry on cryosections

The slides were removed from the -80°C freezer and allowed to equilibrate at RT for 10 min. After equilibration, the slides were dried at 37°C for 30 min, fixed in 1% PFA, washed 2 times in TBS (50 mM Tris-HCl, 150 mM NaCl; pH 7.4) for

5 min and two times in TBS containing 0.025% Triton X-100 (TBST) for 5 min. Sections were then blocked for 2 hrs at RT with TBS containing 10% donkey serum and 1% BSA. The slides were drained for a few seconds and incubated with the primary antibody (rabbit-anti-Rab4 (1:100), Abcam, UK; rabbit-anti-LRP2 (1:100), Joachim Herz, University of Texas, USA; rabbit-anti-TuJ1 (1:500), BabCO, USA; rabbit-anti-P-Smad1/5/8 (1:100), Cell Signaling Technology, USA) in TBS containing 1% BSA at 4°C overnight. The next day, the slides were washed 2 times for 5 min with TBS at RT and the secondary antibody (Cy3 or Cy5 conjugated goat-anti-rabbit (1:400), Jackson Immuno Research Laboratories, USA) was applied in TBS with 1% BSA for 1 hr at RT. Before mounting with glycerol gelatine, the slides were washed 2 times in TBS for 5 min.

4 Results I: Mouse

4.1 Forebrain defects in mice with epiblast-specific lrp2 gene disruption

During early development, LRP2 is expressed in the visceral endoderm of the yolk sac and in the neuroepithelium (Figure 6 A, B). Conceivably, lack of *lrp2* expression in either the embryonic or the extra-embryonic tissues (or both) may be responsible for the brain malformations in mice lacking the receptor. To dissect the contributions of both tissues to the occurrence of forebrain defects, conditional gene targeting was used to inactivate the *lrp2* gene specifically in the embryo proper and retain gene expression in the yolk sac.
A mouse line carrying a *lrp2* gene modified by *loxP* sites (*lrp2* $^{lox/lox}$) was used to achieve tissue-specific receptor gene inactivation (Leheste et al., 2003). *Lrp2* $^{lox/lox}$ animals were bred with mice carrying the *cre* recombinase gene under control of the *mesenchyme homeobox 2* gene promoter (*Meox2* $^{tm1(cre)Sor}$), directing *cre* gene expression to the epiblast (Tallquist and Soriano, 2000). Consistent with this strategy, embryos homozygous for the *loxP*-modified *lrp2*-gene and carrying the *cre* transgene (*lrp2* $^{lox/lox}$/*Meox2* $^{tm1(cre)Sor}$) lacked expression of the receptor in the neuroepithelium (Figure 6 E) but not in the yolk sac (Figure 6 D).
Despite normal expression of LRP2 in the visceral endoderm of the yolk sac, *lrp2* $^{lox/lox}$/*Meox2* $^{tm1(cre)Sor}$ embryos suffered from similar brain defects compared to *lrp2* $^{-/-}$ embryos (Figure 6 C, F), demonstrating that LRP2 activity in the embryo proper is required for brain development. The *cre*-mediated inactivation of the *lrp2* gene in the epiblast of *lrp2* $^{lox/lox}$/*Meox2* $^{tm1(cre)Sor}$ embryos was inefficient, only 1 in 30 embryos showed complete loss of receptor expression in the neuroepithelium. Therefore, mainly *lrp2* $^{-/-}$ animals were used for the following experiments. However, key findings were confirmed in mice with epiblast-specific receptor gene defect.

4.2 Absence of shh expression in the AEP of lrp2-deficient embryos

Embryos lacking functional LRP2 protein display a reduced epithelial wall thickness in the ventral neuroepithelium compared to wildtype embryos (Figure 4 A-C, F-H). Consistent with this finding, cell proliferation in distinct areas of the ventral forebrain, termed anterior entopeduncular area (AEP) and medial ganglionic eminence

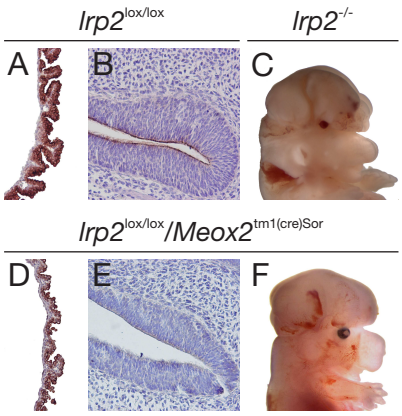

Figure 6: Forebrain abnormalities and LRP2 expression pattern in E14.5 embryos with conditional *lrp2* gene inactivation. (A, B, D, E) Immunohistological detection of LRP2 in yolk sac (A, D) and neuroepithelium (B, E) of E14.5 embryos. *Lrp2* $^{lox/lox}$ embryos express the receptor in the yolk sac (A) and the neuroepithelium (B), whereas *lrp2* $^{lox/lox}$/*Meox2* $^{tm1(cre)Sor}$ embryos express the receptor in the yolk sac (D) but not in the neuroepithelium (E). (C, F) Exencephalus in E14.5 embryos with ubiquitous (*lrp2* $^{-/-}$, C) or with epiblast-specific (*lrp2* $^{lox/lox}$/*Meox2* $^{tm1(cre)Sor}$, F) *lrp2* gene knockout.

(MGE), was found to be significantly reduced in *lrp2* $^{-/-}$ embryos (Figure 4 D, I). Because Shh stimulates proliferation of cell populations in these areas of the ventral forebrain, alterations in the expression of this morphogen as a possible reason for the defects in LRP2-deficient embryos were tested. As seen by *in situ* hybridization (ISH), *shh* is expressed in the notochord, floorplate and ventral prosencephalon at E9.5 (Figure 7 A, B). No differences in this pattern were seen when comparing wildtype and knockout embryos (Figure 7 A, B). However, the situation changed at E10.5. While expression of *shh* in most embryonic tissues, including notochord, floorplate, limb buds and ventral diencephalon, was unaffected in *lrp2* $^{-/-}$ embryos, specific loss of the *shh* signal in the ventral region of the telencephalon anterior to the optic recess was observed (Figure 7 D, arrowhead). By close inspection of frontal head aspects, the *shh* signal lacking in *lrp2* knockout embryos (Figure 7 E, arrowheads) localized to a region of the ventral neural tube in wildtypes that was identical to the area of reduced cell proliferation (Figure 4 D, I). In other regions of the forebrain such as the basal plate of the diencephalon (bpd) and the zona limitans intrathalamica (zli), *shh* expression was identical in wildtypes and knockouts (Figure 7 E, F). This finding was substantiated on coronal brain sections indicating locally restricted loss of *shh* expression in the AEP (Figure 7 H) but not in other

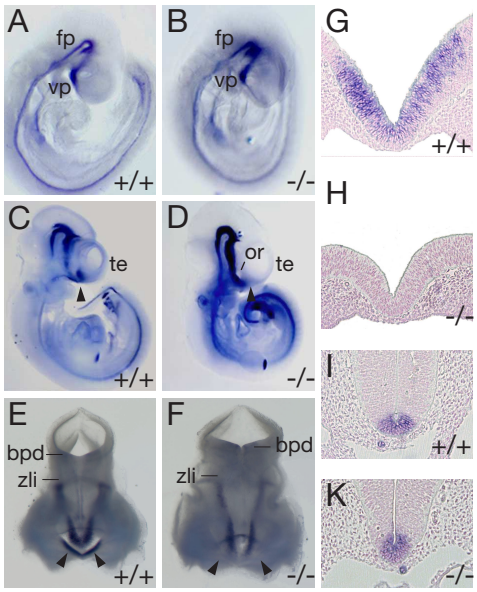

Figure 7: *Shh* expression in wildtype and *lrp2* $^{-/-}$ embryos. (A, B) Whole-mount ISH in E9.5 wildtype (A) and *lrp2* $^{-/-}$ embryos (B), demonstrating an identical expression pattern for *shh* in floorplate and ventral prosencephalon. (C, D) Whole-mount ISH for *shh* in E10.5 embryos, indicating expression in the ventral telencephalon of the wildtype (C, arrowhead) but not in the ventral telencephalic region anterior to the optic recess of *lrp2* $^{-/-}$ embryos (D, arrowhead). (E, F) Frontal head aspects of wildtype (E) and *lrp2* $^{-/-}$ E10.5 embryos (F), depicting *shh* expression in the AEP (arrowheads) of wildtype but not *lrp2* $^{-/-}$ animals. Expression of *shh* in other areas of the forebrain, such as in the basal plate of the diencephalon (bpd) or the zona limitans intrathalamica, is identical in both. (G-K) ISH for *shh* on coronal sections of the rostral (G, H) and the caudal (I, K) neural tube. *Shh* is expressed in the AEP of the rostroventral neural tube of wildtype (G) but not *lrp2* $^{-/-}$ E10.5 embryos (H). Expression in caudal regions of the neural tube is normal in *lrp2* $^{-/-}$ tissues (K). Abbreviations: bpd, basal plate of the diencephalon; fp, floorplate; or, optic recess; te, telencephalon; vp, ventral prosencephalon; zli, zona limitans intrathalamica.

shh expression domains in the ventral neural tube of knockout embryos (Figure 7 K).

The specific loss of *shh*-expression was also observed in mice with an epiblast specific receptor gene defect (Figure 8).

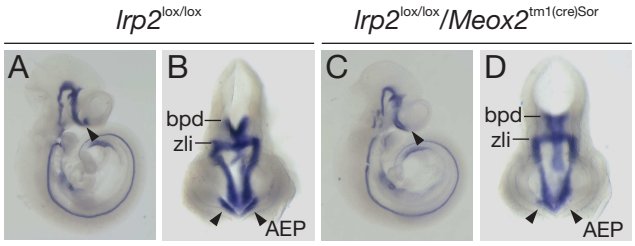

Figure 8: *Shh* expression in *lrp2* $^{lox/lox}$ and *lrp2* $^{lox/lox}$/*Meox2* $^{tm1(cre)Sor}$ E10.5 embryos. Lateral (A, C) and frontal (B, D) head aspects of whole-mount *in-situ* hybridization for *shh* in E10.5 embryos, indicating expression in the AEP of *lrp2* $^{lox/lox}$ (A, B; arrowheads) but not *lrp2* $^{lox/lox}$/*Meox2* $^{tm1(cre)Sor}$ embryos (C, D; arrowheads). Abbreviations: bpd, basal plate of the diencephalon; zli, zona limitans intrathalamica.

4.3 Loss of ventral cell fates in the telencephalon of lrp2-deficient embryos

Shh activity is essential to induce proliferation and differentiation of specific cell populations in the progenitor zone of the ventral neural tube (Marin and Rubenstein, 2001; Nery et al., 2001; Fuccillo et al., 2004). Shh signaling is particularly required for the development of oligodendrocyte precursors that originate from the AEP and migrate tangentially into adjacent areas of the forebrain to develop into myelin-forming glia (Marin and Rubenstein, 2001). As seen by ISH for the mRNA encoding *oligodendrocyte transcription factor 2* (*olig2*), an early marker of the oligodendroglial lineage, expression of *olig2* in E10.5 wildtype embryos (Figure 9 A, arrowhead; C) paralleled the pattern for *shh* expression in the AEP. By contrast, little *olig2* signal was observed in this area of *lrp2* $^{-/-}$ embryos, while expression in the thalamus region of the diencephalon was normal (Figure 9 B, arrowhead; D). The consequence of Shh deficiency on the generation of neuronal precursor populations that arise in the AEP and MGE was analyzed by applying ISH for marker genes highly expressed in these cell types at E10.5 (Sussel et al., 1999; Marin et al., 2000; Fuccillo et al., 2004). The Shh-dependent homeobox gene *thyroid transcription factor 1* (*nkx2.1*) is essential for the production of basal forebrain cholinergic neurons and cortical interneurons (Sussel et al., 1999).
As shown in Figure 9, no expression of *nkx2.1* was detected in the ventral telencephalon of *lrp2*-deficient animals, while expression in other forebrain regions, such as the thalamus of the diencephalon, was normal. *Distal-less homeobox 2* (*Dlx2*), another Shh-dependent homeobox gene, specifies cells that originate in

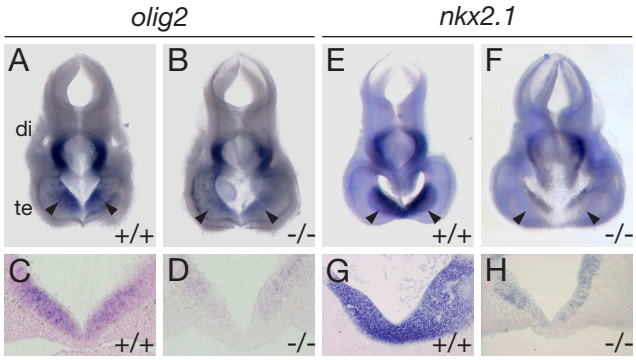

Figure 9: Expression of marker genes of early forebrain development in E10.5 embryos. *In-situ* hybridization (ISH) of frontal head aspects (A, B, E, F) and coronal forebrain sections (C, D, G, H) demonstrate reduced signals for *olig2* and *nkx2.1* in the AEP (B, F, arrowheads) but not in the diencephalon of *lrp2* $^{-/-}$ embryos. Abbreviations: di, diencephalon; te, telencephalon.

the ventral telencephalon and migrate tangentially to populate the cerebral cortex, olfactory bulb and hippocampus, where they differentiate into interneurons (Corbin et al., 2001). Expression of *dlx2* was also absent in the ventral telencephalon and significantly decreased in the thalamus of E10.5 *lrp2* $^{-/-}$ embryos (Figure 10 A, B). Specific loss of ventral neuronal cell populations was confirmed by the lack of neuron-specific class III ß-tubulin (TuJ1) signals in the ventral, but not in the dorsal telencephalon of *lrp2*-deficient animals (Figure 10 E, F). Given the loss of ventral Shh-dependent pathways in *lrp2* $^{-/-}$ embryos, the expression of dorsal markers of the developing brain may be altered in receptor-deficient mice as well.
Wnt1, a marker of early forebrain development, is expressed in the dorsal midline of the di- and mesencephalon, and in the isthmus of wildtypes at E10.5 (Figure 10 L). No differences in expression pattern of *wnt1* were seen in knockouts (Figure 10 M) compared to wildtypes, suggesting normal dorsal patterning of the diencephalon. The situation was different when evaluating dorsal markers also found in the telencephalon. *Pax6* is normally expressed in the dorsal part and ventral thalamus of the diencephalon, in the eyes and in the dorsal telencephalon (Figure 10 C). By contrast, in E10.5 *lrp2* $^{-/-}$ embryos *pax6* expression significantly extended from dorsal areas into ventral areas of the telencephalic neural tube, while expression in the optic vesicles was mostly lost (Figure 10 D, ov). So far, these results show an obvious effect of *lrp2*-deficiency on the specification of ventral cell fate in the rostral ventral forebrain, probably due to locally restricted loss of *shh* in the AEP.

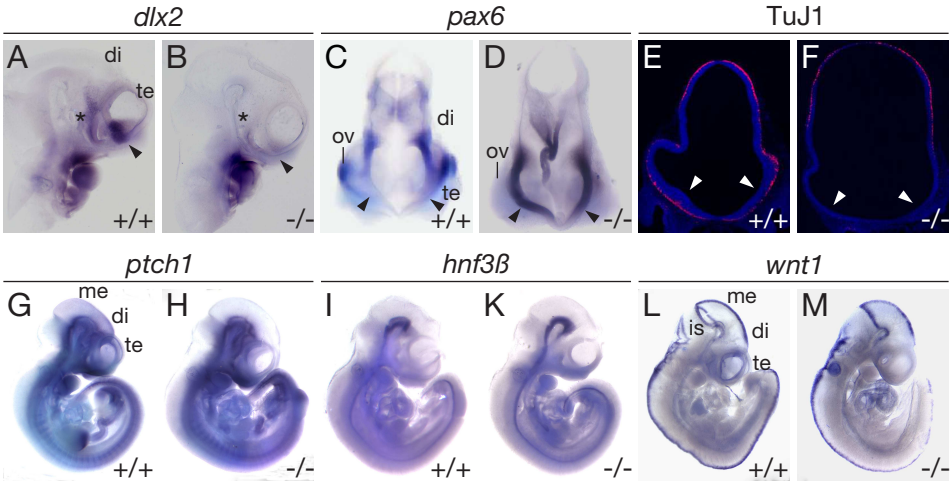

Figure 10: Expression of marker genes of early forebrain development in E10.5 embryos. ISH of lateral (A, B, G-M) and frontal (C, D) head aspects and coronal forebrain sections (E, F). (A, B) Expression of *dlx2* is lost in the ventral telencephalon (arrowheads) and significantly reduced in the ventral thalamus region of the diencephalon (asterisks) of *lrp2* $^{-/-}$ embryos as shown by whole-mount ISH. (C, D) Expression of *pax6* extends from the dorsal into the ventral neural tube of receptor-deficient embryos (D, arrowheads). Also, most knockouts lack the *pax6* signal in the optic vesicle (D). (E, F) Immunohistology of coronal E10.5 forebrain sections indicate lack of TuJ1 expression in the ventral (F, arrowheads), but not in the dorsal telencephalic region of *lrp2* $^{-/-}$ embryos compared with control embryos. (G-M) No differences can be seen in the expression patterns of *ptch1* (G, H; ventral neural tube, including tel-, di- and mesencephalon), *hnf3ß* (L, K; ventral neural tube, including di- and mesencephalon), or *wnt1* (L, M; roof of di- and mesencephalon, isthmus).Abbreviations: di, diencephalon; is, isthmus; me, mesencephalon; ov, optic vesicle; te, telencephalon.

Consistent with normal expression of *shh* in areas of the forebrain other than the AEP, the expression patterns of the receptor *ptch1* (Figure 10 G, H) or the global Shh target gene *hnf3ß* (Figure 10 I, K) were unchanged in *lrp2* $^{-/-}$ mice.

4.4 Enhanced Bmp4 signaling and aberrant fgf8 expression in the dorsal midline of lrp2-deficient mice

Fibroblast growth factor (Fgf) 8 and bone morphogenic protein (Bmp) 4 are morphogens that also play key roles in dorsoventral patterning of the rostral head and that act in precise synergy with Shh to maintain normal prosencephalic develop-

ment (Schneider et al., 2001; Ohkubo et al., 2002). Intriguingly, expression of both morphogens was also significantly altered in mice lacking LRP2.
At E10.5, the expression of *fgf8* was reduced in the rostral ventral telencephalon but extended from the commissural plate along the midline into more dorsal and caudal regions of the forebrain (Figure 11 B, arrowhead). *Bmp4*, demarcating dorsal midline structures, was also aberrantly expressed at E10.5. In wildtypes, *bmp4* expression was restricted to the dorsomedial part of the telencephalon and the dorsal midline of the most anterior diencephalon (Figure 11 C). In mutants, expression in the dorsomedial neuroepithelium of the tel- and diencephalon was significantly increased and extended along the midline into more caudal regions of the roof (Figure 11 D, arrowhead).
Contrary to the findings obtained with Shh (Figure 7 A, B), alterations in Bmp4 and Fgf8 pathways were already evident at E9.5 in *lrp2* $^{-/-}$ embryos. Thus, the expression domain of *fgf8* was reduced in the ventral but increased along the dorsal telencephalic midline (Figure 11 K), while expression of *bmp4* was significantly enhanced in the rostral dorsal telencephalon(Figure 11 M, arrowheads). To evaluate the consequences of this increase in *bmp4* mRNA the intracellular effectors of Bmp4 signaling and the expression levels of downstream target genes were analyzed. Mothers against decapentaplegic homolog (Smad) proteins are the intracellular effectors of Bmp4 signaling. Binding of Bmp4 to its endogenous receptors leads to phosphorylation of the Smad proteins 1, 5 and 8. Subsequently, the phosphorylated Smad (P-Smad) proteins associate with transcription factors and activate downstream target genes.
The increase in *bmp4* mRNA indeed resulted in an increase in P-Smad proteins and in an activation of downstream target genes (Figure 12). As seen by immunofluorescence staining for P-Smad1 at E10.5, overexpression of *bmp4* resulted in enhanced and ventrally expanded Bmp4 signaling in the prosencephalon but not in other areas of the neural tube such as the spinal cord (Figure 12 B, G). At E9.5, enhanced Bmp4 signaling in the forebrain was accompanied by a rise and ventral expansion of P-Smad proteins along the rostral neuroepithelial midline (Figure 12 D, I) and by an aberrantly strong induction of the Bmp4 downstream target gene *mesenchyme homeobox* (*Msx*) *1* transcript *msx1* in this region (Figure 12 K, arrowhead).

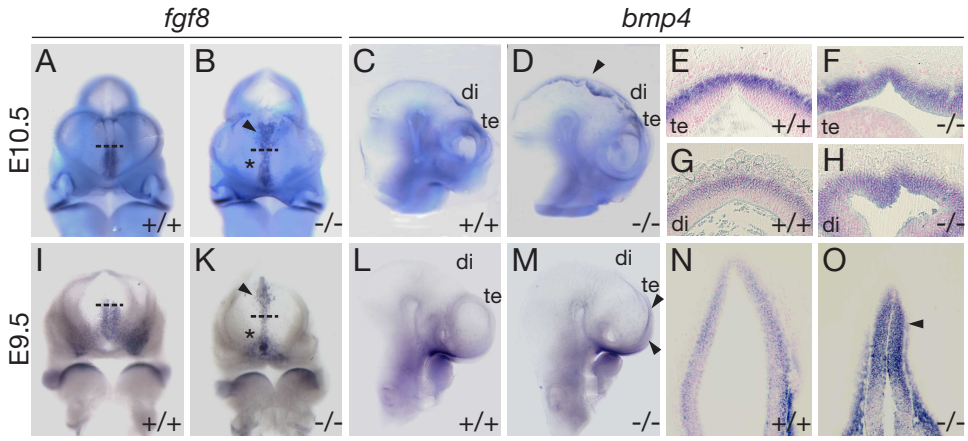

Figure 11: Analysis of Fgf8 and Bmp4 pathways in E9.5 and E10.5 embryos. (A, B) Anteroventral head aspects of E10.5 embryos, demonstrating a reduction of *fgf8* expression in the ventral telencephalon (asterisk) and an extension from the commissural plate (dotted line) into more dorsal regions of the midline (arrowhead) in LRP2-deficient animals. (C, D) lateral head aspects show that *bmp4* expression in wildtypes is restricted to the dorsomedial part of the telencephalon and the dorsal midline of the most anterior diencephalon, whereas in *lrp2* mutants the *bmp4* expression domain extends along the midline into more caudal regions of the roof (D, arrowhead). (E-H) Coronal sections highlight increased *bmp4* signals in the telencephalon and the anterior diencephalon of knockout compared with control embryos. (I, K) At E9.5, the *fgf8* expression domain in *lrp2* $^{-/-}$ animals is reduced in the ventral (K, asterisk), but extended into the dorsal region of the telencephalon (K, arrowhead). (L-O) At E9.5, expression of *bmp4* is increased in the rostral and dorsal telencephalon (M, O, arrowheads) of *lrp2* $^{-/-}$ embryos as shown by whole-mount ISH (L, M) or coronal dorsal forebrain sections thereof (N, O). Abbreviations: di, diencephalon; te, telencephalon.

4.5 LRP2 acts as an endocytic receptor for Bmp4

Based on the distinct alterations in Shh and Bmp4-dependent pathways in the neural tube of *lrp2*-deficient embryos, a direct involvement of this receptor in the activity of either morphogen seems plausible. The ability of LRP2 to bind Shh has been reported before (McCarthy et al., 2002). To also establish a potential role for LRP2 in Bmp4 signaling, the interaction of the receptor with Bmp4 was tested *in vitro*.

LRP2 was immobilized on a sensor chip surface and binding of ligands was detected taking advantage of a phenomenon called surface plasmon resonance (SPR). SPR

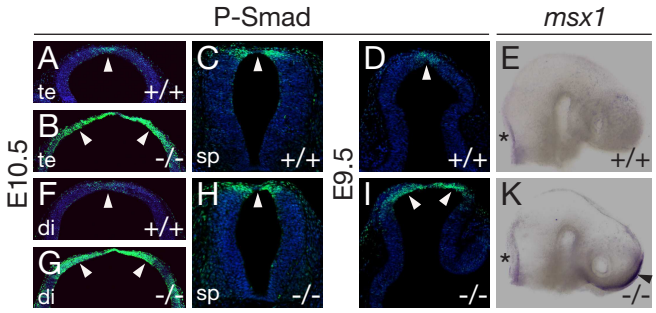

Figure 12: Increased Bmp4 signaling phosphorylates Smad proteins and induces downstream targets. (A-D, F-I) Immunodetection of P-Smad proteins, indicating a signal in E10.5 wildtypes that is restricted to the dorsal midline of the tel- and diencephalon (A, F, arrowheads) but that is significantly enhanced and ventrally expanded (B, G, arrowheads) in *lrp2* $^{-/-}$ littermates. P-Smad signals in the spinal cord are identical in both genotypes (C, H). At E9.5, increases in *bmp4* message result in enhanced phosphorylation of Smad proteins (I, arrowheads) and induced expression of the Bmp4 target gene *Msx1* in the rostral dorsal telencephalon (K, arrowhead). *Msx1* expression in the hindbrain region is unchanged (E; K, asterisks). Abbreviations: di, diencephalon; sp, spinal cord; te, telencephalon.

detects changes in mass on the sensor surface and therefore binding of ligands to the receptor. In this assay, Bmp4 strongly bound to LRP2, while the related factors Bmp5 or Wnt1 did not (Figure 13 A), suggesting a possible function for LRP2 as Bmp4 receptor in the early forebrain. Exposure of LRP2-expressing (BN16) cells to radiolabeled Bmp4 resulted in endocytic uptake and lysosomal degradation of the protein (Figure 13 B).
The cellular catabolism of Bmp4 was mediated by LRP2 because uptake and degradation of ^{125}I-Bmp4 was blocked completely by the LRP2 antagonist receptor-associated protein (RAP) (Christensen and Birn, 2002; Hilpert et al., 1999) and by chloroquine, an inhibitor of lysosomal degradation (Figure 13 B).
Taken together, these findings indicate a possible function of LRP2 as a Bmp4 clearance receptor in the neuroepithelium and increased Bmp signaling in the forebrain as a consequence of the *lrp2* gene defect. LRP2 is involved in the patterning of the rostral neural tube as lack of LRP2 leads to a loss of *shh* expression in the AEP, a region giving rise to oligodendrocytes and interneurons. As seen by ISH for *olig2* and *nkx2.1* (Figure 9), these cell fates are not established in *lrp2* $^{-/-}$ embryos. At the same time, increased *bmp4* expression is observed in the dorsal rostral neural tube (Figure 11 C, D, L, M).

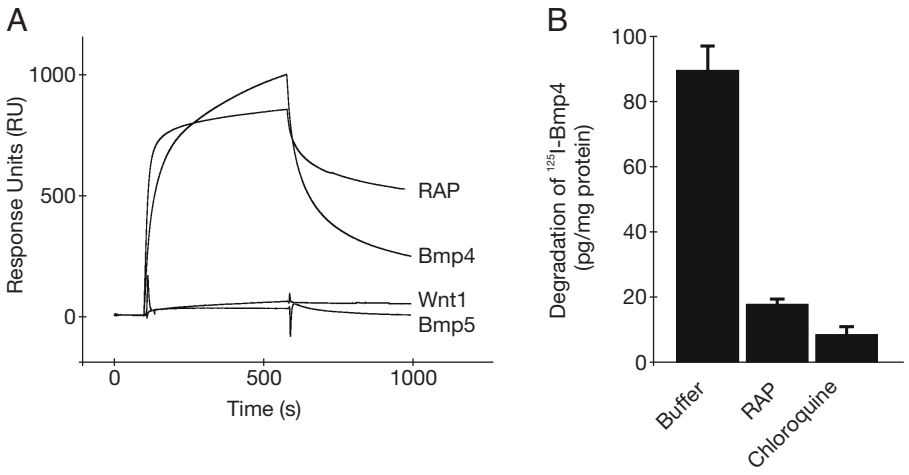

Figure 13: LRP2 mediates binding and cellular catabolism of Bmp4. (A) Surface plasmon resonance (SPR) analysis of binding of 0.5 μmol/l Bmp4, but not of 0.5 μmol/l Bmp5 or Wnt1-conditioned medium to purified LRP2 immobilized on the sensor chip surface. As a positive control, binding of 1 μmol/l receptor-associated protein (RAP) to LRP2 was tested. (B) LRP2-expressing BN16 cells mediate uptake and lysosomal degradation of ^{125}I-Bmp4. Degradation of Bmp4 can be blocked by chloroquine (200 μmol/l) or the receptor-antagonist RAP (100 μg/ml).

Altering the expression patterns of key morphogens in dorsoventral patterning possibly leading to a rescue of the observed phenotype in *lrp2* $^{-/-}$ embryos may help to further elucidate the underlying mechanisms of the defect. One approach could be to decrease Bmp4 signaling in the dorsal rostral neural tube by either reducing *bmp4* expression or by inducing mechanisms that negatively regulate Bmp4 action. For example, overexpression of soluble Bmp4 antagonists or dominant negative pseudo-receptors (Balemans and Van Hul, 2002; Onichtchouk et al., 1999) was described as a method to effectively reduce Bmp4 signaling. Another approach could be to increase Shh signaling in the ventral neural tube either by directly overexpressing *shh* or by overexpressing a constitutively active form of its endogenous receptor *smo*.

5 Results II: Zebrafish

5.1 An alternative animal model: the zebrafish

Realizing the above envisioned experiments in the mouse would inevitably involve generating new transgenic mouse lines that lack or overexpress genes that are involved in dorsoventral patterning of the rostral neural tube. Time-consuming breeding would then be necessary to generate animals that lack *lrp2* and specific genes for dorsoventral patterning. In recent years, animal systems became available where knocking out, knocking down, knocking in or overexpressing specific genes can be accomplished comparably easily. The zebrafish animal model is one of them.
The zebrafish (*Brachydanio rerio*) is a tropical fish that belongs to the minnow family (Cyprinidae). It is native to Eastern India, Pakistan, Bangladesh and Nepal but it has also been introduced and established in Japan and the United States. The fish is omnivorous and feds on various small aquatic insects, crustaceans, worms and plankton. It grows to about 6 cm in length and lives for around 5 years. The fish is named for its five uniformly pigmented, horizontal blue stripes on the side of the body and is considered to be one of the easiest aquarium fish to breed. Under optimal conditions female fish produce around 100 eggs in a single spawning.
Embryonic development is rapid, passing from the egg to the larvae stage in less than three days. A major advantage of this animal system is that the eggs can be easily manipulated in a number of ways, e.g. proteins can be overexpressed ubiquitously in the embryo by injecting mRNA in the yolk of the egg at the one-cell stage. Because the fate map of the dividing egg is very well established, overexpression of proteins can also be directed to specific tissues or areas in the embryo by injecting mRNA into a single progenitor cell.
By the same means it is possible to specifically knock-down protein expression in the whole embryo or in specific tissues of the embryo. This is achieved by injecting synthetic antisense oligonucleotides commonly referred to as "Morpholinos" that target the mRNA of interest. Animals that develop from eggs injected with Morpholinos are referred to as "morphants".
The difference between Morpholinos and the commonly used antisense RNA is the chemical structure of the backbone. Morpholinos have standard nucleic acid bases but the bases are bound to morpholine rings instead of ribose rings as in RNA. The nucleotides of a Morpholino oligonucleotide are linked through phosphorodiamidate

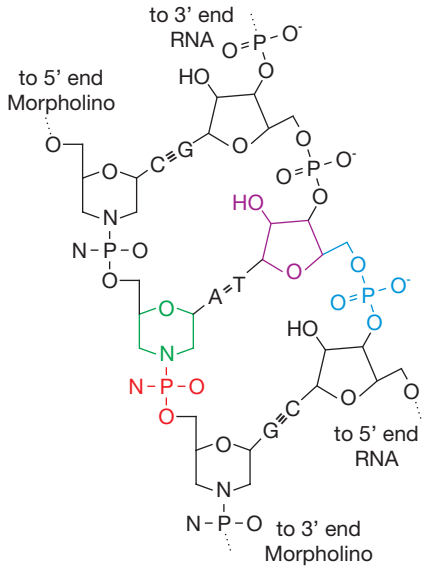

Figure 14: Chemical differences between Morpholino and RNA oligonucleotides. Shown is a trimer segment of a Morpholino-RNA heteroduplex. Morpholinos have standard nucleic acid bases, the bases are bound to morpholine rings (green) instead of deoxyribose rings (purple) as in RNA and linked through phosphorodiamidate groups (red) instead of phosphate groups (blue).

groups instead of phosphate groups as in RNA (Figure 14). As a consequence of this chemical modification, Morpholino oligonucleotides cannot be degraded by exogenous RNA cleaving enzymes (RNases) or by the metabolism of the cell in which it is injected. Thus, Morpholinos exert their function for a comparably long time, usually they remain sufficiently active until day 5 of embryonic development. Protein expression can be blocked by injecting Morpholinos targeting the initiation site of translation or by injecting Morpholinos that target splice donor- or acceptor-sites in the pre-mRNA. As a consequence of the latter, the pre-mRNA cannot be processed correctly producing an mRNA that lacks the intronic sequences associated with the targeted splicing site. If the intronic sequence is spliced out in frame, the synthesized protein is smaller in size because the amino acids encoded by the removed intronic sequence are missing. If the removal of the intronic sequence leads to a frameshift, the result can either be a protein with a different amino acid sequence after the removed intron or a premature termination of translation by a newly formed stop codon. In general, targeting the initiation site of translation is the method of choice for abolishing protein expression most effectively.

Transplantation experiments are also feasible and are usually done 2 to 5 hours after fertilization at the blastula stage. Wildtype cells can be easily transplanted in a mutated background or vice versa and the behavior of the transferred cells in the altered background can be observed. An additional advantage is the fact that the eggs are completely transparent until the onset of pigmentation after two days of development, allowing to observe the outcome of the above mentioned manipulations directly.
The zebrafish has become a popular model organism for studies of vertebrate development and gene function because of the afore described properties. For genetic research groups, the zebrafish is an excellent test subject and is used in many labs to replace or to supplement higher vertebrate models such as rats and mice. Provided that the *lrp2* ortholog exists in the zebrafish, this model might prove useful in further dissecting the function of *lrp2* in dorsoventral patterning of the neural tube.

5.2 Identification of the LRP2 ortholog in the zebrafish

The intracellular, carboxy-terminal part of the amino acid sequence encoding LRP2 of the rat (gene bank accession ID 68436945) was used to search the Sanger Zv4.0 genomic sequence zebrafish database (http://www.ensembl.org/Danio_rerio/blastview) because this part of the receptor is highly conserved among species. The search identified a short fragment of a putative LRP2 ortholog in the zebrafish (zf-LRP2). The retrieved amino acid sequence was analyzed for common functional and structural motifs with the protein motif prediction tool "Simple Modular Architecture Research Tool" (SMART; http://smart.embl-heidelberg.de).
According to this software, the sequence contained a short extracellular stretch of 45 amino acids followed by a hydrophobic transmembrane domain consisting of 20 amino acids (Figure 15, underlined sequence) and the intracellular part of the protein. Due to the incomplete annotation of the zebrafish genomic sequence database, most of the sequence encoding the extracellular domain of the zf-LRP2 could not be retrieved. The amino acid sequence of proteins that serve important functions in the cellular metabolism or the development of the organism are usually highly conserved among species. To determine the extent of conservation of zf-LRP2 compared to human LRP2, the amino acid sequences of the corresponding proteins were aligned using the software "ClustalW" (ver 1.83; http://www.ebi.ac.uk/clustalw).

```
Human     CRCMHGGNCYFDETDLPKCKCPSGYTGKYCEMAFSKGISPGTTAVAVLL
Zebrafish CRCMNGGTCFTDEGGLPKCKCPYGYSGSYCEMGKSRGAPAG-TAVTVLL
          ****:**.*: ** .******* **:*.****. *:* ..* ***:***

Human     TILLIVVIGALAIAGFFHYRRTGSLLPALPKLP-SLSSLVKPSENGNGV
Zebrafish AVVIILVTGALVVGVFLNYRRTGSLIPSMPNYPGSLSSLVKSGDTGNGV
          ::::*:* ***.:. *::*******:*::*: * *******.::.****

Human     TFRSGADLNMDIGVSGFGPETAIDRSMAMSEDFVMEMGKQPIIFENPMY
Zebrafish SFHSGDNVTMDLEPQTLG-VSFIDRAMQLVNLHHFTSGRNGMLFYYLLF
          :*:** ::.**:  . :*  : ***:* : : . :  *:: ::*   ::

Human     SARDSAVKVVQP--IQVTVSENVDNKNYGSPINPSEIVPETNPTSPAAD
Zebrafish YYLFLFYLHLNYNYILCLFNQIYIIQESKWSFFKRKLKPSTTFENPTYS
                    ::   *   ..:    ::   .:   :: *.*.  .*: .

Human     GTQVTKWNLFKRKSKQTTNFENPIYAQMENEQKESVAATPPPSPSLPAK
Zebrafish --EESKWSFFKRKLKPSTTFENPTYSEMQDEQTPGAADSSSTAEPSPFV
            : :**.:**** * :*.**** *::*::**. ..* :...: . *

Human     PKPPSRRDPTPTYSATEDTFKDTANLVKEDSEV
Zebrafish PPKPPKREKLSTFTPTEDTFRDTANLVKEDSDI
          *  *.:*:  .*::.*****:**********::
```

Figure 15: Amino acid sequence alignment of human LRP2 with the zebrafish ortholog. Sequence comparison of both orthologs shows 49.6% identity and 65.7% similarity (identity indicated by asterisks, high similarity indicated by colons and low similarity indicated by dots). The transmembrane segment of both sequences is underlined, NpxY-motifs are highlighted red.

The retrieved partial sequence of zf-LRP2 is indeed highly conserved across species, displaying 49.5% identity and 65.2% similarity. Motifs that are important for binding intracellular adaptor proteins and for endocytosis have been conserved, e.g. two NPxY motifs (Figure 15, NPxY motifs highlighted in red) are present in the zebrafish sequence.
The zebrafish belongs to the teleosts that all harbour duplicated genomes (Amores et al., 1998). This duplication event took place early in the evolution of the teleosts, probably more than 300 million years ago (Taylor et al., 2001). At present, many genes of the zebrafish have functional duplicates, whereas duplicates of other genes have lost their function or adopted new functions. The "Basic Local Alignment Search Tool" (BLAST) and the "Sequence Search and Alignment by Hashing Algorithm" (SSAHA) were used to retrieve information about the existence of ad-

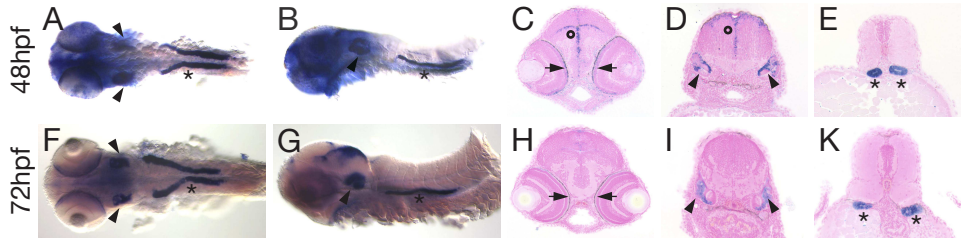

Figure 16: Expression pattern of zf-*lrp2* at 48hpf (A-E) and 72hpf (F-K) analyzed in wildtypes by ISH. The yolk and tail of the embryos were removed in A, B, F and G. At 48hpf (A, dorsal aspect; B, lateral aspect; C-E, transversal sections) zf-*lrp2* is weakly but uniformly expressed in the forebrain and midbrain of the embryo (C, D, open circle). Stronger sites of expression are the otic vesicles (A, B, D, arrowheads), the retina (C, arrows) and the pronephric tubules (A, B, E, asterisk). At 72hpf (F, dorsal aspect; G, lateral aspect; H-K, transversal sections) expression levels of zf-*lrp2* in the forebrain and midbrain is decreased compared to 48hpf. Expression in the otic vesicles (F, G, I, arrowheads) and in the retina (H, arrows) as well as in the pronephric tubules (F, G, K, asterisk) remains strong.

ditional copies of the zf-LRP2.
Both approaches failed to identify additional copies of the zf-*lrp2* gene in the zebrafish genome. The partly identified zf-*lrp2* is therefore the only copy of this receptor present within the zebrafish genome, based on the Sangers Zv4.0 database which covers about 60% of the genomic sequence.

5.3 The expression pattern of zf-lrp2 and mouse-lrp2 is conserved

ISH was used to visualize *lrp2* expression in zebrafish embryos at various stages of development. At 48 hours post fertilization (hpf) *lrp2* is strongly expressed in the pronephric tubules (Figure 16 A, B, E, asterisk) and in the structures giving rise to the ears (otic vesicles, Figure 16 A, B, D, arrowheads). Weak expression of zf-*lrp2* mRNA can be observed in the retina (Figure 16 C, arrows). Expression is diffuse but strong in the forebrain and midbrain at 48hpf (Figure 16 A, B; C, D, open circle), whereas expression of zf-*lrp2* in the brain is regulated down at 72hpf (Figure 16 F-I), but remains strong in the otic vesicles (Figure 16 F, G, I, arrowheads) and in the pronephric tubules (Figure 16 F, G, K, asterisk).
To examine the expression domains of zf-*lrp2* more thoroughly, earlier timepoints

were analyzed by ISH. In addition, the expression domains of *lrp2* were correlated with the expression domains of *cubilin*, *dab2*, *wt1* and *pax2.1* that are key marker genes for brain and kidney development.
Cubilin is a membrane protein that is non-covalently bound to the cell membrane. It is always found coexpressed with *lrp2* (but not neccessarily vice versa) and acts as a coreceptor expanding the range of ligands that can be endocytosed by LRP2 (Assemat et al., 2005). Dab2 is an intracellular adapter protein that binds to NPxY motifs and is essential for endocytosis. Mice that are conditionally deficient for *dab2* in the renal proximal tubules of the kidney display low molecular weight proteinuria, emphasizing an essential function of the protein in renal reabsorption (Morris et al., 2002). The *Wilms Tumor 1* (*Wt1*) gene plays an important role for kidney development in mammals (Menke and Schedl, 2003). One main site of expression in mammals is in the podocytes of the glomeruli of the kidney (Menke and Schedl, 2003). Pax2.1 is expressed in the midbrain/hindbrain boundary, in motoneurons and in the pronephric tubules. In zebrafish that are deficient for functional *pax2.1* the pronephric tubules do not form (Majumdar et al., 2000). The expression patterns of these genes were analyzed by ISH for 20, 24, 48 and 72hpf. Between 20 and 24hpf, *lrp2* and *dab2* displayed overlapping expression patterns within the anterior third of the pronephric duct (Figure 17 A, B, I, K). Whereas expression of *cubilin* was not detectable at 20hpf, it was largely overlapping with *lrp2* and *dab2* at 24hpf (Figure 17 B, F, K).
By 48hpf, the bilateral nephron primordia integrate to form central pronephric glomeruli that express *wt1* (Figure 17 P) and tubules that express *pax2.1* (Figure 17 T). At this stage, *lrp2*, *dab2*, and *cubilin* are expressed in an expanded proximal portion of the pronephric duct but not in pronephric tubules (Figure 17 C, G, L). Finally, by 72hpf, *lrp2*, *dab2*, and *cubilin* were expressed in a proximal portion of the pronephric duct and a small distal portion of the tubule epithelium (Figure 17 D, arrows; H, M).

5.4 Functional analysis of zf-LRP2 protein

To make sure that zf-LRP2 had not lost its physiological relevance in the zebrafish, the functional conservation of the protein was analyzed in the zebrafish pronephros before analyzing the function of the receptor in brain development.
In adult mammals, LRP2 is mainly expressed in the proximal tubules of the kidney where it is responsible for reabsorbing metabolites from the glomerular filtrate. To further characterize those regions of the pronephric duct involved in renal clearance of metabolites in the zebrafish, tracer molecules of defined molecular weight

were injected into the cardinal vein of 72hpf wildtype embryos as previously described (Drummond et al., 1998). 70 kDa fluorescein-labeled dextran (FD) was used as a fluid phase marker and was taken up into the proximal third of the pronephric duct and the distal tubule within minutes after injection (Figure 18 A). To define whether the region involved in renal clearance of metabolites corresponds to the *lrp2* expression domain (McCarthy et al., 2002), the receptor was co-visualized on whole-mounts with an anti-rat LRP2 antibody. Indeed, renal reuptake of 70kDa-FD occurred in a proximal-to-distal gradient of intensity that was entirely enclosed within the *lrp2* expression domain (Figure 18 A-C). Transverse sections of these embryos showed apical LRP2 localization and confirmed that the 70 kDa-FD molecules were

distributed as punctuate vesicles in the pronephric duct epithelial cells (Figure 18 D-F). To confirm that the tubular uptake is dependent on glomerular filtration, the clearance of 10 kDa rhodamine labeled dextran (RD) was compared to 500 kDa-FD, which should not pass the ultrafiltration barrier (Drummond et al., 1998). Whereas 10 kDa-RD was cleared from the proximal third of the pronephric duct and the distal tubule within minutes after injection (Figure 19 A) and was distributed as punctuate vesicles on transverse sections (Figure 19 B), no uptake of 500 kDa-FD was observed, confirming that glomerular ultrafiltration prevents passage of this large molecular weight tracer into the pronephric duct (Figure 19 D). To visualize the reuptake of a known LRP2 ligand *in vivo*, Cy2-labeled rat receptor-associated protein (Cy2-RAP) was injected into the circulation of 72hpf wildtype embryos. Cy2-RAP was rapidly cleared from the pronephric duct and internalized into apical vesicles of anterior pronephic duct tubular cells in a pattern identical to that observed for 70 kDa-FD (Figure 19 C). Thus, 70 kDa-FD visualizes LRP2 dependent uptake processes and was used as a marker for further tests.

5.5 Generation of lrp2-deficient zebrafish embryos

One method of choice to elucidate a protein's function *in vivo* is to analyze the phenotype of animals that are deficient for the protein of interest. In mice, this is usually achieved by targeted gene disruption, a method where a mutation is introduced in the gene of interest via homologous recombination. This results in a protein with an altered amino acid sequence that has usually lost its function.
In the zebrafish, where the targeted gene disruption technology is not available, expression of a specific protein is suppressed by deploying a Morpholino antisense approach that either efficiently interferes with the splicing of the pre-mRNA or

with the initiation of translation (Heasman et al., 2000; Nasevicius and Ekker, 2000). To achieve the latter, the Morpholino has to be complementary in sequence to the region 5' of the start codon of the targeted mRNA. Because so far no information about this region was available in the zebrafish genome database, an approach was chosen that interfered with the splicing of the zf-*lrp2* pre-mRNA resulting in the removal of the exon coding for the transmembrane segment.
Two independent Morpholinos were designed, one targeting the splice donor site of the exon coding for the transmembrane region (*lrp2*MO1), the other targeting the splice donor site of the next 5' exon (*lrp2*MO2).
This should lead to downstream nonsense mutations resulting in a premature stop of protein translation. The truncated protein should lack the transmembrane segment and should thereby not be incorporated into the plasma membrane but excreted. This approach was used successfully before in the mouse to ablate *lrp2* expression (Willnow et al., 1996a).
The efficiency of both Morpholinos was verified on the nucleotide level by RT-PCR as well as on the protein level by Western Blotting with an antibody specific for zf-LRP2.
As can be seen in Figure 20, both Morpholino oligonucleotides efficiently interfered with the splicing of the zf-*lrp2* pre-mRNA at 48hpf, yielding RT-PCR products of the indicated size. Embryos that developed from eggs injected with either oligonucleotide were deficient for zf-LRP2 protein at 48hpf as seen by Western Blotting of total membrane extracts of these embryos with an antibody specific for zf-LRP2 (Figure 20). Extracts from wildtype embryos displayed a prominent immunoreactive band of approximately 250 kDa that likely represented the major proteolytic breakdown product of the receptor described before (Bachinsky et al., 1993; Orlando and Farquhar, 1993) and that was completely absent from the morphants.
Sequencing of the RT-PCR products indeed confirmed the predicted alterations in sequence. As indicated by the dashed lines (Figure 21 A), the targeted exons were precisely removed from the zf-*lrp2*-mRNA in embryos that were injected with *lrp2*MO1 and *lrp2*MO2 at the one-cell stage.
Translation of the altered mRNA sequences of these embryos with the "Expert Protein Analysis System" (ExPASy) translate tool (http://www.expasy.ch/tools/dna.html) showed that the aberrant splicing led to a reading frame shift for *lrp2*MO1 as well as for *lrp2*MO2.
This resulted in a completely different downstream amino acid sequence, eventually leading to a premature derogation of translation because of newly formed

stop-codons (Figure 21 B; stop-codons highlighted in red). The aberrant amino acid sequences were then analyzed using the SMART motif prediction algorithm to verify that the transmembrane domain was completely gone. Indeed, no transmembrane domain was predicted for both Morpholinos rendering it highly unlikely that the aberrant protein is still able to integrate into the cell membrane.
Phenotypically, the overall embryonic and larval anatomy appeared unchanged throughout the entire observation period (7dpf; Figure 22 A-F) of embryonic development. Moreover, acridine orange vital embryonic staining failed to reveal increased apoptotic cell death in zf-*lrp2* morphants compared to controls at 3.5dpf (Figure 22 F-I). To investigate the relevance of zf-*lrp2* in zebrafish tubular clearance mechanisms, morpholino antisense oligonucleotide mediated knock-down of zf-*lrp2* (Heasman et al., 2000; Nasevicius and Ekker, 2000) was performed. To assess whether knock-down of zf-*lrp2* affected formation of the pronephric duct and nephron, the expression of key differentiation markers was visualized by ISH in wildtype and morphant embryos using the same markers that were used for characterizing the expression domains of zf-LRP2. As can be seen in Figure 23, the expression of the analyzed marker genes in the morphants is comparable to that of the wildtype.

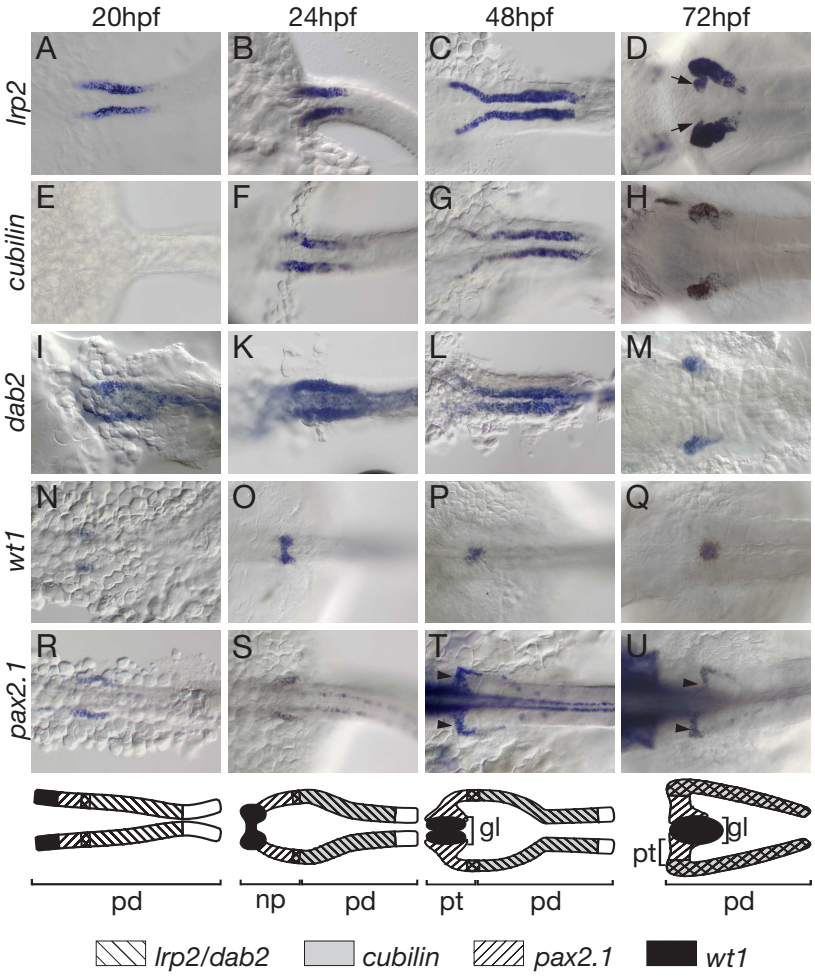

Figure 17: Expression of *lrp2*, *cubilin*, *dab2*, *wt1* and *pax2.1* in the developing pronephros. Dorsal view of wildtype embryos at 20hpf (A, E, I, N, R), 24hpf (B, F, K, O, S), 48hpf (C, G, L, P, T), and 72hpf (D, H, M, Q, U) analyzed for expression of *lrp2* (A-D), *cubilin* (E-H), *dab2* (I-M), *wt1* (N-Q) and *pax2.1* (R-U). Combinatorial gene expression patterns are indicated in the model. Arrows indicate the tubular expression of *lrp2* (D); arrowheads point at the pronephros expression domain of *pax2.1* (T, U). Abbreviations: gl, glomerulus; np, nephric primordium; pd, pronephric duct; pt, pronephric tubule.

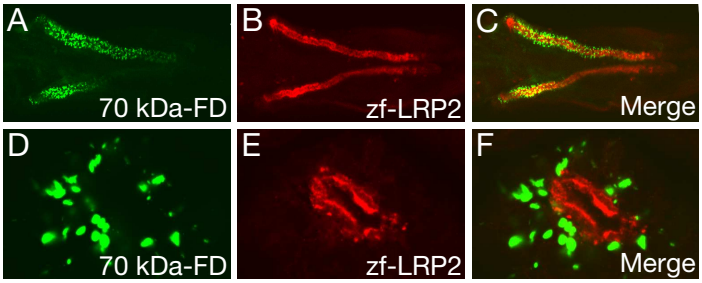

Figure 18: Renal clearance of tracers within the proximal pronephric duct is restricted to the LRP2 expression domain. Wildtype embryos (72hpf) were injected with 70 kDa-FD (green) and renal clearance of tracer into the pronephric duct tubular cells evaluated 1.5 hours later on whole-mounts (A, C) or transversal sections (D, F) by confocal fluorescence microscopy. Immunostaining for LRP2 (B, C; red) demonstrates that renal clearance of 70 kDa-FD occurs within the expression domain of the receptor. (E, F) Transversal sections show apical localization of LRP2.

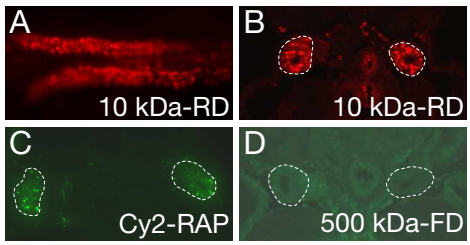

Figure 19: Renal clearance of tracers occurs within the proximal pronephric duct. Wildtype embryos (72 hpf) were injected with 10 kDa-RD (A, B; red), Cy2-RAP (C; green), or 500 kDa-FD (D; green), and renal clearance of tracer into the pronephric duct tubular cells evaluated 1.5 hours later on whole-mounts (A) or transversal sections (B-D) by fluorescence microscopy. 10 kDa-RD is cleared from the proximal third of the pronephric duct (A) and taken up into punctuate vesicles (B). Cy2-RAP is also endocytosed efficiently by cells of the proximal tubule. There is no tubular uptake of the 500 kDa-FD tracer (D). White dotted lines demarcate the position of the pronephric ducts in B-D.

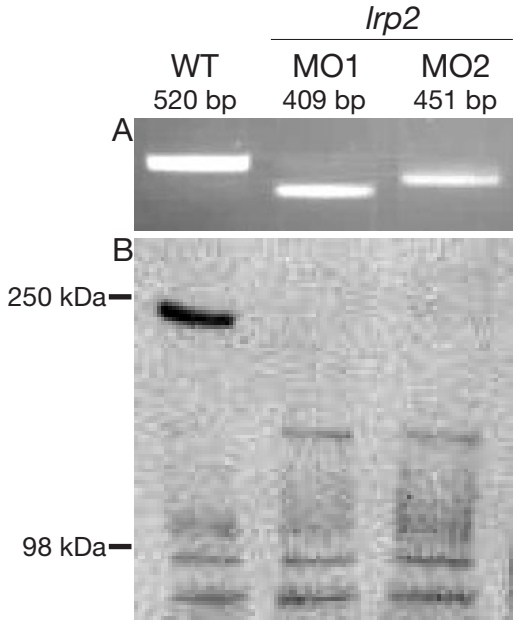

Figure 20: Molecular characterization of the *lrp2* morphant embryos. Wildtype embryos were injected with buffer (WT) or with two different *lrp2* splice variant Morpholinos (*lrp2*MO1; *lrp2*MO2). Embryo extracts were generated at 48hpf and analyzed by RT-PCR (A) or by Western blot analysis of membrane fractions (B). Injection of *lrp2*MO1 and *lrp2*MO2 resulted in aberrant splicing of the*lrp2* transcript as evidenced by truncated RT-PCR products of the cDNA encoding the transmembrane and intracellular portions of the receptor (A) and by the absence of LRP2 immunoreactivity compared to controls (B).

A

```
wt       AGTGCAAGTGTCCGTACGGTTACTCTGGTAGTTACTGCGAAATGGGCAAGT
lrp2MO1  AGTGCAAGTGTCCGTACGGTTACTCTGGTAGTTACTGCGAAATGGGCAAGT
lrp2MO2  AGTGCAAGT----------------------------------------

wt       CTAGAGGAGCTCCCGCTGGCACAGCGGTGACGGTACTGTTAGCAGTGGTGA
lrp2MO1  CTAGAGGAGCTCCCGCTGGCACAG-------------------------
lrp2MO2  ----------------------CGGTGACGGTACTGTTAGCAGTGGTGA

wt       TTATTCTGGTGACTGGAGCTCTGGTTGTGGGAGTTTTCCTCAACTACAGGA
lrp2MO1  -------------------------------------------------
lrp2MO2  TTATTCTGGTGACTGGAGCTCTGGTTGTGGGAGTTTTCCTCAACTACAGGA

wt       GAACTGGATCTCTCATCCCGTCAATGCCTAAACTCCCCAGTCTGAGCAGTC
lrp2MO1  ----------------------------------TCTGAGCAGTC
lrp2MO2  GAACTGGATCTCTCATCCCGTCAATGCCTAAACTCCCCAGTCTGAGCAGTC
```

B

```
wt       LPKCKCPYGYSGSYCEMGKSRGAPAGTAVTVLLAVVIILVTGALVVGVFLN
lrp2MO1  LPKCNGDGTVSSGDYSGDWSSGCGSFPQLQENWSHPVNAStopTTQSEQSG
lrp2Mo2  LPKCKCPYGYSGSYCEMGKSRGAPAGTVStopAVWStopSLEIRGMECPFI
```

Figure 21: Sequence analysis of RT-PCR products of Morpholino injected embryos. RT-PCR products (Figure 20 A) were sequenced, aligned (A) and translated (B). (A) Aligned mRNA sequences, the dashed line indicates the location of the removed sequences caused by aberrant splicing for *lrp2*MO1 and *lrp2*MO2 injected animals. (B) Amino acid sequences obtained by *in vitro* translation of the mRNA sequences with the "Expert Protein Analysis System" (ExPASy) translate tool. The transmembrane domain is underlined in the wildtype sequence. Stop-codons are highlighted in red in *lrp2*MO1 and *lrp2*MO2 injected animals.

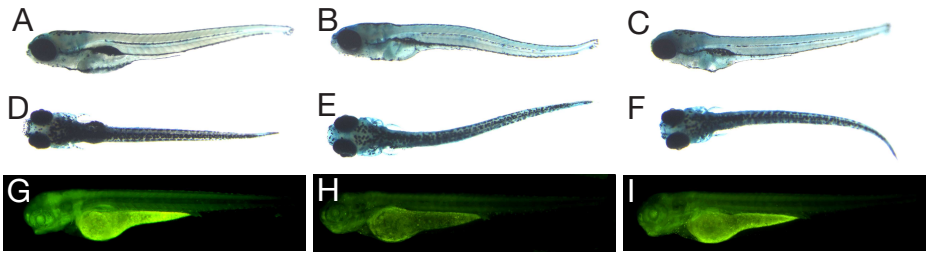

Figure 22: *Lrp2* morphant embryos are phenotypically normal. Brightfield pictures (A-F) of 7dpf, respectively acridine orange vital stainings (G-I) of 3.5dpf wildtype (A, C, G), *lrp2*MO1 (B, E, H) and *lrp2*MO2 (C, F, I) embryos do not show any differences in physiological appearance or the rate of apoptosis.

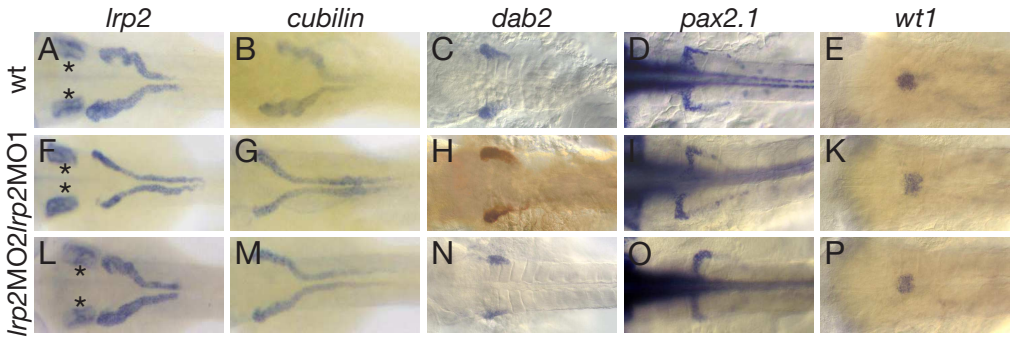

Figure 23: The renal system is developed normally in zf-*lrp2* morphants. 72hpf wildtype (A-E), *lrp2*MO1 (F-K) and *lrp2*MO2 (L-P) morphants. There is no apparent difference in the expression pattern of the marker genes analyzed. *Cubilin* (B, G, M) shows a complete overlap of expression with *lrp2* (A, F,L), whereas *dab2* expression (C, H, N) overlaps with *lrp2* expression only in the pronephric ducts. *Pax2.1* (D, I, O) is strongly expressed in the pronephric ducts and to a slighter extent in the pronephric tubules. The glomerulus is the only site of expression for *wt1* (E, K, P).

5.6 Zebrafish-lrp2 is essential for tubular clearance of metabolites via receptor-mediated endocytosis

Mice that are deficient for functional LRP2 protein display low molecular weight proteinuria in line with an essential function of this receptor in renal physiology. To adress the question whether the zf-*lrp2* ortholog is also necessary for the zebrafish kidney to function properly, morphant embryos for zf-*lrp2* were injected with fluorecently labeled dextranes of different molecular weight and with Cy2-RAP.
Consistent with the anticipated critical role for zf-*lrp2* in pronephric duct clearance, both independent zf-*lrp2* morphants exhibited an almost complete failure of renal uptake of the tracers as shown by fluorescence microscopy on whole-mount embryos (Figure 24).

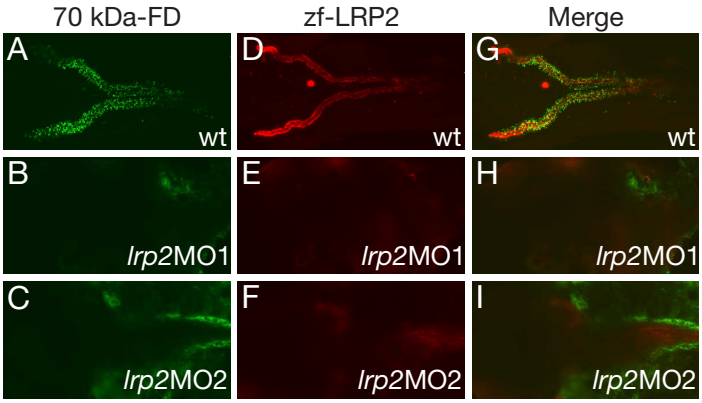

Figure 24: Tubular clearance defects in zf-*lrp2* morphants. Wildtype embryos (A, D, G) and *lrp2* morphants (B, E, H, C, F, I). Renal clearance of the injected tracer dye (70 kDa-FD; green) occurs in wildtype (A, G) but not in *lrp2*MO1 (B, H) respectively *lrp2*MO2 (C, I) morphants. Renal clearance of tracer into the pronephric duct tubular cells was evaluated after fixation and immunostaining against zf-LRP2 (D-F; red) on whole-mounts by confocal fluorescence microscopy.

Staining with an antibody specific for zf-LRP2 on these specimen showed that the embryos were completely devoid of the receptor (Figure 24 E, F). The tubular clearance defects were also analyzed by injecting tracer in 3, 4 and 5dpf wildtype and morphant embryos. Embryos that showed renal uptake were counted and expressed as percentage of the total number of animals injected (Figure 25). In comparison with the wildtype embryos, fewer *lrp2* morphant embryos showed renal uptake of the dye. Even at 5dpf there was a massive decrease in the number

of morphants showing renal uptake, only the percentage of Cy2-RAP injected *lrp2*MO2 morphants showing renal uptake was increased at 4dpf (50%), resp. 5dpf (60%). This may reflect an inefficient injection of the *lrp2*MO2 morpholino at the one-cell stage in these animals resulting in a Morpholino concentration that was too low to efficiently interfere with the splicing of zf-*lrp2* mRNA at 4 and 5dpf.

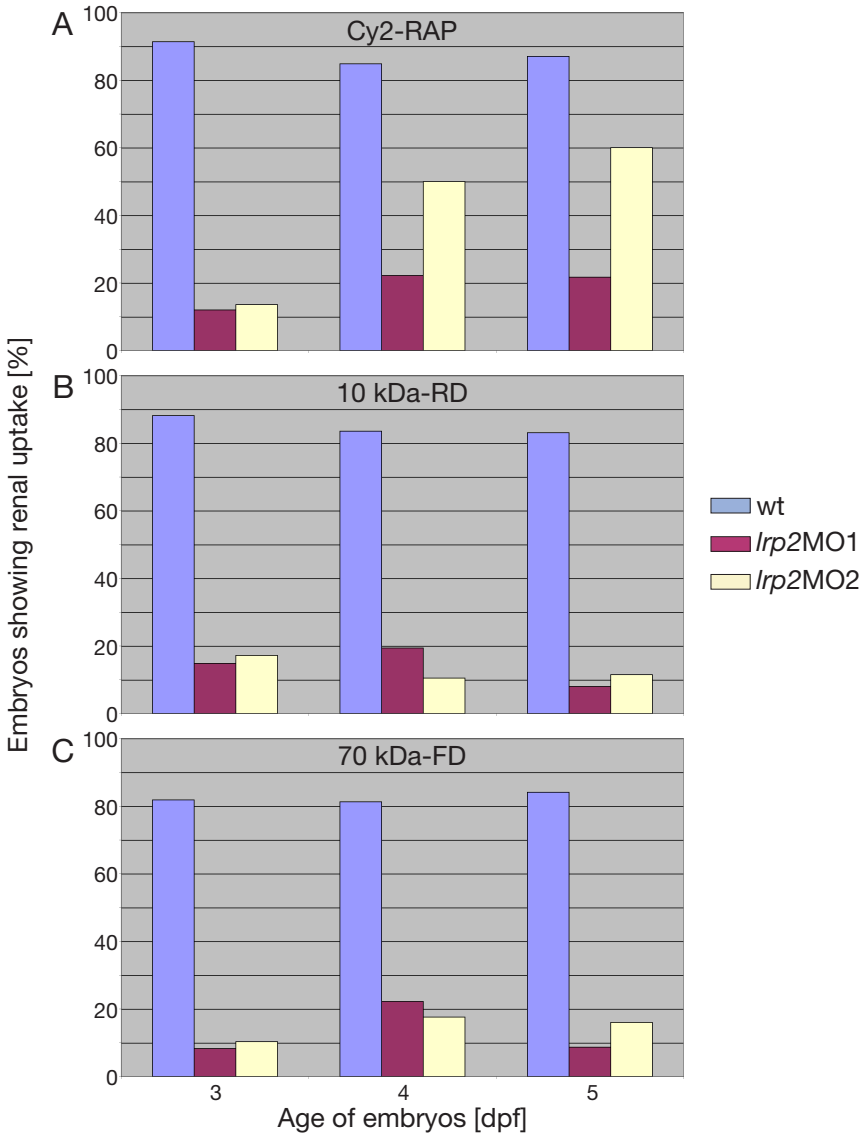

Figure 25: Statistical analysis of tubular clearance defects in zf-*lrp2* morphants. Animals were injected at three different time points (3, 4 and 5dpf) with Cy2-RAP (A), 10 kDa-RD (B), 70 kDa-FD (C). Compared to the wildtype, the percentage of zf-*lrp2* morphants showing renal uptake of the dye is decreased for all time points analyzed. Data are given as percent of all animals injected [70 kDa-FD: wt= 45/55 embryos (81.8%); *lrp2*MO1= 2/24 embryos (8.3%); *lrp2*MO2= 3/29 embryos (10.3%); 10k Da-RD: wt= 46/52 embryos (88.5%); *lrp2*MO1= 4/27 embryos (14.8%); *lrp2*MO2= 5/29 embryos (17.2%); Cy2-RAP: wt= 42/46 embryos (91.3%); *lrp2*MO1= 3/25 embryos (12.0%); *lrp2*MO2= 3/22 embryos (13.6%)

5.7 Tracer accumulates in vesicles that are positive for the early endosomal marker Rab4.

As shown in Figure 18 D and in Figure 19 B and C, the injected tracer dye accumulates in vesicular structures of the renal tubules. These vesicles were postive for Rab4, a protein that is found exclusively in an endosomal subfraction termed early endosomes. Embryos were injected with 70 kDa-FD at 72hpf, sectioned and stained for Rab4 (Figure 26).

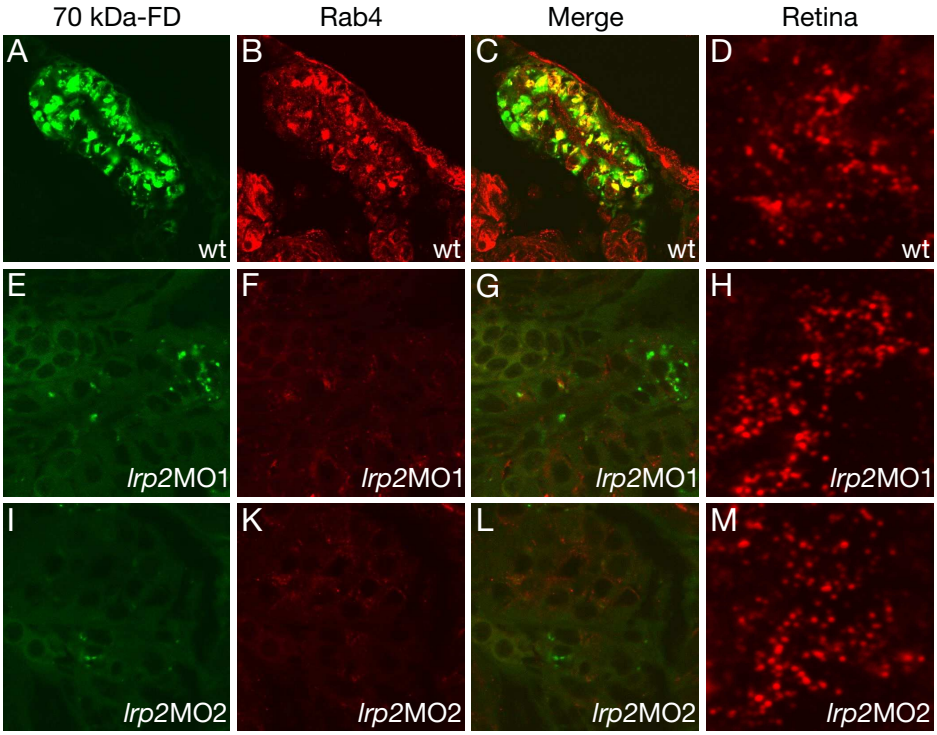

Figure 26: *Lrp2* morphant embryos are negative for Rab4 positive early endosomes. Wildtype (A-D) and morphant (E-M) embryos were injected with 70 kDa-FD (A, E, I; green), fixed and cryosectioned. The sections were then subjected to antibody staining for Rab4 (B, F, K, red). In the wildtype, most endosomes containing the tracer co-stain for Rab4 (C), but surprisingly, no Rab4 positive endosomes were detected in either morphant (F, K). Rab4 positive endosomes were present at comparable levels in the wildtype as well as in the morphants in extrarenal tissue such as the retina (D, H, M).

Morphant embryos did not accumulate tracer dye, but even more surprising was the complete lack of Rab4 positive endosomes (Figure 26 F, K).
However, Rab4-positive endosomes were still present in extra-renal tissues such as the retina (Figure 26 H, M). These findings not only confirm a conserved function for zf-LRP2 as clearance receptor in the zebrafish renal tubular epithelium but also highlight a crucial role for this protein in proper formation of early endosomes in this cell type.

5.8 Mechanisms of receptor mediated endocytosis are functionally conserved between the zebrafish larval pronephros and the adult mammalian kidney.

The results so far clearly indicate that zf-*lrp2* plays a crucial role in receptor mediated endocytosis in the renal tubules of the zebrafish. Injecting fluorescent marker dyes to asses renal function in the zebrafish could be used to easily identify additional components that are essential for receptor mediated endocytosis. To demonstrate that this is indeed possible, Dab2 was choosen to be analyzed in the zebrafish.
Dab2 is an intracellular adaptor protein of LRP2 that is binding to the NPxY motifs of the receptor and is essential for protein reabsorption in the renal proximal tubules of the mouse kidney (Morris et al., 2002). The zebrafish ortholog of *dab2* has been predicted by automated computational analysis of annotated genomic sequence (genomic contig ID: NW 634710; gene bank accession ID: XM 687541). It is expressed in an overlapping pattern with zf-*lrp2* as shown by ISH (Figure 17 I-M), but whether it is also functionally conserved was not known so far.
Using again a Morpholino antisense approach, the expression of the protein was knocked-down and the consequences for renal function analyzed. This time a morpholino was designed to interfere with the initiation of protein translation by binding to the ATG region of the *dab2* mRNA (*dab2*MO). Animals that were injected with the *dab2*MO at the one-cell stage were phenotypically normal and viable for the period of observation (7dpf; Figure 27 A-D). Acridine orange vital embryonic staining failed to reveal increased apoptotic cell death in *dab2* morphants compared to controls at 3.5dpf (Figure 27 E, F).

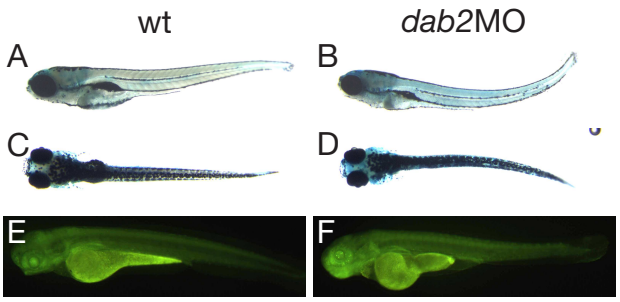

Figure 27: *Dab2* morphants are phenotypically normal. The physiological appearance at 7dpf is indistinguishable between wildtype (A, lateral view; C, dorsal view) and *dab2* morphants (B, lateral view; C, dorsal view). Acridine orange vital staining for appoptotic cells in the wildtype (E, lateral view) also fails to show any difference compared with the *dab2* morphants (F, lateral view).

5.9 Dab2 is essential for tubular clearance of metabolites via receptor-mediated endocytosis

Dab2 morphants were injected with 70 kDa-FD at 3dpf and analyzed for renal reabsorption of the dye. Consistent with the anticipated critical role for Dab2 in pronephric duct clearance, *Dab2* morphants exhibited an almost complete failure of renal uptake of the tracer as shown by fluorescence microscopy on whole-mounts (Figure 28 B, F). Staining with an antibody specific for zf-LRP2 on these specimen showed that knock-down of *dab2* did not interfere with zf-LRP2 expression (Figure 28 D, F) and could be excluded as possible reason for the lack of endocytic activity. The tubular clearance defects were again analyzed by injecting tracer in 3, 4 and 5dpf wildtype and morphant embryos. Embryos that showed renal uptake were counted and expressed as percentage of the total number of animals injected (Figure 29). In comparison with the wildtype embryos, fewer *dab2* morphant embryos showed renal uptake of the dye. The effect was most pronounced at 3dpf, but even at 5dpf there was a massive decrease in the number of morphants showing renal uptake. To verify the specificity of the *dab2* morphant phenotype, an mRNA rescue was performed by co-injecting full-length *dab2* transcripts with silent sequence alterations that rendered the mRNA resistant to the *dab2*MO. Animals injected with the *dab2* morpholino and the modified *dab2* mRNA indeed exhibited a rescue of

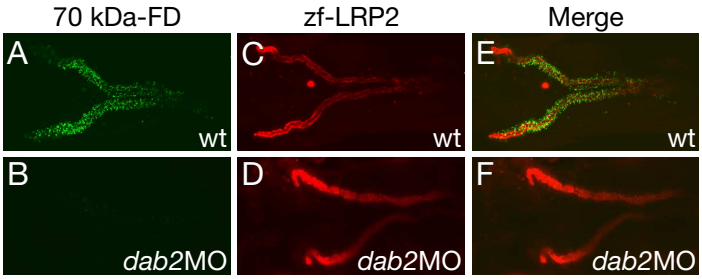

Figure 28: Tubular clearance defects in *dab2* morphants. (A, C, E) wildtype embryos, (B, D, F) *dab2* morphants. Renal clearance of the injected tracer dye (70 kDa-FD; green) occurs in wildtype (A, E) but not in *dab2*MO (B, F) embryos. Renal clearance of tracer into the pronephric duct tubular cells was evaluated after fixation and immunostaining against zf-LRP2 (C-F; red) on whole-mounts by confocal fluorescence microscopy.

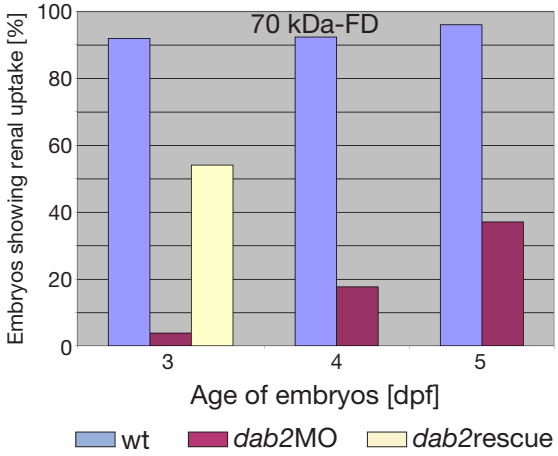

Figure 29: Statistical analysis of tubular clearance defects in *dab2* morphants. *dab2* morphant, and *dab2* rescued embryos were injected with 70 kDa-FD at the indicated time points and the number of embryos exhibiting tubular accumulation of tracers evaluated by fluorescence microscopy. Data are given as percent of all animals injected [70 kDa-FD, 3dpf: wt= 34/37 embryos (91,9%); *dab2*MO= 2/52 embryos (3,8%); *dab2* rescue= 26/48 embryos (54.2%); 4dpf: wt=24/26 embryos (92,3); *dab2*MO= 3/17 embryos (17,6%); 5dpf: wt=24/25 embryos (96,0); *dab2*MO= 20/54 embryos (37,0%)

the phenotype at 3dpf with 54,2% of the embryos showing renal uptake (Figure 29). *Lrp2* morphant embryos are negative for Rab4 positive early endososmes in the renal tubular epithelium (Figure 26). To evaluate whether knock-down of *dab2* also leads to a loss of the Rab4 positive early endosomal fraction, embryos were injected with 70 kDa-FD, and stained for early endosomes with a Rab4 antibody. As can be clearly seen in Figure 30, there are no Rab4 positive vesicles present in the renal tubular epithelium of the *dab2* morphants (Figure 30 E, F).

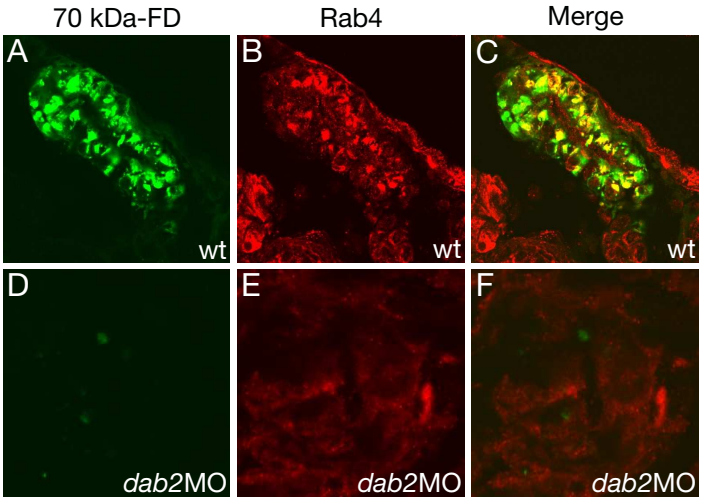

Figure 30: *Dab2* morphant embryos are negative for Rab4 positive early endosomes. Wildtype (A-C) and morphant (D-F) embryos were injected with 70 kDa-FD (A, D; green), fixed and cryosectioned. The sections were then subjected to antibody staining for Rab4 (B, E; red), a marker for the early endosomal fraction. In the wildtype, most endosomes containing the tracer co-stain for Rab4 (C), but no Rab4 positive endosomes were detected in the morphant (E).

These findings suggest that Dab2 is an essential component of LRP2-mediated endocytosis in the zebrafish pronephros and argue for a functional conservation of renal clearance pathways in the zebrafish. Zf-LRP2 expression and apical localization is not affected by the knock-down of *dab2* as seen in Figure 28. To exclude the possibilty that the clearance defects in *dab2* morphants are due to a misslocalization of the zf-LRP2 protein, wildtype and *dab2* morphants were injected with tracer, cryosectioned and stained for zf-LRP2 expression. As can be seen in Figure 31, knock-down of Dab2 protein expression did not affect the apical localization of zf-LRP2 (Figure 31 E, F).

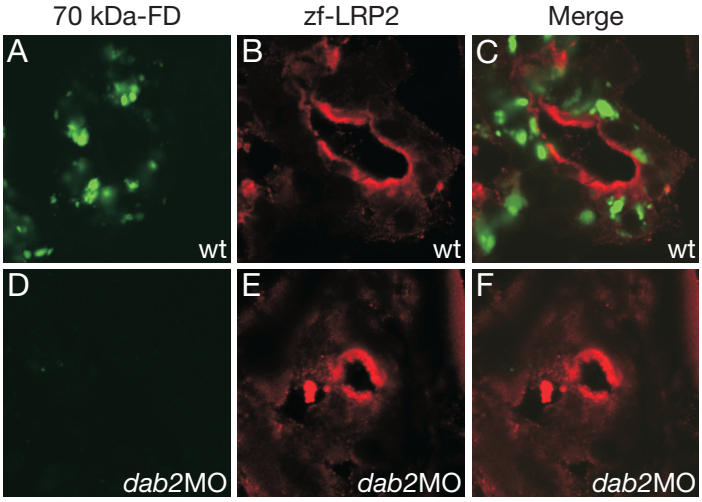

Figure 31: Localization of zf-LRP2 in *dab2* morphants is not changed. Wildtype (A-C) and *dab2* morphants (D-F) were injected with 70 kDa-FD, cryosectioned and stained for zf-LRP2. Wildtype animals show uptake of the dye (A, C) and a clear apical localization of zf-LRP2 (B, C), whereas no tracer uptake occurs in *dab2* morphants (D, F) despite correct apical localization of zf-LRP2 (E, F).

5.10 Analyzing new components for their role in endocytic processes in the zebrafish pronephros

As a proof of concept that this assay system can also be used to identify components that have not been associated with renal clearance pathways so far, two additional candidate genes were analyzed. Numerous reports have been implicating an important role for kinase signaling events to be involved in various endocytic processes (Conner and Schmid, 2003; Pelkmans et al., 2005). A recent study analyzed human kinases with respect to their involvement in endocytosis by a functional RNA interference assay (Pelkmans et al., 2005). Among others, the atypical protein kinase C iota (PRKCi) was implicated in endocytic processes. The relevance of PRKCi and its apical scaffolding partner, the membrane-associated guanylate kinase (MAGUK) subfamily member 5 (Mpp5) were choosen to be investigated, because the mutant zebrafish lines for these proteins were available and well characterized at our institution. The zebrafish strain carrying the naturally occuring mutated form of PRKCi has been termed heart and soul (*has* ^{m567}, Wei and Malicki (2002)), the strain where the Mpp5 protein is mutated has been termed

nagie oko (*nok* ^{s305}, Peterson et al. (2001)). Zebrafish embryos that are homozygous for either mutation die between 4 and 5 days post fertilization from cardiac malformations and lack of blood circulation. Because *has* ^{m567} and *nok* ^{s305}mutants lack circulation, injection of tracer molecules for analysis of uptake was not possible.

This problem was circumvented by using transgenic lines of zebrafish that express either wildtype PRKCi or Mpp5 under the control of the *cardiac myosin light chain 2* (*cmlc2*) promoter region (Huang et al., 2003) within all myocardial cells of the mutated backgrounds *nok* ^{s305} and *has* ^{m567} [*Tg(cmlc2:nok)* (generated by Nana Bit-Avragim) or *Tg(cmlc2:has)* (generated by Stefan Rohr), respectively] (Rohr et al., 2006). In these *Tg(cmlc2:nok)* and *Tg(cmlc2:has)* transgenic embryos cardiac morphogenesis and peripheral circulation is significantly restored while producing the complete range of epithelial defects characteristic of the mutants (Rohr et al., 2006).

Transgenic animals *Tg(cmlc2:has)* with restored circulation that were injected with 70 kDa-FD completely lacked uptake of tracer molecules from the pronephric duct (Figure 32 G, I), whereas *Tg(cmlc2:nok)* mutants showed robust presence of endocytic vesicles filled with tracer, albeit at weaker levels than their wildtype siblings (Figure 32 D, F). Mislocalization of the zf-LRP2 protein could be excluded as reason for the lack of uptake for *Tg(cmlc2:has)* mutants because similar to its localization in the wildtype, zf-LRP2 was still present apically in pronephric-duct epithelial cells (Figure 32 H, I). Therefore, apical-basal polarity of pronephric duct cells or apical localization of zf-LRP2 is not affected in *Tg(cmlc2:has)* mutants.

The presence of early endosomes was assesed using an anti-Rab4 antibody. Whereas wildtype and *Tg(cmlc2:nok)* mutants had significant amounts of Rab4-positive endosomes, *Tg(cmlc2:has)* mutants lacked clearly recognizable amounts of this vesicle type (Figure 33 H, I). These findings implicated *Tg(cmlc2:has)* but not *Tg(cmlc2:nok)* in the zf-LRP2 retrieval pathway, which is essential for the presence of Rab4-positive endosomes within the pronephric duct.

An explanation for the loss of endocytic activity in *Tg(cmlc2:has)* mutants could be the absence of ligands due to defective glomerular filtration. Alternatively, PRKCi might have a direct regulatory role in tubular endocytic processes. To discriminate between both possibilities, a mosaic clonal analysis of PRKCi function for endocytic activity was performed. A transgenic line of zebrafish that expresses membrane-tethered GFP (lynGFP) under control of the epithelial *claudin B* promoter *(clndB:GFP)* (obtained from S. Seyfried, MDC, Berlin) was used to genetically mark pronephric duct epithelial cells. Animals trangenic for *(clndB:GFP)*

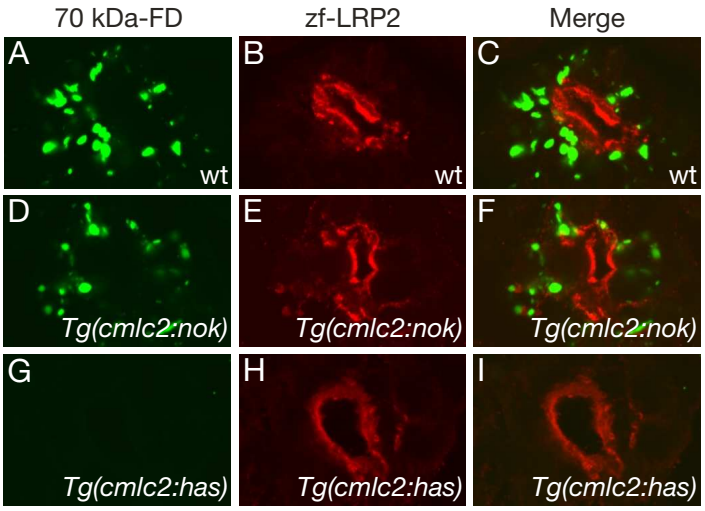

Figure 32: Lack of renal clearance in *Tg(cmlc2:has)* mutants. Transverse sections of 72 hpf wildtype embryos (A-C), *Tg(cmlc2:nok)* mutants (D-F), and *Tg(cmlc2:has)* mutants (G-I) injected with 70 kDa-FD (green) and immunostained for zf-LRP2 (B, C, E, F, H, I). *Tg(cmlc2:prkci)* mutants completely lack uptake of the tracer (G, I). The apical localization of zf-LRP2 protein is not affected in *Tg(cmlc2:nok)* and *Tg(cmlc2:has)* mutants (E, F, H, I).

were injected with the *has*MO to ablate expression of PRKCi (Horne-Badovinac et al., 2001; Rohr et al., 2006) and used as donors for transplantation into unmarked wildtype hosts (transplantation was carried out by F. Rudolph, MDC, Berlin). The efficiency and specificity of the *has*MO used in this experiment has been demonstrated in several studies (Horne-Badovinac et al., 2001; Rohr et al., 2006). Subsequently, *has* morphant pronephric duct clones within otherwise wildtype hosts were easily identified by GFP expression. In these transplants, *prkci* morphant pronephric duct clones showed robust uptake of 10 kDa-FD (Figure 34 C, arrowhead).

This result excludes a direct role of PRKCi in tubular endocytosis. Rather, lack of renal uptake in *Tg(cmlc2:has)* mutants most probably indicates defective glomerular filtration and, as a consequence, absence of ligands in the duct lumen.

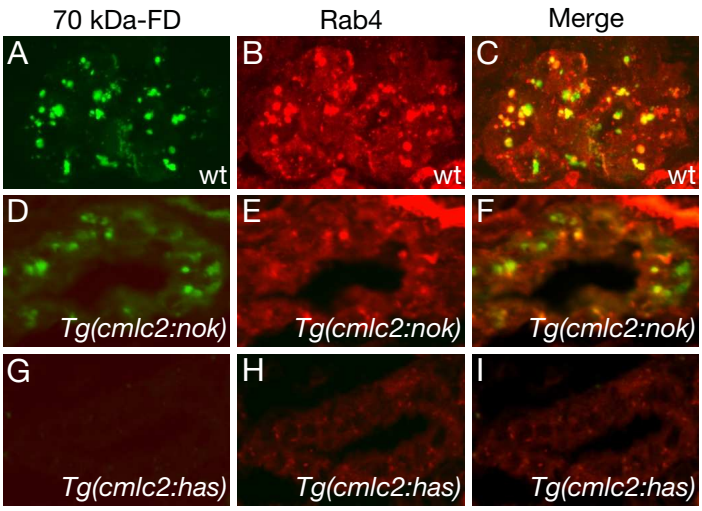

Figure 33: Lack of Rab4-positive early endosomes in *Tg(cmlc2:has)* mutants. Transverse sections of 72 hpf wildtype embryos (A-C), *Tg(cmlc2:nok)* mutants (D-F), and *Tg(cmlc2:has)* (G-I) injected with 70 kDa-FD (green) and immunostained for the early endosomal marker Rab4 (B, C, E, F, H, I). Whereas *Tg(cmlc2:nok)* mutants show a robust presence of Rab4-positive endocytic vesicles filled with the tracer (D, F), *Tg(cmlc2:has)* mutants completely lack Rab4 positive vesicles (G, I).

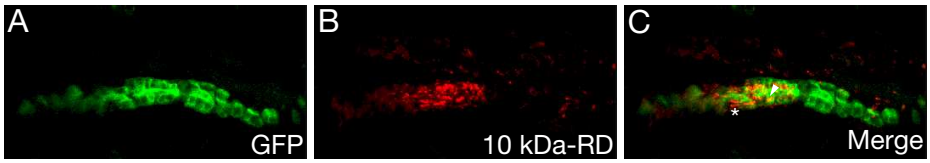

Figure 34: Mosaic clonal analysis of *prkci* function in tubular endocytic processes. Confocal fluorescence microscopy on whole-mounts of wildtype host embryos (non-GFP) injected with 10 kDa-FD that contain pronephric duct clones of animals trangenic for *(clndB:GFP)* injected with the *has*MO. (C) Endocytic punctate vesicles filled with the tracer are present within *has* morphant cell clones (arrowhead) and wildtype host neighboring cells (asterisk).

5.11 Zf-LRP2 and forebrain development

The results so far clearly indicate that the Morpholino approach to knock-down protein expression of zf-LRP2 is working efficiently and that the phenotypes concerning kidney function in the zebrafish are comparable to the phenotypes observed

for *lrp2* deficient mice.
To answer the question whether zf-*lrp2* is also involved in forebrain development, brain structures of wildtypes and *lrp2* morphants were analyzed on paraffin sections at different time points of embryonic development.
There were no obvious morphological differences between the brain structures of wildtypes and morphants for the analyzed time points (Figure 35). All major structural hallmarks were present and unchanged in the morphants. The sections shown (Figure 35) are representative for all animals analyzed, the plane of section (PoS) is indicated in the schematics. All other areas of the brain were also not changed.

5.12 Expression of early forebrain marker genes is unchanged

Although the overall physiological morphology of the brain did not seem to be changed in *lrp2* morphants (Figure 35), the expression patterns of key marker genes of early brain development could be altered. The key ventral forebrain marker genes that were found to be aberrantly expressed in the mouse knockout model for *lrp2* included *shh*, *nkx2.1* and *olig2*. Expression of these genes was therefore also analyzed in the zebrafish on sections and on whole-mount ISH.
Shh was expressed strongly in the central nervous system (CNS) of the developing embryo but also in parts of the intestinal tract at 48hpf. Expression domains in the (CNS) included the ventral neural tube and the notochord, the emenentia thalami (Figure 36 A, E; EmT) and the ventral thalamus (Figure 36 A, E; VT).
Expression domains in the intestinal tract included the anlage for the mouth (Figure 36 A, E; Mt) and the anlage for the pharynx (Figure 36 A, E; Ph). Expression of *shh* at 72hpf was weaker than at 48hpf, but the *shh* expression pattern was identical to the pattern observed for 48hpf. No differences between wildtypes and *lrp2* morphants were seen for the expression pattern of *shh* on whole-mounts (Figure 36 A, C, E, G) or on transversal sections (Figure 36 B, D, F, H) thereof for 48hpf and 72hpf.
Expression of *nkx2.1* at 10.5dpc was found to be significantly reduced in the AEP of *lrp2* $^{-/-}$ mouse embryos compared to wildtypes. In the zebrafish, expression of *nkx2.1* was restricted to brain structures at 48hpf and 72hpf. At 48hpf it was found to be expressed in the pallium, subpallium, ventral thalamus, eminentia thalamica, preoptic region and the dorsal part of the posterior tuberculum (Figure 37 A, E; P, S, VT, EmT, Po, Ptd). The expression level of *nkx2.1* at 72hpf was only

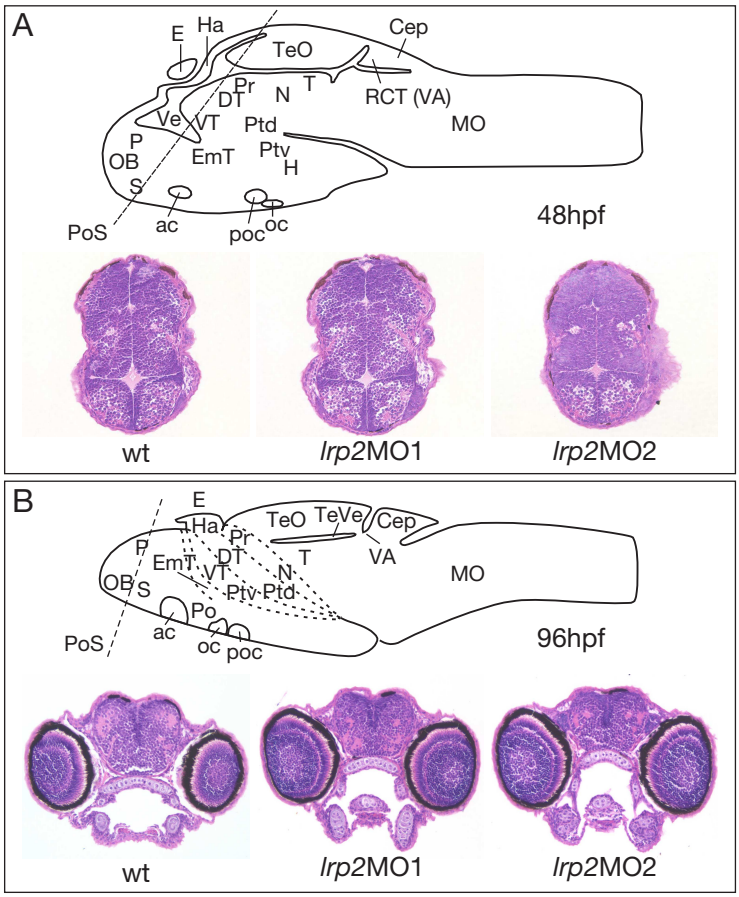

Figure 35: Histological analysis of Hematoxylin and Eosin stained paraffin sections of 48hpf (A) and 96hpf (B) wildtype and morphant animals. The plane of section (PoS) is indicated in the models by dashed straight lines in (A) and (B). No obvious morphological changes were observed when analyzing stacks of sections along the rostral to caudal body axis of *lrp2*MO1 and *lrp2*MO2 injected animals. The depicted sections are representative for all animals analyzed. Abbreviations: ac, anterior comissure; CeP, cerebellar plate; DT, dorsal thalamus; E, epiphysis; EmT emenentia thalami; H, hypothalamus; Ha, habenula; MO, medulla oblongata; N, region of the nucleus of the medial longitudinal fascicle; OB, olfactory bulb; oc, optic chiasma; P, pallium; Po, preoptic region; Poc, postoptic commissure; Pr, pretectum; PTd, dorsal part of posterior tuberculum; PTv, ventral part of posterior tuberculum; RCT, rostral cerebellat thickening (valvula); S, subpallium; T, midbrain tectum; TeO, tectum opticum; Va, valvula cerebelli; Ve, brain ventricle; VT, ventral thalamus (prethalamus). Models modified from Mueller and Wullimann (2005).

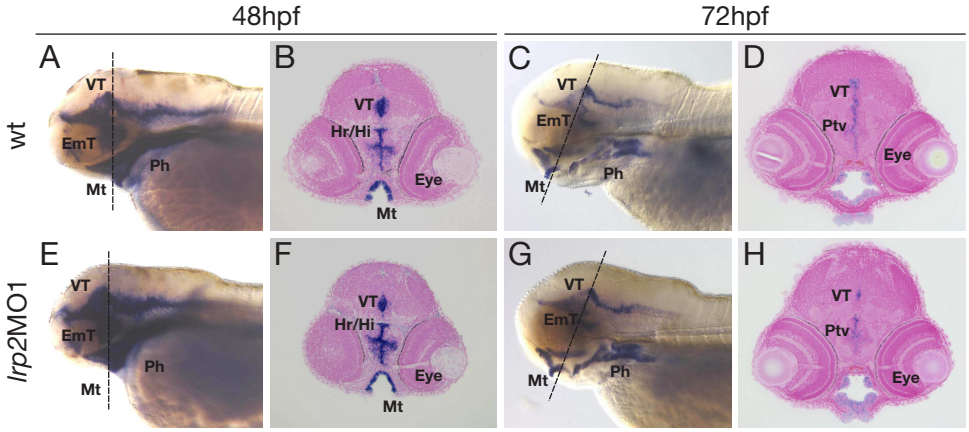

Figure 36: Expression of *shh* in wildtype (A-D) and *lrp2* morphant (E-H) animals at 48hpf (A, B, E, F) and 72hpf (C, D, G, H). Analysis of *shh* expression on whole-mounts (A, C, E, G) and on sections (B, D, F, H) did not reveal differences between wildtype and *lrp2* morphant animals. The plane of section for B, D, F and H is indicated by a dashed line in the corresponding whole-mount ISH (A, C, E, G). Abbreviations: Emt, eminentia thalami; Hi, intermediate hypothalamus; Hr, rostral hypothalamus; Mt, mouth; Ph, pharynx; VT, ventral thalamus.

slightly lower than at 48hpf, the expression domains remained the same. Unlike the situation in the mouse, no differences between wildtypes and *lrp2* morphants were seen for the expression pattern of *nkx2.1* on whole-mounts (Figure 37 A, C, E, G) or on transversal sections (Figure 37 B, D, F, H) thereof for 48hpf and 72hpf.

Another marker gene displaying a reduced expression level in the AEP of 10.5 dpc *lrp2* $^{-/-}$ mouse embryos was *olig2*. The expression of the zebrafish ortholog of *olig2* was restricted to areas of the forebrain and midbrain of the developing embryo.

At 48hpf it was expressed mainly in the eminentia thalami, the pallium, subpallium, ventral thalamus and the retina (Figure 38 B, F; Emt, P, S, VT, Eye). At 72hpf, main sites of expression were the midbrain-hindbrain boundary and motoneurons (Figure 38 C, G; Mhb, Mn).

However, no differences between wildtypes and *lrp2* morphants were seen for the expression pattern of *olig2* on whole-mounts (Figure 38 A, C, E, G) or on transversal sections (Figure 38 B, D, F, H) thereof for 48hpf and 72hpf.

Taken together, these findings indicate that the brain development is not disturbed in zebrafish embryos that have been injected with the *lrp2*MO1 or *lrp2*MO2 Mor-

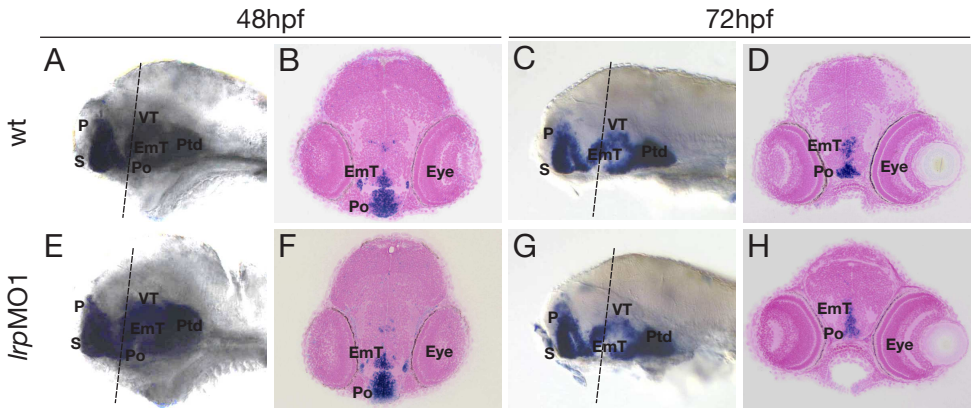

Figure 37: Expression of *nkx2.1* in wildtype (A-D) and *lrp2* morphant (E-H) animals at 48hpf (A, B, E, F) and 72hpf (C, D, G, H). Analysis of *nkx2.1* expression on whole-mounts (A, C, E, G) and on sections (B, D, F, H) did not reveal differences between wildtype and *lrp2* morphant animals. The plane of section for B, D, F and H is indicated by a dashed line in the corresponding whole-mount ISH (A, C, E, G). The yolk has been removed in A, C, E and G. Abbreviations: Emt, eminentia thalami; P, pallium; Po, preoptic region; Ptd, dorsal part of posterior tuberculum; S, subpallium; VT, ventral thalamus.

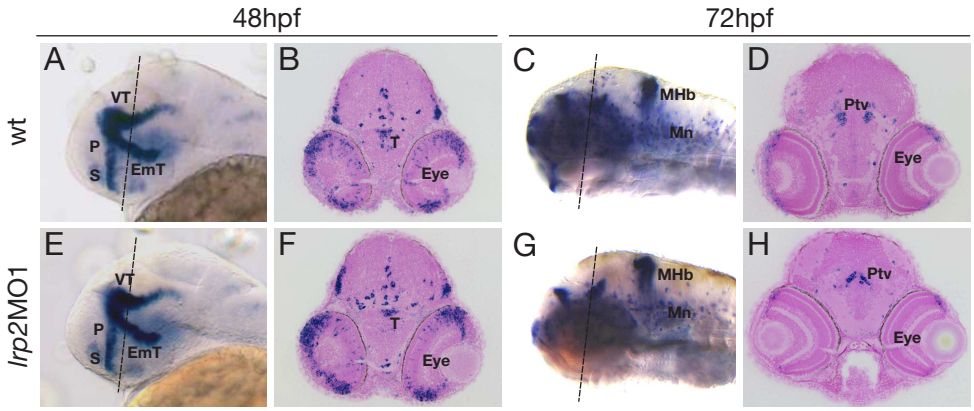

Figure 38: Expression of *olig2* in wildtype (A-D) and *lrp2* morphant (E-H) animals at 48hpf (A, B, E, F) and 72hpf (C, D, E, F). Analysis of *olig2* expression on whole-mounts (A, C, E, G) and on sections (B, D, F, H) did not reveal differences between wildtype and *lrp2* morphant animals. The plane of section for B, D, F and H is indicated by a dashed line in the corresponding whole-mount ISH (A, C, E, G). The yolk sac has been removed in C and G. Abbreviations: Emt, eminentia thalami; P, pallium; S, subpallium; VT, ventral thalamus.

pholino.

5.13 Zf-lrp2 mRNA is provided maternally

Proteins or mRNAs important for the early development of the zebrafish embryo are provided maternally with the yolk of the egg. In this scenario, splice variant Morpholinos would not be effective because the *lrp2* mRNA is already spliced and would be translated normally into functional zf-LRP2. This might be one explanation for the seemingly normal brain development in the *lrp2* morphant embryos. RT-PCR analysis of early stages of zebrafish development indeed revealed the presence of zf-*lrp2* transcripts (Figure 39).

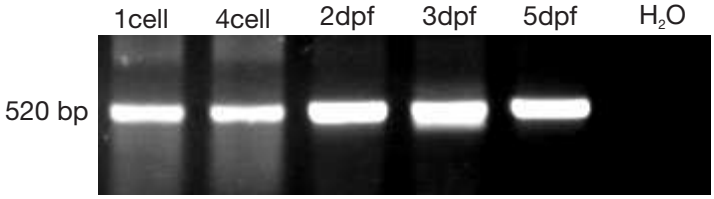

Figure 39: RT-PCR for zf-*lrp2* transcripts at various stages of development. Zf-*lrp2* transcripts were already present at the one-, respectively four-cell stage of development. The expression level for zf-*lrp2* at 2, 3 and 5dpf of embryonic development was found to be higher than for the early stages.

6 Discussion

The function of LRP2 in forebrain development has been analyzed using knockout mouse models. Lack of the receptor results in defects in Shh and Bmp4 pathways in the neural tube and in impaired establishment of ventral cell fate, particularly affecting oligodendroglial and interneuronal cell populations. The similarities between *lrp2* knockout mice and mouse models with altered Shh or Bmp4 activities in the forebrain indicated a crucial role for this receptor in morphogen pathways that specify early dorsoventral patterning of the prosencephalon. A zebrafish animal model was established to further elucidate the function of LRP2 in forebrain development in an alternative system amenable to rapid transgenic manipulations.

6.1 Analysis of LRP2 function in the mouse model

6.1.1 The role of lrp2 in forebrain development: yolk sac or neuroepithelium?

Previously, deficiency for *lrp2* in the yolk sac and/or in the neuroepithelium was held responsible for the holoprosencephalic symptoms in *lrp2* $^{-/-}$mice (Farese and Herz, 1998; McCarthy and Argraves, 2003; Willnow et al., 1996a). Using *cre*-mediated conditional gene inactivation, a mouse line was generated that had lost LRP2 expression in the embryo but not in the yolk sac. Surprisingly, expression of LRP2 in the yolk sac alone did not prevent forebrain malformation as embryos with epiblast specific *lrp2* gene deletion were phenotypically indistinguishable from embryos with complete *lrp2* gene deletion (Figure 6 F, page 42). The limited number of *lrp2* $^{lox/lox}$/*meox2* $^{tm1(cre)Sor}$ embryos available (n=15) precluded a detailed comparison of the phenotypes of mice with complete and with epiblast-specific *lrp2* gene deletion. Thus it cannot be excluded that some phenotypic differences exist in forebrain abnormalities in these two lines that reflect the influence of LRP2 in the yolk sac on neural tube formation. However, similar alterations in *fgf8*, *shh* and *bmp4* expression in both lines strongly suggest that *lrp2*-deficiency in the neuroepithelium is the main cause of the observed forebrain defects.

6.1.2 Lrp2-deficiency impairs Shh-dependent ventral cell fate

While the role of LRP2 in the yolk sac still awaits elucidation, experimental evidence in this study identified the contribution of this receptor in the neuroepithelium to

specification of dorsal and ventral signaling pathways in the anterior neural tube. Axial patterning of the neural tube is controlled by secreted factors that have distinct expression domains in the rostral forebrain. In particular, an intricate balance of the morphogens Shh and Bmp4 is crucial for specifying dorsoventral forebrain patterning (Ohkubo et al., 2002; Sasai and De Robertis, 1997). Shh activity defines the ventral neural tube and establishes ventral neuronal and oligodendroglial cell populations (Lu et al., 2000; Marin and Rubenstein, 2001; Nery et al., 2001; Rowitch et al., 1999). Inactivation of the *shh* gene in the mouse causes defective axial patterning, cyclopia and absence of ventral cell types (Chiang et al., 1996). Surprisingly, lack of LRP2 resulted in loss of *shh* expression specifically in the AEP, whereas expression in further caudal regions of the neural tube was not affected (Figure 7, page 43). The identical phenotype is seen in other models of abnormal dorsoventral patterning and HPE, in particular in those with increased Bmp4 activity, as discussed below. Why some defects impair Shh activity exclusively in the AEP is unclear at present, but region-specific differences in the molecular mechanism of Shh action in the rostral forebrain compared with more caudal regions, such as the spinal cord, are clearly established (Dale et al., 1997). For example, ventral diencephalic midline cells of the neural tube rostral to the zona limitans intrathalamica (zli) require the morphogens Bmp7 and Shh in order to differentiate correctly whereas ventral midline cells caudal to the zli do not require Bmp7 (Dale et al., 1997).

The spatially restricted loss of *shh* in the AEP may explain why no overt changes in some components of the global Shh signaling pathway, e.g. Hnf3ß (Figure 10, page 46) were detectable in *lrp2* $^{-/-}$embryos at E10.5, and why some defects in *shh* knockout mice (such as absence of distal limb structures) were not shared by *lrp2*-deficient animals. In the AEP, the *shh* signal peaks around E10.5, when it overlaps with *olig2* and *nkx2.1*, markers of oligodendroglial and neuronal lineages, respectively (Figure 9, page 45). Ectopic expression of *shh* locally induces differentiation of oligodendrocytes from ventral neuroepithelial precursors (Nery et al., 2001), a process blocked by anti-Shh antibodies (Orentas et al., 1999). Consistent with loss of *shh* in the AEP, *lrp2*-deficient embryos suffered from impaired establishment of neuroepithelial progenitors and from a dramatic reduction in oligendroglial and interneuronal cell populations, as demonstrated by the almost complete absence of *olig2*, *nkx2.1*, *dlx2* and TuJ1-positive cells in the ventral (but not in the dorsal) forebrain (Figure 9, page 45 and Figure 10, page 46). Potentially, lack of proliferation, increased cell death or impaired differentiation may be held responsible for the absence of ventral cell fate specification. Decreased mitotic activity was de-

tected in the AEP of *lrp2* $^{-/-}$embryos (Figure 4, page 13). Thus, this effect clearly contributes to forebrain anomalies in this mouse line. However, the absence of proliferative defects in other areas of the rostral forebrain and the normal expression of many ventral marker genes (e.g. *ptch1* and *hnf3ß*) strongly suggested that alterations in Shh-dependent differentiation processes also play a causative role. This hypothesis is in agreement with recent findings in which Shh signaling was disrupted in the ventral telencephalon of mice at E9.5 using conditional targeting of the *smo* gene. Spatial and temporary specific ablation of ventral *shh* activity results in a complete absence of oligodendrocytes and interneurons in the ventral forebrain, due to impaired differentiation rather than altered proliferation or apoptosis of progenitor cells (Fuccillo et al., 2004).
The spatial restricted loss of *shh* in the AEP, the restricted loss of ventral cell types and the normal expression of global Shh target genes like *hnf3ß* oppose findings from McCarthy et al. (2002) who implicated a role for LRP2 as Shh clearance receptor *in vitro*. If LRP2 were involved in Shh signaling, other areas of the neural tube than the AEP would likely be affected as well.

6.1.3 Lrp2-deficiency increases Bmp4 activity in the rostral dorsal neural tube

Whereas Shh specifies ventral cell fate, Bmps provide inductive signals for dorsal cell types such as the astroglial lineage (Gross et al., 1996; Liem et al., 1995; Timmer et al., 2002). They act through suppression of cell proliferation and induction of apoptosis (Furuta et al., 1997), and function as potent antagonists of the ventral neural tube by blocking Shh action on dorsal cell types and by inhibiting ventral cell fate (Lim et al., 2000; McMahon et al., 1998). Consistent with an opponent action of dorsal and ventral signaling pathways in the neural tube, increased activity of Bmps suppressed the expression of *shh* in the rostral ventral neuroepithelium. For example, when beads soaked with recombinant Bmp4 or Bmp5 are implanted into the neural tube of the chicken forebrain, loss of *shh* expression in the ventral forebrain is observed to cause cyclopia and HPE (Golden et al., 1999). In mice genetically deficient for *noggin*, a Bmp4 antagonist, expression of dorsal cell fates is normal but Shh-dependent ventral cell fate is lost progressively (McMahon et al., 1998). Finally, in mice homozygous for the deletion of *chordin* and heterozygous for the *noggin* gene defect, deficiencies for both Bmp antagonists also cause loss of *shh* expression, specifically in the AEP, and holoprosencephalic syndrome, a phenotype highly reminiscent of defects in *lrp2* $^{-/-}$embryos (Anderson et al., 2002).

As well as with alterations in Bmp4 and Shh pathways, *lrp2*-deficient embryos also displayed changes in expression of *fgf8* and *pax6*. Fgf8 promotes rather than induces rostroventral telencephalic fate (Wilson and Houart, 2004), and its expression is considered to be dependent on coordinated *shh* and *bmp* signaling (Ohkubo et al., 2002). Therefore reduction in ventral *fgf8* gene expression and the extension of the signal along the dorsal midline probably reflected secondary alterations in dorsoventral patterning of the forebrain and abnormalities in formation of midline tissue. Similarly, the expansion of *pax6* into ventral parts of the telencephalon of receptor-deficient mice was probably a consequence of the absence of Shh in the AEP, as described for other models with specific loss of *shh* expression in the rostral forebrain (Gofflot et al., 1999; Huh et al., 1999).

6.1.4 A role for LRP2 in patterning the rostral neural tube: a working model

What may be the mechanism whereby LRP2 affects dorsoventral specification of the neural tube? Given the competing action of dorsal and ventral signaling factors on neural tube patterning one may envision two scenarios. In one model, the receptor may be essential to induce *shh* expression in cells of the AEP, its absence resulting in the loss of Shh activity and in an impaired ventral cell fate (Figure 40 B). This idea is supported by a recent study that identified three novel regulatory enhancer elements necessary for directing *shh* expression to distinct areas of the rostroventral neural tube (Jeong et al., 2006). Two of these novel enhancers are necessary for inducing *shh* expression in the subventricular zone of the anterior entopeduncular area (AEP). This is consistent with the finding that *lrp2*-deficient animals lacked *shh* expression (Figure 7 D and F, page 43) and displayed a reduction in neuroepithelial wall thickness in this area of the ventral forebrain (Figure 4 G and H, page 13). In this scenario, LRP2 might be necessary to specifically activate regulatory elements that are essential for *shh* expression in the AEP. As a consequence of the lack of ventral Shh signals, dorsal markers such as Bmp4 would be overexpressed.
In an alternative model, LRP2 may act as a negative regulator of Bmp4 activity in the dorsal neuroepithelium and receptor deficiency may cause an increase in dorsal Bmp4 signals, an effect known to suppress *shh* (Figure 40 C, Golden et al. (1999); Lim et al. (2000); McMahon et al. (1998)). Based on the fact that increases in *bmp4* expression and signaling through phosphorylated Smad (P-Smad) proteins at E9.5 clearly precede defects observed for *shh* expression at E10.5, the latter

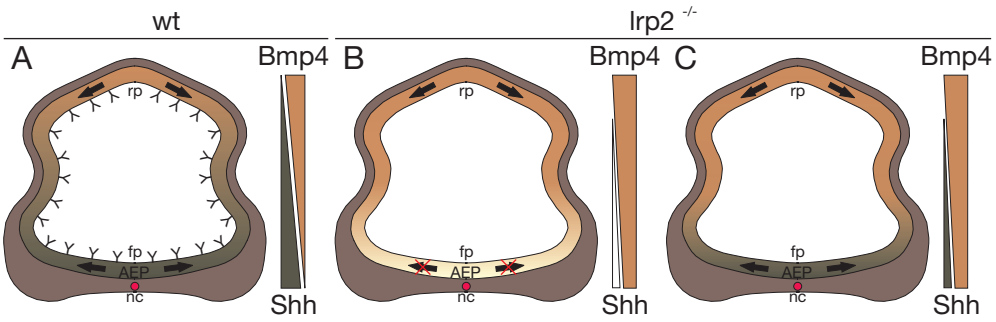

Figure 40: Schematic working models of a possible role for LRP2 in patterning of the rostral neural tube. Depicted is the situation in the wildtype (A) and two possible situations in the *lrp2* $^{-/-}$animals (B, C). In the wildtype, Shh is expressed in the notochord (nc) and in the floor plate (fp) of the neural tube, whereas Bmp4 is expressed in the roof plate (rp) of the neural tube.The two key morphogens of dorsoventral patterning form a defined directly opposed gradient, thereby specifying cell fates in a concentration dependant manner. In the first scenario (B), the lack of LRP2 leads to a lack of *shh* expression in the AEP, as a consequence ventral cell fates become dorsalized. In the second scenario (C), lack of LRP2 in the dorsal neural tube leads to an increase in the range of action of Bmp4, resulting again in suppression of ventral cell fates. Abbreviations: AEP, anterior entopeduncular area; fp, floor plate; nc; notochord; rp, roofplate.

model seems to be more likely.
A role for LRP2 in restricting the range of action of Bmp4 is supported by findings obtained in this study and by work from others. In the early forebrain, Bmp4 is believed to induce its own expression via a positive feedback loop; thus, increases in Bmp4 activity are expected to induce *bmp4* transcription (Blitz et al., 2000). Furthermore, the importance of restricting Bmp signals during development is well established and several mechanisms have evolved to negatively regulate the range of action of the morphogen at various points in the signal transduction cascade.
First, the range of action is limited by soluble, excreted proteins such as Chordin or Noggin that bind to Bmp4 and thereby prevent binding to its endogenous receptors (Bmp-receptor I and II, Balemans and Van Hul (2002)). The concentration of Bmp4 available for signaling is further reduced by dominant negative pseudoreceptors like the Bmp activin membrane bound inhibitor (BAMBI) that binds Bmp4 but does not relay the signal (Onichtchouk et al., 1999). The Bmp signal can also be attenuated intracellularly by inactivating Smad (I-Smad) proteins and Smad ubiquitin regulatory factors (Smurfs) that mediate the proteasomal degrada-

tion of the intracellular effectors of Bmp4 signaling (von Bubnoff and Cho, 2001). Taken together with the ability of LRP2 to internalize Bmp4 (Figure 13, page 50), these findings provide an explanatory model in which LRP2 acts as an endocytic receptor for Bmp4 in the neural tube, antagonizing morphogen signaling. As a consequence of receptor deficiency, Bmp4 activity may be locally increased, causing activation of *bmp4* transcription and stimulation of rostral and dorsal patterning and suppression of ventral patterning. A similar function for LRP2 as a clearance receptor for parathyroid hormone (PTH) suppressing signaling via the PTH receptor in the kidney has been documented before (Hilpert et al., 1999).
Few established cell lines express the receptor LRP2, and BN16 cells are the system of choice for testing LRP2-dependent endocytosis. The lack of expression of Bmp receptors in BN16 cells (R. Spoelgen, MDC, Berlin; unpublished) currently precludes testing the consequence of LRP2 activity on Bmp signaling in these cells directly. Therefore, future efforts should be directed toward establishing suitable cellular systems (e.g. neural tube explants) to address this question.
In conclusion, the studies in the mouse model have uncovered an important novel activity of LRPs as modifiers of Bmp4- and Shh-dependent patterning of the forebrain, and the role that is played by LRP2 in this process. These findings have identified LRP2 as an important factor in axial embryonic pattern formation and characterized a novel molecular pathway that contributes to abnormal specification of the ventral forebrain and to HPE, the most common developmental brain anomaly in humans (Wallis and Muenke, 1999).

6.2 Analysis of LRP2 function in the zebrafish model

6.2.1 Expression of the LRP2 ortholog in the zebrafish pronephros

The expression domain of *lrp2* was compared to the expression domains of established marker genes for renal development. Expression of *lrp2*, *dab2*, and *cubilin* overlap in a defined domain of the zebrafish pronephric duct (Figure 17, page 60) that is involved in renal clearance processes as indicated by tracer uptake studies (Figure 18, page 61).
At 3dpf, this expression domain comprises a sharply defined segment within the proximal half of the duct epithelium and a short distal segment of the pronephric tube. This segment likely corresponds to the proximal convoluted tubule (PCT), a nephron segment that is central to the tubular resorption of solutes in the mammalian kidney (Jacobson, 1981). Expression mapping of transport proteins involved

in osmoregulation in the *Xenopus* larval pronephric kidney predicts the presence of several distinct transport domains involved in renal clearance along the proximal-distal axis suggesting a segmented complexity that is similar to that of mammalian nephrons (Eid and Brandli, 2001; Zhou and Vize, 2004).
The data of this study provide the first functional evidence for a segmental subdivision of the zebrafish pronephric duct epithelium. Mapping of the *lrp2* expression domain in the zebrafish pronephros largely parallels the distinct expression of the receptor in the PCT of the developing mouse kidney, a pattern that is prototypic for most mammalian species. The situation is somewhat different in the rat embryo, where expression of the receptor can also be detected in podocytes in the glomerulus (Assemat et al., 2005).
It is not known how the expression of *lrp2*, *cubilin* and *dab2* is controlled but proximal-distal patterning of the pronephric duct most likely is involved. The field of the pronephric kidney has attributes of a prepatterned tissue based on partially overlapping expression patterns of *wt1*, *pax2.1* and *simple minded 1* (*sim1*), a basic helix-loop-helix factor, that are consistent with lineage relationships of segments of pronephric progenitor cells (Serluca and Fishman, 2001). The expression domains of *lrp2* and *cubilin* are overlapping with different combinatorial codes of *wt1* and *pax2.1* expression (Figure 17, page 60). However, the expression patterns of *wt1* and *pax2.1* are independent of *lrp2* and *dab2* function. It remains to be seen whether, conversely, the combinatorial codes of these transcription factors may affect the expression of *lrp2*, *cubilin* and *dab2* and thereby the functional specialization of the pronephric tubule.

6.2.2 Functional analysis of zf-LRP2 in the zebrafish pronephros

Visualization of receptor-mediated endocytosis can be easily accomplished within the zebrafish pronephros, making the zebrafish an ideal model organism to dissect the molecular components of receptor-mediated endocytosis. To prove that this is indeed possible, known components of the endocytic machinery in mammals were analyzed. In line with a central role for LRP2 in renal uptake processes, knock-down of this scavenger receptor or its adaptor Dab2 interfered with endocytic clearance of metabolites into the pronephric duct (Figure 24, page 65 and Figure 28, page 71), demonstrating functional conservation of this endocytic pathway across species. The ease with which endocytic processes can be manipulated in zebrafish larvae should allow for the systematic characterization of additional components required for LRP2 trafficking and function *in vivo*.

To this end, a number of cytoplasmic adaptors have been identified by yeast-2-hybrid screening that interact with the intracellular domain of LRP2 (Gotthardt et al., 2000; Oleinikov et al., 2000; Petersen et al., 2003; Rader et al., 2000). Apart from Dab2, the significance of these adaptors for receptor function *in vivo* remains unclear. Where applicable, the relevance of these proteins for receptor function may now be identified using the respective morphants.
Intriguingly, knock-down of *lrp2* and *dab2* in the zebrafish pronephros not only impairs tubular clearance of receptor ligands (such as RAP, Figure 25; page 67) but also abolishes the uptake of fluid-phase markers (Figure 25 B and C, page 67) or the formation of Rab4-positive endosomes (Figure 26, page 68 and Figure 30, page 72). These findings may reflect the fact that other endocytic receptors only contribute insignificantly to renal clearance processes in the absence of LRP2 activity. Alternatively, LRP2 function may be directly required for establishment of an endocytic apparatus in this cell type, a hypothesis strongly supported by previous observations in *lrp2*-deficient mice (Christensen and Willnow, 1999; Nykjaer et al., 1999). In these animals, lack of the receptor also results in complete absence of detectable endocytic structures including endosomes and dense apical tubules (recycling membrane vesicles) as shown by morphological analysis using electron microscopy (Christensen and Willnow, 1999; Nykjaer et al., 1999).
A central role for the LRP2 receptor in formation of endocytic structures was also demonstrated by inactivation of PRKCi and its scaffolding partner Mpp5. These proteins have been recently identified in an *in vitro* assay to be directly involved in endocytic uptake processes (Pelkmans et al., 2005). However, the *in vivo* relevance of these findings for the kidney was not adressed. Therefore, expression of both proteins was abolished and the consequences for the larval pronephros, resp. renal uptake of tracer dye were evaluated.
Inactivation of Mpp5 only mildly affected renal clearance processes, whereas inactivation of PRKCi did impair tubular clearance processes and formation of early endosomes (Figure 33, page 76). Surprisingly however, this defect is not due to an abnormal epithelial cell polarity of the pronephros or an inability of zf-LRP2 to perform endocytosis as indicated by the correct localization of the receptor to the apical membrane (Figure 32, page 75). Rather, the finding that *prkci* mutants fail to form Rab4-positive endosomes in pronephric duct epithelial cells and fail to clear tracers, suggests that glomerular filtration is impaired in these mutants and that reduced availability of ligands for zf-LRP2 prevents formation of early endocytic vesicles.
This conclusion was confirmed by clonal analysis of morphant cells in otherwise

wildtype hosts (with normal glomerular filtration) demonstrating that zf-LRP2 is active in PRKCi-deficient tubules (Figure 34, page 76). It might also be possible that the presence of un-liganded receptor accelerates the kinetic of dissociation of Rab4 with endosomes thus reducing the amount of Rab4 that can be detected by immunofluorescence. However, complete absence of endosomal structures in *lrp2*-deficient mouse proximal convoluted tubule (PCT) cells (Nykjaer et al., 1999)) strongly supports the concept that absence of receptor activity in the larval pronephros also impairs formation of a proper endocytic machinery in this tissue.
Taken together, these findings highlight the evolutionary conservation of renal tubular clearance mechanisms from fish to mammals and the central role played by ligand-induced LRP2 activity in this process. The experimental model system established in this study provides a framework for detailed approaches to dissect the molecular components involved in this important endocytic receptor pathway.

6.2.3 Role of the LRP2 ortholog in kidney and forebrain development of the zebrafish

The zebrafish ortholog of LRP2 is also abundantly expressed in brain structures, the retina and the otic vesicles (Figure 16, page 55). Surprisingly, knockdown of expression of the zf-LRP2 protein does not result in malformation of the brain as observed in the *lrp2* $^{-/-}$mouse model. Also, expression patterns of morphogens such as *shh*, *nkx2.1* or *olig2* that were found to be altered in *lrp2* $^{-/-}$embryos, were not changed in *lrp2* morphant animals (Figure 36, page 79; Figure 37, page 80 and Figure 38, page 80).
One possible explanation might be that the LRP2 ortholog in the zebrafish has lost its importance in forebrain development, resp. that the mammalian LRP2 gained its importance during evolution. However, this possibility seems unlikely because even in organisms that are evolutionary more distantly related to mammals than the zebrafish, LRP2 plays a crucial role during development (Figure 41). The receptor is for example essential for growth and development of the nematode *Caenorhabditis elegans* as a mutation in the gene of the *lrp2* ortholog of the nematode causes an inability to shed and degrade the old cuticle at each of the larval molts (Yochem et al., 1999).
A more likely explanation for the lack of a forebrain phenotye may be attributed to technical difficulties in generating the *lrp2* morphant animals. These animals were generated by injecting splice variant Morpholino antisense oligonucleotides

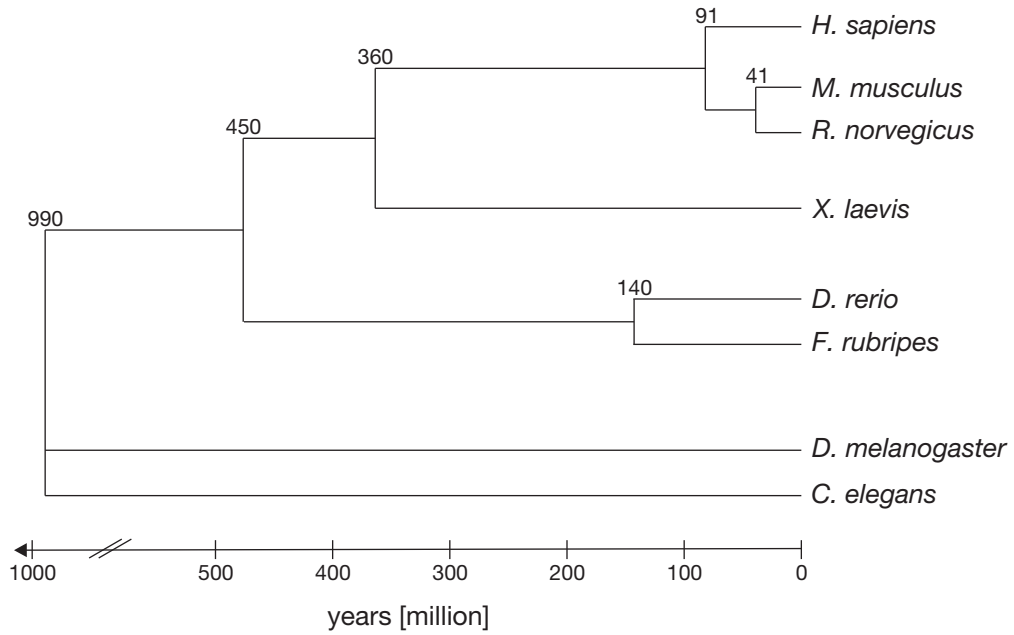

Figure 41: Phylogenetic tree of different species illustrating evolutionary distance in million years. The vertical lines indicate the last common ancestor for the two species branching off. The last common ancestor for *H. sapiens* and for *M. musculus* existed 360 million years ago, the last common ancestor for *D. rerio* and *H. sapiens* existed 450 million years ago, whereas the last common ancestor for *C. elegans* and *H. sapiens* existed 990 million years ago.

that interfere with the correct splicing of the pre-mRNA of *zf-lrp2*. As opposed to ATG Morpholinos that affect translation, splice variant Morpholinos cannot target already spliced *zf-lrp2*-mRNA. Proteins or mRNA for proteins that are essential for early embryonic development are supplied maternaly in the yolk of the egg. The early presence of already spliced maternal *zf-lrp2*-mRNA might be sufficient to trigger normal forebrain development. Indeed, RT-PCR analysis of zebrafish eggs at early stages of embryonic development reveals the presence of significant amounts of *zf-lrp2*-mRNA (Figure 39, page 82).
At present, the only possibility to knock down zf-LRP2 protein expression is the splice variant Morpholino approach, because sequence information about the ATG-region of the *zf-lrp2* gene to generate an ATG-Morpholino is not available to date. The success of further elucidating the function of LRP2 in forebrain development in the zebrafish is therefore critically dependent on interfering with LRP2 expres-

sion or function as early as possible during embryonic development. This may be achieved in a direct or indirect manner. Directly interfering with LRP2 expression involves cloning of the ATG-region of zf-*lrp2* in order to generate a Morpholino that blocks the initiation of translation of the protein.
Introducing mutations that ablate *lrp2* gene expression would be another direct approach. Since the technique of targeted gene disruption is not available so far in this animal model, artificial mutagenesis may be used to introduce mutations. A method that earned much attention is the "Targeting Induced Local Lesions IN Genomes" (TILLING) approach because it combines the efficiency of ethyl methanesulfonate (EMS)-induced mutagenesis (Koornreef et al., 1982) with the ability of fast detection of base pair changes in the genomic region of interest (McCallum et al., 2000). Although this method is fast and automatable it is nevertheless introducing mutations randomly and therefore not guaranteed to succeed.
An indirect approach to interfere with LRP2 function would be overexpression of a receptor antagonist that blocks binding sites for other ligands. The receptor associated protein (RAP) normally resides in the endoplasmic reticulum (ER) of the cell acting as a chaperone for LDL receptor gene family members. Removal of the ER retention signal leads to excretion of RAP into the extracellular space where it binds to the receptors and blocks binding sites for other ligands artificially. This strategy has been successfully applied in the mouse to transiently inactivate LRP *in vivo* (Rohlmann et al., 1996). The disadvantage of this approach is that RAP binds to and therefore blocks all members of the LDL receptor gene family, rendering it difficult to discern defects specific for the loss of LRP2 function.
Interfering with LRP2 function may also be achieved by ablating expression of intracellular adaptor proteins. That this is feasible has been shown in this study for the intracellular LRP2 adaptor protein Dab2 . Numerous additional intracellular adaptor proteins for LRP2 have been identified so far *in vitro*. Some of these adaptors are involved in regulating endocytic pathways, such as the outer membrane protein (OMP) 25 that has been implicated in vesicular transport processes (Nemoto and De Camilli, 1999), or the Disabled homolog (Dab) 1 that prevents clustering of the receptor into clathrin coated pits (Gotthardt et al., 2000). Proteins important for neurotransmission like the postsynaptic density (Psd) protein 95 (Sheng and Pak, 1999) and the carboxyl-terminal PDZ ligand of neuronal nitric oxide synthase (Capon) have also been shown to bind to LRP2 (Gotthardt et al., 2000). There are also adaptor proteins with unknown physiological function that bind to LRP2 like the LRP2 binding protein (LRP2BP) (Petersen et al., 2003) or the M-SemF cytoplasmic domain-associated protein (SEMCAP) 1 (Gotthardt

et al., 2000). Assuming that some of these intracellular adaptor proteins may specifically be involved in LRP2 mediated signaling in the brain, a Morpholino based knock-down approach of these adaptors might help to ablate the function of LRP2 in the brain.
Generating zebrafish that are devoid of functional LRP2 signaling by one of the above described approaches will certainly help to further elucidate the function of this protein in forebrain development.

Bibliography

A. Amores, A. Force, Yan Y. L., L. Joly, C. Amemiya, A. Fritz, R. K. Ho, J. Langeland, V. Prince, Y. L. Wang, M. Westerfield, M. Ekker, and J. H. Postlethwait. Zebrafish hox Clusters and Vertebrate Genome Evolution. *Science*, 282(5394): 1711–4, November 1998.

O. M. Andersen, V. Schmidt, R. Spoelgen, J. Gliemann, J. Behlke, D. Galatis, W. J. McKinstry, M. W. Parker, C. L. Masters, B. T. Hyman, R. Cappai, and T. E. Willnow. Molecular Dissection of the Interaction between Amyloid Precursor Protein and Its Neuronal Trafficking Receptor SorLA/LR11. *Biochemistry*, 45 (8):2618–28, Feb 2006.

O.M. Andersen, C.H. Yeung, H. Vorum, M. Wellner, T.K. Andreassen, B. Erdmann, E.C. Mueller, J. Herz, A. Otto, T.G. Cooper, and T.E. Willnow. Essential Role of the Apolipoprotein E Receptor-2 in Sperm Development. *J. Biol. Chem.*, 278(26):23989–23995, June 27 2003.

R. M. Anderson, A. R. Lawrence, R. W. Stottmann, D. Bachiller, and J. Klingensmith. Chordin and noggin promote organizing centers of forebrain development in the mouse. *Development*, 129(21):4975–87, 2002. 0950-1991 Journal Article.

E. Assemat, F. Chatelet, J. Chandellier, F. Commo, O. Cases, P. Verroust, and R. Kozyraki. Overlapping expression patterns of the multiligand endocytic receptors cubilin and megalin in the CNS, sensory organs and developing epithelia of the rodent embryo. *Gene Expr. Patterns*, 6(1):69–78, July 2005.

D. R. Bachinsky, G. Zheng, J. L. Niles, M. McLaughlin, M. Abbate, G. Andres, D. Brown, and R. T. McCluskey. Detection of two forms of GP330. Their role in Heymann nephritis. *Am J Pathol*, 143:598–611, 1993.

W. Balemans and W. Van Hul. Extracellular regulation of BMP signaling in vertebrates: a cocktail of modulators. *Dev Biol*, 250(2):231–50, 2002. 0012-1606 Journal Article Review.

A. Bansal and L. M. Gierasch. The NPxY Internalization signal of the LDL receptor adopts a reverse-turn conformation. *Cell*, 67(6):1195–201, 1991. 0092-8674 (Print) Journal Article.

A. Barrallo-Gimeno, J. Holzschuh, W. Driever, and E. W. Knapik. Neural crest survival and differentiation in zebrafish depends on mont blanc/tfap2a gene function. *Development*, 131(7):1463–77, Apr 2004.

U. Beisiegel, W. Weber, G. Ihrke, J. Herz, and K. K. Stanley. The LDL-receptor-related protein, LRP, is an apolipoprotein E-binding protein. *Nature*, 341(6238): 162–4, 1989. 0028-0836 (Print) Journal Article.

U. Beisiegel, W. Weber, and G. Bengtsson-Olivecrona. Lipoprotein lipase enhances the binding of chylomicrons to low density lipoprotein receptor-related protein. *Proc Natl Acad Sci U S A*, 88(19):8342–6, 1991. 0027-8424 (Print) Journal Article.

S. Bieri, J. T. Djordjevic, N. L. Daly, R. Smith, and P. A. Kroon. Disulfide bridges of a cysteine-rich repeat of the LDL receptor ligand-binding domain. *Biochemistry*, 34(40):13059–65, 1995. 0006-2960 (Print) Journal Article.

I. L. Blitz, O. Shimmi, K. Wunnenberg-Stapleton, M. B. O'Connor, and K. W. Cho. Is chordin a long-range- or short-range-acting factor? Roles for BMP1-related metalloproteases in chordin and BMP4 autofeedback loop regulation. *Dev Biol*, 223(1):120–38, 2000. 0012-1606 Journal Article.

P. Boucher, M. Gotthardt, W. P. Li, R. G. Anderson, and J. Herz. LRP: role in vascular wall integrity and protection from atherosclerosis. *Science*, 300(5617): 329–32, 2003. 1095-9203 (Electronic) Journal Article.

M. M. Bradford. A rapid and sensitive method for the quantitation of microgram quantities of protein utilizing the principle of protein-dye binding. *Anal Biochem*, 72:248–54, May 1976.

M. S. Brown and J. L. Goldstein. A receptor-mediated pathway for cholesterol homeostasis. *Science*, 232(4746):34–47, 1986. 0036-8075 (Print) Journal Article Review.

M. S. Brown, J. Herz, and J. L. Goldstein. LDL-receptor structure. Calcium cages, acid baths and recycling receptors. *Nature*, 388(6643):629–30, 1997. 0028-0836 (Print) Comment News.

S. D. Brown, R. C. Twells, P. J. Hey, R. D. Cox, E. R. Levy, A. R. Soderman, M. L. Metzker, C. T. Caskey, J. A. Todd, and J. F. Hess. Isolation and characterization of LRP6, a novel member of the low density lipoprotein receptor gene family. *Biochem Biophys Res Commun*, 248(3):879–88, 1998. 0006-291X (Print) Journal Article.

W. J. Chen, J. L. Goldstein, and M. S. Brown. NPXY, a sequence often found in cytoplasmic tails, is required for coated pit-mediated internalization of the low density lipoprotein receptor. *J Biol Chem*, 265(6):3116–23, 1990. 0021-9258 (Print) Journal Article.

C. Chiang, Y. Litingtung, E. Lee, K. E. Young, J. L. Corden, H. Westphal, and P. A. Beachy. Cyclopia and defective axial patterning in mice lacking Sonic hedgehog gene function. *Nature*, 383(6599):407–13, 1996. 0028-0836 Journal Article.

E. I. Christensen and H. Birn. Megalin and cubilin: multifunctional endocytic receptors. *Nat Rev Mol Cell Biol*, 3(4):256–66, 2002. 1471-0072 (Print) Journal Article Review.

E. I. Christensen and T. E. Willnow. Essential role of megalin in renal proximal tubule for vitamin homeostasis. *J Am Soc Nephrol*, 10(10):2224–36, Oct 1999.

Jr. Cohen, M. M. and K. Shiota. Teratogenesis of holoprosencephaly. *Am J Med Genet*, 109(1):1–15, 2002. 0148-7299 (Print) Journal Article Review.

S. D. Conner and S. L. Schmid. Regulated portals of entry into the cell. *Nature*, 422(6927):37–44, Mar 2003.

J. G. Corbin, S. Nery, and G. Fishell. Telencephalic cells take a tangent: non-radial migration in the mammalian forebrain. *Nat Neurosci*, 4 Suppl:1177–82, 2001. 1097-6256 Journal Article Review Review, Tutorial.

J. K. Dale, C. Vesque, T. J. Lints, T. K. Sampath, A. Furley, J. Dodd, and M. Placzek. Cooperation of BMP7 and SHH in the induction of forebrain ventral midline cells by prechordal mesoderm. *Cell*, 90(2):257–69, 1997. 0092-8674 Journal Article.

G. D'Arcangelo, R. Homayouni, L. Keshvara, D.S. Rice, M. Sheldon, and T. Curran. Reelin is a ligand for lipoprotein receptors. *Neuron*, 24(2):471–9, Oct 1999.

Y. Dong, W. Lathrop, D. Weaver, Q. Qiu, J. Cini, D. Bertolini, and D. Chen. Molecular cloning and characterization of LR3, a novel LDL receptor family protein with mitogenic activity. *Biochem Biophys Res Commun*, 251(3):784–90, 1998. 0006-291X (Print) Journal Article.

I. A. Drummond, A. Majumdar, H. Hentschel, M. Elger, L. Solnica-Krezel, A. F. Schier, S. C. Neuhauss, D. L. Stemple, F. Zwartkruis, Z. Rangini, W. Driever, and M. C. Fishman. Early development of the zebrafish pronephros and analysis of mutations affecting pronephric function. *Development*, 125(23):4655–67, Dec 1998.

S. R. Eid and A. W. Brandli. Xenopus Na,K-ATPase: primary sequence of the beta2 subunit and in situ localization of alpha1, beta1, and gamma expression during pronephric kidney development. *Differentiation*, 68(2-3):115–25, Sep 2001.

D.S. Falconer. Two new mutations, trembler and reeler, with neurological actions in the house mouse. *J. Genet.*, 50:192–201, 1951.

Jr. Farese, R. V. and J. Herz. Cholesterol metabolism and embryogenesis. *Trends Genet*, 14(3):115–20, 1998. 0168-9525 Journal Article Review Review, Tutorial.

D. Fass, S. Blacklow, P. S. Kim, and J. M. Berger. Molecular basis of familial hypercholesterolaemia from structure of LDL receptor module. *Nature*, 388 (6643):691–3, 1997. 0028-0836 (Print) Journal Article.

P. J. Fraker and Jr. Speck, J. C. Protein and cell membrane iodinations with a sparingly soluble chloroamide, 1,3,4,6-tetrachloro-3a,6a-diphrenylglycoluril. *Biochem Biophys Res Commun*, 80(4):849–57, 1978. 0006-291X (Print) Journal Article.

P. K. Frykman, M. S. Brown, T. Yamamoto, J. L. Goldstein, and J. Herz. Normal plasma lipoproteins and fertility in gene-targeted mice homozygous for a disruption in the gene encoding very low density lipoprotein receptor. *Proc Natl Acad Sci U S A*, 92(18):8453–7, 1995. 0027-8424 (Print) Journal Article.

M. Fuccillo, M. Rallu, A. P. McMahon, and G. Fishell. Temporal requirement for hedgehog signaling in ventral telencephalic patterning. *Development*, 131(20): 5031–40, 2004. 0950-1991 Journal Article.

Y. Furuta, D. W. Piston, and B. L. Hogan. Bone morphogenetic proteins (BMPs) as regulators of dorsal forebrain development. *Development*, 124(11):2203–12, 1997. 0950-1991 Journal Article.

L.G. Gafvels, M.E. andPaavola, C.O. Boyd, P.M. Nolan, F. Wittmaack, A. Chawla, M.A. Lazar, M. Bucan, B.O. Angelin, and J.F. Strauss. Cloning of a complementary deoxyribonucleic acid encoding the murine homolog of the very low density lipoprotein/apolipoprotein-E receptor: expression pattern and assignment of the gene to mouse chromosome 19. *Endocrinology*, 135(1):387–394, 1994.

J. Gliemann. Receptors of the low density lipoprotein (LDL) receptor family in man. Multiple functions of the large family members via interaction with complex ligands. *Biol Chem*, 379(8-9):951–64, 1998. 1431-6730 (Print) Journal Article Review.

F. Gofflot, M. Kolf-Clauw, F. Clotman, C. Roux, and J. J. Picard. Absence of ventral cell populations in the developing brain in a rat model of the Smith-Lemli-Opitz syndrome. *Am J Med Genet*, 87(3):207–16, 1999. 0148-7299 Journal Article.

J. A. Golden, A. Bracilovic, K. A. McFadden, J. S. Beesley, J. L. Rubenstein, and J. B. Grinspan. Ectopic bone morphogenetic proteins 5 and 4 in the chicken forebrain lead to cyclopia and holoprosencephaly. *Proc Natl Acad Sci U S A*, 96 (5):2439–44, 1999. 0027-8424 Journal Article.

Y. Gong, R. B. Slee, N. Fukai, G. Rawadi, S. Roman-Roman, A. M. Reginato, H. Wang, T. Cundy, F. H. Glorieux, D. Lev, M. Zacharin, K. Oexle, J. Marcelino, W. Suwairi, S. Heeger, G. Sabatakos, S. Apte, W. N. Adkins, J. Allgrove, M. Arslan-Kirchner, J. A. Batch, P. Beighton, G. C. Black, R. G. Boles, L. M. Boon, C. Borrone, H. G. Brunner, G. F. Carle, B. Dallapiccola, A. De Paepe, B. Floege, M. L. Halfhide, B. Hall, R. C. Hennekam, T. Hirose, A. Jans, H. Juppner, C. A. Kim, K. Keppler-Noreuil, A. Kohlschuetter, D. LaCombe, M. Lambert, E. Lemyre, T. Letteboer, L. Peltonen, R. S. Ramesar, M. Romanengo, H. Somer, E. Steichen-Gersdorf, B. Steinmann, B. Sullivan, A. Superti-Furga, W. Swoboda, M. J. van den Boogaard, W. Van Hul, M. Vikkula, M. Votruba,

B. Zabel, T. Garcia, R. Baron, B. R. Olsen, and M. L. Warman. LDL receptor-related protein 5 (LRP5) affects bone accrual and eye development. *Cell*, 107 (4):513–23, 2001. 0092-8674 (Print) Journal Article.

M. Gotthardt, M. Trommsdorff, M. F. Nevitt, J. Shelton, J. A. Richardson, W. Stockinger, J. Nimpf, and J. Herz. Interactions of the low density lipoprotein receptor gene family with cytosolic adaptor and scaffold proteins suggest diverse biological functions in cellular communication and signal transduction. *J Biol Chem*, 275(33):25616–24, 2000. 0021-9258 (Print) Journal Article.

J.R. Goudriaan, P.J. Tacken, V.E.H. Dahlmans, M.J.J. Gijbels, K.W. van Dijk, L.M. Havekes, and M.C. Jong. Protection From Obesity in Mice Lacking the VLDL Receptor. *Arterioscler Thromb Vasc Biol*, 21(9):1488–1493, 2001.

R. E. Gross, M. F. Mehler, P. C. Mabie, Z. Zang, L. Santschi, and J. A. Kessler. Bone morphogenetic proteins promote astroglial lineage commitment by mammalian subventricular zone progenitor cells. *Neuron*, 17(4):595–606, 1996. 0896-6273 Journal Article.

R. J. Havel. Biology of cholesterol, lipoproteins and atherosclerosis. *Clin Exp Hypertens A*, 11(5-6):887–900, 1989. 0730-0077 (Print) Journal Article Review.

J. Heasman, M. Kofron, and C. Wylie. Beta-catenin signaling activity dissected in the early Xenopus embryo: a novel antisense approach. *Dev Biol*, 222(1): 167–80, Jun 2000.

L. Hermo, M. Lustig, S. Lefrancois, W. S. Argraves, and C. R. Morales. Expression and regulation of LRP-2/megalin in epithelial cells lining the efferent ducts and epididymis during postnatal development. *Mol Reprod Dev.*, 53(3):282–93, Jul 1999.

J. Herz, U. Hamann, S. Rogne, O. Myklebost, H. Gausepohl, and K.K. Stanley. Surface location and high affinity for calcium of a 500-kd liver membrane protein closely related to the LDL-receptor suggest a physiological role as lipoprotein receptor. *EMBO J.*, 7(13):4119–27, Dec 20 1988.

J. Herz, D.E. Clouthier, and R.E. Hammer. LDL receptor-related protein internalizes and degrades uPA-PAI-1 complexes and is essential for embryo implantation. *Cell*, 71(3):411–21, Oct 1993.

P. J. Hey, R. C. Twells, M. S. Phillips, Nakagawa Yusuke, S. D. Brown, Y. Kawaguchi, R. Cox, Xie Guochun, V. Dugan, H. Hammond, M. L. Metzker, J. A. Todd, and J. F. Hess. Cloning of a novel member of the low-density lipoprotein receptor family. *Gene*, 216(1):103–11, 1998. 0378-1119 (Print) Journal Article.

T. Hiesberger, M. Trommsdorff, B. W. Howell, A. Goffinet, M. C. Mumby, J. A. Cooper, and J. Herz. Direct binding of Reelin to VLDL receptor and ApoE receptor 2 induces tyrosine phosphorylation of disabled-1 and modulates tau phosphorylation. *Neuron*, 24(2):481–9, 1999. 0896-6273 Journal Article.

J. Hilpert, A. Nykjaer, C. Jacobsen, G. Wallukat, R. Nielsen, S. K. Moestrup, H. Haller, F. C. Luft, E. I. Christensen, and T. E. Willnow. Megalin antagonizes activation of the parathyroid hormone receptor. *J Biol Chem*, 274(9):5620–5, 1999. 0021-9258 Journal Article.

G. Hjalm, E. Murray, G. Crumley, W. Harazim, S. Lundgren, I. Onyango, B. Ek, M. Larsson, C. Juhlin, P. Hellman, H. Davis, G. Akerstrom, L. Rask, and B. Morse. Cloning and sequencing of human gp330, a Ca(2+)-binding receptor with potential intracellular signaling properties. *Eur J Biochem*, 239(1):132–7, 1996. 0014-2956 (Print) Journal Article.

S. Horne-Badovinac, D. Lin, S. Waldron, M. Schwarz, G. Mbamalu, T. Pawson, Y. Jan, D. Y. Stainier, and S. Abdelilah-Seyfried. Positional cloning of heart and soul reveals multiple roles for PKC lambda in zebrafish organogenesis. *Curr Biol*, 11(19):1492–502, Oct 2001.

C. Houston, D.W. Wylie. Cloning and expression of Xenopus Lrp5 and Lrp6 genes. *Mech Dev.*, 117(1-2):337–42, Sep 2002.

B. W. Howell, T. M. Herrick, and J. A. Cooper. Reelin-induced tryosine phosphorylation of disabled 1 during neuronal positioning. *Genes Dev*, 13(6):643–8, 1999. 0890-9369 (Print) Journal Article.

C. J. Huang, C. T. Tu, C. D. Hsiao, F. J. Hsieh, and H. J. Tsai. Germ-line transmission of a myocardium-specific GFP transgene reveals critical regulatory elements in the cardiac myosin light chain 2 promoter of zebrafish. *Dev Dyn*, 228(1):30–40, Sep 2003.

S. Huh, V. Hatini, R. C. Marcus, S. C. Li, and E. Lai. Dorsal-ventral patterning defects in the eye of BF-1-deficient mice associated with a restricted loss of shh expression. *Dev Biol*, 211(1):53–63, 1999. 0012-1606 Journal Article.

H. Iijima, M. Miyazawa, J. Sakai, K. Magoori, M. R. Ito, H. Suzuki, M. Nose, Y. Kawarabayasi, and T. T. Yamamoto. Expression and characterization of a very low density lipoprotein receptor variant lacking the O-linked sugar region generated by alternative splicing. *J Biochem (Tokyo)*, 124(4):747–55, 1998. 0021-924X (Print) Journal Article.

P. W. Ingham and A. P. McMahon. Hedgehog signaling in animal development: paradigms and principles. *Genes Dev*, 15(23):3059–87, 2001. 0890-9369 (Print) Journal Article Review.

T. Inoue, S. Nakamura, and N. Osumi. Fate mapping of the mouse prosencephalic neural plate. *Dev Biol*, 219(2):373–83, 2000. 0012-1606 (Print) Journal Article.

S. Ishibashi, M. S. Brown, J. L. Goldstein, R. D. Gerard, R. E. Hammer, and J. Herz. Hypercholesterolemia in low density lipoprotein receptor knockout mice and its reversal by adenovirus-mediated gene delivery. *J Clin Invest*, 92(2): 883–93, 1993. 0021-9738 (Print) Journal Article.

L. Jacobsen, P. Madsen, S.K. Moestrup, A.H. Lund, N. Tommerup, A. Nykjaer, L. Sottrup-Jensen, J. Gliemann, and C.M. Petersen. Molecular characterization of a novel human hybrid-type receptor that binds the alpha2-macroglobulin receptor-associated protein. *J Biol Chem.*, 271(49):31379–83, Dec 1996.

H. R. Jacobson. Functional segmentation of the mammalian nephron. *Am J Physiol*, 241(3):F203–18, Sep 1981.

H. Jeon, W. Meng, J. Takagi, M. J. Eck, T.A. Springer, and S. C. Blacklow. Implications for familial hypercholesterolemia from the structure of the LDL receptor YWTD-EGF domain pair. *Nat Struct Biol.*, 8(6):499–504, Jun 2001.

Y. Jeong, K. El-Jaick, E. Roessler, M. Muenke, and D.J. Epstein. A functional screen for sonic hedgehog regulatory elements across a 1 Mb interval identifies long-range ventral forebrain enhancers. *Development*, 133(4):761–72, Feb 2006.

E. B. Johnson, R. E. Hammer, and J. Herz. Abnormal development of the apical ectodermal ridge and polysyndactyly in Megf7-deficient mice. *Hum Mol Genet*, 14(22):3523–38, November 2005.

R. L. Kelley, E. Roessler, R. C. Hennekam, G. L. Feldman, K. Kosaki, M. C. Jones, J. C. Palumbos, and M. Muenke. Holoprosencephaly in RSH/Smith-Lemli-Opitz syndrome: does abnormal cholesterol metabolism affect the function of Sonic Hedgehog? *Am J Med Genet*, 66(4):478–84, 1996. 0148-7299 Journal Article.

D. Kerjaschki and M. G. Farquhar. The pathogenic antigen of Heymann nephritis is a membrane glycoprotein of the renal proximal tubule brush border. *Proc Natl Acad Sci U S A*, 79(18):5557–61, 1982. 0027-8424 (Print) Journal Article.

D. H. Kim, Iijima H., K. Goto, J. Sakai, H. Ishii, H.J. Kim, H. Suzuki, H. Kondo, S. Saeki, and T. Yamamoto. Human Apolipoprotein E Receptor 2. *J. Biol. Chem.*, 271(14):8373–8380, 1996.

C. B. Kimmel, W. W. Ballard, S. R. Kimmel, B. Ullmann, and T. F. Schilling. Stages of embryonic development of the Zebrafish. *Dev Dyn*, 203(3):253–310, Jul 1995.

M. Koornreef, L. W. Dellaert, and J. H. van der Veen. EMS- and radiation-induced mutation frequencies at individual loci in Arabidopsis thaliana (L.) Heynh. *Mutat Res*, 93(1):109–23, Mar 1982.

M. Z. Kounnas, J. Henkin, W. S. Argraves, and D. K. Strickland. Low density lipoprotein receptor-related protein/alpha 2-macroglobulin receptor mediates cellular uptake of pro-urokinase. *J Biol Chem*, 268(29):21862–7, 1993. 0021-9258 (Print) Journal Article.

M. Z. Kounnas, C. C. Haudenschild, D. K. Strickland, and W. S. Argraves. Immunological localization of glycoprotein 330, low density lipoprotein receptor related protein and 39 kDa receptor associated protein in embryonic mouse tissues. *In Vivo*, 8(3):343–51, 1994. 0258-851X (Print) Journal Article.

M. Z. Kounnas, R. D. Moir, G. W. Rebeck, A. I. Bush, W. S. Argraves, R. E. Tanzi, B. T. Hyman, and D. K. Strickland. LDL receptor-related protein, a multifunctional ApoE receptor, binds secreted beta-amyloid precursor protein and mediates its degradation. *Cell*, 82(2):331–40, 1995. 0092-8674 (Print) Journal Article.

K. Kozarsky, D. Kingsley, and M. Krieger. Use of a mutant cell line to study the kinetics and function of O-linked glycosylation of low density lipoprotein

receptors. *Proc Natl Acad Sci U S A*, 85(12):4335–9, 1988. 0027-8424 (Print) Journal Article.

S. Langbein, O. Szakacs, M. Wilhelm, F. Sukosd, S. Weber, A. Jauch, B.A. Lopez, Alken P., T. Kalble, and G. Kovacs. Alteration of the LRP1B gene region is associated with high grade of urothelial cancer. *Lab Investig.*, 82(5):639–43, May 2002.

L. Lanoue, D. B. Dehart, M. E. Hinsdale, N. Maeda, G. S. Tint, and K. K. Sulik. Limb, genital, CNS, and facial malformations result from gene/environment-induced cholesterol deficiency: further evidence for a link to sonic hedgehog. *Am J Med Genet*, 73(1):24–31, 1997. 0148-7299 (Print) Journal Article.

L.Y. Lee, W.A. Mohler, B.L. Schafer, Freudenberger J.S., N. Byrne-Connolly, K.B. Eager, S.T. Mosley, J.K. Leighton, R.N. Thrift, and Davis R.A. Nucleotide sequence of the rat low density lipoprotein receptor cDNA. *Nucleic Acids Res.*, 17(3):1259–1260, February 11 1989.

J. R. Leheste, B. Rolinski, H. Vorum, J. Hilpert, A. Nykjaer, C. Jacobsen, P. Aucouturier, J. O. Moskaug, A. Otto, E. I. Christensen, and T. E. Willnow. Megalin knockout mice as an animal model of low molecular weight proteinuria. *Am J Pathol*, 155(4):1361–70, 1999. 0002-9440 Journal Article.

J. R. Leheste, F. Melsen, M. Wellner, P. Jansen, U. Schlichting, I. Renner-Muller, T. T. Andreassen, E. Wolf, S. Bachmann, A. Nykjaer, and T. E. Willnow. Hypocalcemia and osteopathy in mice with kidney-specific megalin gene defect. *Faseb J*, 17(2):247–9, 2003. 1530-6860 Journal Article.

Jr. Liem, K. F., G. Tremml, H. Roelink, and T. M. Jessell. Dorsal differentiation of neural plate cells induced by BMP-mediated signals from epidermal ectoderm. *Cell*, 82(6):969–79, 1995. 0092-8674 Journal Article.

D. A. Lim, A. D. Tramontin, J. M. Trevejo, D. G. Herrera, J. M. Garcia-Verdugo, and A. Alvarez-Buylla. Noggin antagonizes BMP signaling to create a niche for adult neurogenesis. *Neuron*, 28(3):713–26, 2000. 0896-6273 (Print) Journal Article.

C. X. Liu, Y. Li, L. M. Obermoeller-McCormick, A. L. Schwartz, and G. Bu. The putative tumor suppressor LRP1B, a novel member of the low density lipoprotein (LDL) receptor family, exhibits both overlapping and distinct properties with the

LDL receptor-related protein. *J Biol Chem*, 276(31):28889–96, 2001. 0021-9258 (Print) Journal Article.

Q. R. Lu, D. Yuk, J. A. Alberta, Z. Zhu, I. Pawlitzky, J. Chan, A. P. McMahon, C. D. Stiles, and D. H. Rowitch. Sonic hedgehog-regulated oligodendrocyte lineage genes encoding bHLH proteins in the mammalian central nervous system. *Neuron*, 25(2):317–29, 2000. 0896-6273 Journal Article.

A. Majumdar, K. Lun, M. Brand, and I. A. Drummond. Zebrafish no isthmus reveals a role for pax2.1 in tubule differentiation and patterning events in the pronephric primordia. *Development*, 127(10):2089–98, 2000.

O. Marin and J. L. Rubenstein. A long, remarkable journey: tangential migration in the telencephalon. *Nat Rev Neurosci*, 2(11):780–90, 2001. 1471-003x Journal Article Review Review, Tutorial.

O. Marin, S. A. Anderson, and J. L. Rubenstein. Origin and molecular specification of striatal interneurons. *J Neurosci*, 20(16):6063–76, 2000. 0270-6474 Journal Article.

P. Marschang, J. Brich, E. J. Weeber, J. D. Sweatt, J.M. Shelton, J.A. Richardson, R.E. Hammer, and J. Herz. Normal Development and Fertility of Knockout Mice Lacking the Tumor Suppressor Gene LRP1b Suggest Functional Compensation by LRP1. *Mol. Cell. Biol.*, 24(9):3782–3793, 2004.

E. Matsunaga and K. Shiota. Holoprosencephaly in human embryos: epidemiologic studies of 150 cases. *Teratology*, 16(3):261–72, 1977. 0040-3709 (Print) Journal Article.

C. M. McCallum, L. Comai, E. A. Greene, and S. Henikoff. Targeted screening for induced mutations. *Nature Biotechnol*, 18(4):455–7, Apr 2000.

R. A. McCarthy and W. S. Argraves. Megalin and the neurodevelopmental biology of sonic hedgehog and retinol. *J Cell Sci*, 116(Pt 6):955–60, 2003. 0021-9533 Journal Article Review.

R. A. McCarthy, J. L. Barth, M. R. Chintalapudi, C. Knaak, and W. S. Argraves. Megalin functions as an endocytic sonic hedgehog receptor. *J Biol Chem*, 277 (28):25660–7, 2002. 0021-9258 Journal Article.

J. A. McMahon, S. Takada, L. B. Zimmerman, C. M. Fan, R. M. Harland, and A. P. McMahon. Noggin-mediated antagonism of BMP signaling is required for growth and patterning of the neural tube and somite. *Genes Dev*, 12(10): 1438–52, 1998. 0890-9369 Journal Article.

A. L. Menke and A. Schedl. WT1 and glomerular function. *Semin Cell Dev Biol*, 14(4):233–40, August 2003.

S. K. Moestrup, J. Gliemann, and G. Pallesen. Distribution of the alpha 2-macroglobulin receptor/low density lipoprotein receptor-related protein in human tissues. *Cell Tissue Res*, 269(3):375–82, 1992. 0302-766X (Print) Journal Article.

S. K. Moestrup, H. Birn, P. B. Fischer, C. M. Petersen, P. J. Verroust, R. B. Sim, E. I. Christensen, and E. Nexo. Megalin-mediated endocytosis of transcobalamin-vitamin-B12 complexes suggests a role of the receptor in vitamin-B12 homeostasis. *Proc Natl Acad Sci U S A*, 93(16):8612–7, 1996. 0027-8424 (Print) Journal Article.

S.K. Moestrup, I. Schousboe, C. Jacobsen, J. R. Leheste, E. I. Christensen, , and T. E. Willnow. Beta2-glycoprotein-i (apolipoprotein h) and beta2-glycoprotein-i-phospholipid complex harbor a recognition site for the endocytic receptor megalin. *J Clin Invest*, 102(5):902–9, Sep 1998.

S. M. Morris, M. D. Tallquist, C. O. Rock, and J. A. Cooper. Dual roles for the Dab2 adaptor protein in embryonic development and kidney transport. Dual roles for the Dab2 adaptor protein in embryonic development and kidney transport. Dual roles for the Dab2 adaptor protein in embryonic development and kidney transport. *EMBO J.*, 21(7):1555–64, April 2002.

S. Morwald, H. Yamazaki, H. Bujo, J. Kusunoki, T. Kanaki, K. Seimiya, N. Morisaki, J. Nimpf, W.J. Schneider, and Y. Saito. A novel mosaic protein containing LDL receptor elements is highly conserved in humans and chickens. *Arterioscler Thromb Vasc Biol.*, 17(5):996–1002, May 1997.

T. Mueller and M. F. Wullimann. *Atlas of Early Zebrafish Brain Development Atlas of early Zebrafish brain development. A Tool for Molecular Neurogenetics.* Elsevier, 2005.

M. Nakayama, D. Nakajima, T. Nagase, N. Nomura, N. Seki, and O. Ohara. Identification of high-molecular-weight proteins with multiple EGF-like motifs by motif-trap screening. *Genomics*, 51(1):27–34, 1998. 0888-7543 (Print) Journal Article.

A. Nasevicius and S. C. Ekker. Effective targeted gene 'knockdown' in zebrafish. *Nat Genet*, 26(2):216–20, Oct 2000.

Y. Nemoto and P. De Camilli. Recruitment of an alternatively spliced form of synaptojanin 2 to mitochondria by the interaction with the PDZ domain of a mitochondrial outer membrane protein. *EMBO J.*, 18(11):2991–3006, Jun 1999.

S. Nery, H. Wichterle, and G. Fishell. Sonic hedgehog contributes to oligodendrocyte specification in the mammalian forebrain. *Development*, 128(4):527–40, 2001. 0950-1991 Journal Article.

S. Novak, T. Hiesberger, W. J. Schneider, and J. Nimpf. A New Low Density Lipoprotein Receptor Homologue with 8 Ligand Binding Repeats in Brain of Chicken and Mouse. *J. Biol. Chem.*, 271(20):11732–11736, 1996.

A. Nykjaer, D. Dragun, D. Walther, H. Vorum, C. Jacobsen, J. Herz, F. Melsen, E. I. Christensen, and T. E. Willnow. An endocytic pathway essential for renal uptake and activation of the steroid 25-(OH) vitamin D3. *Cell*, 96(4):507–15, 1999. 0092-8674 Journal Article.

K. Offe, S. E. Dodson, J. T. Shoemaker, J. J. Fritz, M. Gearing, AI. Levey, and J. J. Lah. The lipoprotein receptor LR11 regulates amyloid beta production and amyloid precursor protein traffic in endosomal compartments. *J Neurosci.*, 26 (5):1596–603, Feb 2006.

Y. Ohkubo, C. Chiang, and J. L. Rubenstein. Coordinate regulation and synergistic actions of BMP4, SHH and FGF8 in the rostral prosencephalon regulate morphogenesis of the telencephalic and optic vesicles. *Neuroscience*, 111(1): 1–17, 2002. 0306-4522 Journal Article.

A. V. Oleinikov, J. Zhao, and S. P. Makker. Cytosolic adaptor protein Dab2 is an intracellular ligand of endocytic receptor gp600/megalin. *Biochem J*, 347(3): 613–21, May 2000.

D. Onichtchouk, Y. G. Chen, R. Dosch, V. Gawantka, H. Delius, J. Massague, and C. Niehrs. Silencing of TGF-beta signalling by the pseudoreceptor BAMBI. *Nature*, 401(6752):480–5, 1999. 0028-0836 Journal Article.

D. M. Orentas, J. E. Hayes, K. L. Dyer, and R. H. Miller. Sonic hedgehog signaling is required during the appearance of spinal cord oligodendrocyte precursors. *Development*, 126(11):2419–29, 1999. 0950-1991 Journal Article.

R. A. Orlando and M. G. Farquhar. Identification of a cell line that expresses a cell surface and a soluble form of the gp330/receptor-associated protein (RAP) Heymann nephritis antigenic complex. *PNAS*, 90:4082–6, 1993.

L. Pelkmans, E. Fava, H. Grabner, M. Hannus, B. Habermann, E. Krausz, and M. Zerial. Genome-wide analysis of human kinases in clathrin- and caveolae/raft-mediated endocytosis. *Nature*, 436(7047):78–86, Jul 2005.

H. H. Petersen, J. Hilpert, D. Militz, V. Zandler, C. Jacobsen, A. J. Roebroek, and T. E. Willnow. Functional interaction of megalin with the megalinbinding protein (MegBP), a novel tetratrico peptide repeat-containing adaptor molecule. *J Cell Sci*, 116(Pt 3):453–61, 2003. 0021-9533 (Print) Journal Article.

R. T. Peterson, J. D. Mably, J. N. Chen, and M. C. Fishman. Convergence of distinct pathways to heart patterning revealed by the small molecule concentramide and the mutation heart-and-soul. *Curr Biol*, 11(19):1481–91, Oct 2001.

K. I. Pinson, J. Brennan, S. Monkley, B. J. Avery, and W. C. Skarnes. An LDL-receptor-related protein mediates Wnt signalling in mice. *Nature*, 407(6803): 535–8, 2000. 0028-0836 Journal Article.

J. A. Porter, K. E. Young, and P. A. Beachy. Cholesterol modification of hedgehog signaling proteins in animal development. *Science*, 274(5285):255–9, 1996. 0036-8075 Journal Article.

K. Rader, R. A. Orlando, X. Lou, and M. G. Farquhar. Characterization of ANKRA, a novel ankyrin repeat protein that interacts with the cytoplasmic domain of megalin. *J Am Soc Nephrol*, 11(12):2167–78, Dec 2000.

E. Roach, W. Demyer, P. M. Conneally, C. Palmer, and A. D. Merritt. Holoprosencephaly: birth data, benetic and demographic analyses of 30 families. *Birth Defects Orig Artic Ser*, 11(2):294–313, 1975. 0547-6844 (Print) Journal Article.

E. Roessler, E. Belloni, K. Gaudenz, P. Jay, P. Berta, S. W. Scherer, L. C. Tsui, and M. Muenke. Mutations in the human Sonic Hedgehog gene cause holoprosencephaly. *Nat Genet*, 14(3):357–60, 1996. 1061-4036 Journal Article.

A. Rohlmann, M. Gotthardt, T. E. Willnow, R. E. Hammer, and J. Herz. Sustained somatic gene inactivation by viral transfer of Cre recombinase. *Nat Biotechnol*, 14(11):1562–5, Nov 1996.

S. Rohr, N. Bit-Avragim, and S. Abdelilah-Seyfried. Heart and soul/PRKCi and nagie oko/Mpp5 regulate myocardial coherence and remodeling during cardiac morphogenesis. *Development*, 133(1):107–15, Jan 2006.

D. H. Rowitch, S. Jacques B, S. M. Lee, J. D. Flax, E. Y. Snyder, and A. P. McMahon. Sonic hedgehog regulates proliferation and inhibits differentiation of CNS precursor cells. *J Neurosci*, 19(20):8954–65, 1999. 1529-2401 Journal Article.

J. L. Rubenstein, K. Shimamura, S. Martinez, and L. Puelles. Regionalization of the prosencephalic neural plate. *Annu Rev Neurosci*, 21:445–77, 1998. 0147-006X (Print) Journal Article Review.

G. Rudenko, L. Henry, K. Henderson, K. Ichtchenko, M. S. Brown, J. L. Goldstein, and J. Deisenhofer. Structure of the LDL receptor extracellular domain at endosomal pH. *Science*, 298(5602):2353–8, 2002. 1095-9203 (Electronic) Journal Article.

Thomas Sadler. *Langman's Medical Embryology*. Lippincott, Williams, Wilkins, 2003.

A. Saito, S. Pietromonaco, A. K. Loo, and M. G. Farquhar. Complete cloning and sequencing of rat gp330/"megalin," a distinctive member of the low density lipoprotein receptor gene family. *Proc Natl Acad Sci U S A*, 91(21):9725–9, 1994. 0027-8424 Journal Article.

Y. Sasai and E. M. De Robertis. Ectodermal patterning in vertebrate embryos. *Dev Biol*, 182(1):5–20, 1997. 0012-1606 Journal Article Review.

R. A. Schneider, D. Hu, J. L. Rubenstein, M. Maden, and J. A. Helms. Local retinoid signaling coordinates forebrain and facial morphogenesis by maintaining FGF8 and SHH. *Development*, 128(14):2755–67, 2001. 0950-1991 Journal Article.

F. C. Serluca and M. C. Fishman. Pre-pattern in the pronephric kidney field of zebrafish. *Development*, 128(12):2233–2241, Jun 2001.

M. Sheng and D. T. Pak. Glutamate receptor anchoring proteins and the molecular organization of excitatory synapses. *Ann N Y Acad Sci*, 868:483–93, Apr 1999.

D. Simon-Chazottes, S. Tutois, M. Kuehn, M. Evans, F. Bourgade, S. Cook, M. T. Davisson, and J. L. Guenet. Mutations in the gene encoding the low-density lipoprotein receptor LRP4 cause abnormal limb development in the mouse. *Genomics*, Epup ahead of print, March 2006.

R. Spoelgen, A. Hammes, U. Anzenberger, D. Zechner, O. M. Andersen, B. Jerchow, and T. E. Willnow. LRP2/megalin is required for patterning of the ventral telencephalon. *Development*, 132(2):405–14, Jan 2005.

S. Stefansson, D. A. Chappell, K. M. Argraves, D. K. Strickland, and W. S. Argraves. Glycoprotein 330/low density lipoprotein receptor-related protein-2 mediates endocytosis of low density lipoproteins via interaction with apolipoprotein B100. *J Biol Chem*, 270(33):19417–21, 1995a. 0021-9258 (Print) Journal Article.

S. Stefansson, M. Z. Kounnas, J. Henkin, R. K. Mallampalli, D. A. Chappell, D. K. Strickland, and W. S. Argraves. gp330 on type II pneumocytes mediates endocytosis leading to degradation of pro-urokinase, plasminogen activator inhibitor-1 and urokinase-plasminogen activator inhibitor-1 complex. *J Cell Sci*, 108 (Pt 6):2361–8, 1995b. 0021-9533 (Print) Journal Article.

W. Stockinger, E. Hengstschlager-Ottnad, S. Novak, A. Matus, M. Huttinger, J. Bauer, H. Lassmann, W. J. Schneider, and J. Nimpf. The low density lipoprotein receptor gene family. Differential expression of two alpha2-macroglobulin receptors in the brain. *J. Biol. Chem.*, 273(48):32213–32221, 1998.

L. Sussel, O. Marin, S. Kimura, and J. L. Rubenstein. Loss of Nkx2.1 homeobox gene function results in a ventral to dorsal molecular respecification within the basal telencephalon: evidence for a transformation of the pallidum into the striatum. *Development*, 126(15):3359–70, 1999. 0950-1991 Journal Article.

H. O. Sweet, R. T. Bronson, K. R. Johnson, S. A. Cook, and M. T. Davisson. Scrambler, a new neurological mutation of the mouse with abnormalities of

neuronal migration. *Mamm Genome*, 7(11):798–802, 1996. 0938-8990 (Print) Journal Article.

S. Takahashi, Y. Kawarabayasi, T. Nakai, J. Sakai, and T. Yamamoto. Rabbit Very Low Density Lipoprotein Receptor: A Low Density Lipoprotein density Receptor-Like Protein with Distinct Ligand Specificity. *PNAS*, 89(19):9252–9256, Oct 1992.

M. D. Tallquist and P. Soriano. Epiblast-restricted Cre expression in MORE mice: a tool to distinguish embryonic vs. extra-embryonic gene function. *Genesis*, 26 (2):113–5, 2000. 1526-954x Journal Article.

K. Tamai, M. Semenov, Y. Kato, R. Spokony, C. Liu, Y. Katsuyama, F. Hess, J. P. Saint-Jeannet, and X. He. LDL-receptor-related proteins in Wnt signal transduction. *Nature*, 407(6803):530–5, 2000. 0028-0836 (Print) Journal Article.

J. S. Taylor, Y. Van de Peer, I. Braasch, and A. Meyer. Comparative genomics provides evidence for an ancient genome duplication event in fish. *Philosophical Transactions of the Royal Society B: Biological Sciences*, 356(1414):1661–79, October 2001.

J. R. Timmer, C. Wang, and L. Niswander. BMP signaling patterns the dorsal and intermediate neural tube via regulation of homeobox and helix-loop-helix transcription factors. *Development*, 129(10):2459–72, 2002. 0950-1991 Journal Article.

M. Trommsdorff, M. Gotthardt, T. Hiesberger, J. Shelton, W. Stockinger, J. Nimpf, R. E. Hammer, J. A. Richardson, and J. Herz. Reeler/Disabled-like disruption of neuronal migration in knockout mice lacking the VLDL receptor and ApoE receptor 2. *Cell*, 97(6):689–701, 1999. 0092-8674 Journal Article.

A. von Bubnoff and K. W. Cho. Intracellular BMP signaling regulation in vertebrates: pathway or network? *Dev Biol*, 239(1):1–14, 2001. 0012-1606 (Print) Journal Article Review.

D. E. Wallis and M. Muenke. Molecular mechanisms of holoprosencephaly. *Mol Genet Metab*, 68(2):126–38, 1999. 1096-7192 Journal Article Review Review, Tutorial.

M. Wehrli, S. T. Dougan, K. Caldwell, L. O'Keefe, S. Schwartz, D. Vaizel-Ohayon, E. Schejter, A. Tomlinson, and S. DiNardo. arrow encodes an LDL-receptor-related protein essential for Wingless signalling. *Nature*, 407(6803):527–30, 2000. 0028-0836 Journal Article.

X. Wei and J. Malicki. nagie oko, encoding a MAGUK-family protein, is essential for cellular patterning of the retina. *Nat Genet*, 31(2):150–7, Jun 2002.

T. E. Willnow. Receptor-associated protein (RAP): a specialized chaperone for endocytic receptors. *Biol Chem*, 379(8-9):1025–31, 1998. 1431-6730 (Print) Journal Article Review.

T. E. Willnow and J. Herz. Animal models for disorders of hepatic lipoprotein metabolism. *J Mol Med*, 73(5):213–20, 1995. 0946-2716 Journal Article Review Review, Tutorial.

T. E. Willnow, J. L. Goldstein, K. Orth, M. S. Brown, and J. Herz. Low density lipoprotein receptor-related protein and gp330 bind similar ligands, including plasminogen activator-inhibitor complexes and lactoferrin, an inhibitor of chylomicron remnant clearance. *J Biol Chem*, 267(36):26172–80, 1992. 0021-9258 Journal Article.

T. E. Willnow, K. Orth, and J. Herz. Molecular dissection of ligand binding sites on the low density lipoprotein receptor-related protein. *J Biol Chem*, 269(22): 15827–32, 1994. 0021-9258 Journal Article.

T. E. Willnow, J. Hilpert, S. A. Armstrong, A. Rohlmann, R. E. Hammer, D. K. Burns, and J. Herz. Defective forebrain development in mice lacking gp330/megalin. *Proc Natl Acad Sci U S A*, 93(16):8460–4, 1996a. 0027-8424 Journal Article.

T. E. Willnow, A. Rohlmann, J. Horton, H. Otani, J. R. Braun, R. E. Hammer, and J. Herz. RAP, a specialized chaperone, prevents ligand-induced ER retention and degradation of LDL receptor-related endocytic receptors. *Embo J*, 15(11): 2632–9, 1996b. 0261-4189 Journal Article.

S. W. Wilson and C. Houart. Early steps in the development of the forebrain. *Dev Cell*, 6(2):167–81, 2004. 1534-5807 Journal Article Review.

K.L. Wyne, R.K. Pathak, M.C. Seabra, and H.H. Hobbs. Expression of the VLDL Receptor in Endothelial Cells. *Arterioscler Thromb Vasc Biol*, 16(3):407–415, 1996.

H. Yamazaki, H. Bujo, J. Kusunoki, K. Seimiya, T. Kanaki, N. Morisaki, W.J. Schneider, and Y. Saito. Elements of neural adhesion molecules and a yeast vacuolar protein sorting receptor are present in a novel mammalian low density lipoprotein receptor family member. *J Biol Chem.*, 271(40):24761–8, Oct 1996.

J. Yochem, S. Tuck, I. Greenwald, and M. Han. A gp330/megalin-related protein is required in the major epidermis of Caenorhabditis elegans for completion of molting. *Development*, 126(3):597–606, Feb 1999.

G. Zheng, D. R. Bachinsky, M. Abbate, G. Andres, D. Brown, I. Stamenkovic, J. L. Niles, and R. T. McCluskey. gp330: receptor and autoantigen. *Ann N Y Acad Sci*, 737:154–62, 1994. 0077-8923 Journal Article Review Review, Tutorial.

X. Zhou and P. D. Vize. Proximo-distal specialization of epithelial transport processes within the Xenopus pronephric kidney tubules. *Dev Biol*, 271(2):322–38, Jul 2004.

7 Appendix

7.1 Abbreviations

asn	asparagine
asp	aspartate
ATP	adenosin triphosphate
bp	basepairs
CCD	charged coupled device
CTP	cytidine triphosphate
dATP	deoxyadenosine triphosphate
dCTP	deoxycytidine triphosphate
ddH_2O	double distilled H_2O
dGTP	deoxyguanosin triphosphate
DIG	digoxygenin
dNTP	deoxynucleotide triphosphate
dUTP	deoxyuridine triphosphate
DNA	desoxyribonucleic acid
E	embryonic day
EDTA	ethylenediaminetetraacetic acid
EGTA	ethyleneglycoltetraacetic acid
g	gram
glx	glutamine or glutamic acid
GTP	guanosine triphosphate
HCl	hydrogen chloride
HEPES	hydroxyethylpiperazineethanesulfonic acid
hrs	hours
K	potassium
KCl	potassium chloride
kDa	kilodalton
kV	kilovolt
l	liter
LB	lysogeny broth
mg	miligram
$MgCl_2$	magnesium chloride

min	minute
ml	milliliter
mM	millimolar
mRNA	messenger ribonucleic acid
M	molar
N	asparagine
NaCl	sodium chloride
NaOH	sodiumhydroxide
ng	nanogram
nl	nanoliter
P	proline
pH	potential of hydrogen
PMSF	phenylmethanesulfonyl fluoride
pro	proline
RT	room temperature
RNA	ribonucleic acid
S	serine
sec	second
SDS	sodium dodecyl sulfate
SOC	super optimal broth with catabolite repression
Taq	*thermus aquaticus*
Tris	trishydroxymethylaminomethane
TUNEL	terminal transferase dUTP nick end labeling
Tyr	tyrosine
U	unit
UTP	uridine triphosphate
UV	ultraviolett
V	volt
wt	wildtype
Y	tyrosine
μ	micro

7.2 Danksagung

Ich bedanke mich herzlichst bei Prof. Dr. Thomas E. Willnow für die Überlassung des Themas, für die stets ausgezeichnete Betreuung meiner Arbeit sowie für die erstklassigen Arbeitsbedingungen in seinem Labor. Ein großes Dankeschön gilt meinen Arbeitskollegen der AG Willnow. Namentlich erwähnen möchte ich meinen Bürokollegen Dr. Tilman Breiderhoff, der stets den ein oder anderen klugen Lösungsansatz bei experimentellen Problemen jedweder Art parat hatte. Für die Einführung in die BIAcore Analysetechnik bedanke ich mich bei Dr. Olav Andersen. Bei Dr. Annette Hammes-Lewin und Dr. Robert Spoelgen bedanke ich mich für die Hilfe beim Präparieren von Mäuseembryonen und für die Einarbeitung in die Technik der *In-situ*-Hybridisierungen. Bei allen anderen Kollegen möchte ich mich für das gute Arbeitsklima und die stete Bereitschaft zur Problemdiskussion bedanken.

Mein besonderer Dank gilt Prof. Dr. Wolfgang Lockau von der Humboldt Universität zu Berlin für die Betreuung meiner Arbeit.

Bei den technischen Assistenten der AG Willnow möchte ich mich ebenfalls bedanken, Charlotte Räder für die Hilfe bei der Genotypisierung transgener Tiere, Donate Vetter für die Unterstützung bei der ein oder anderen PCR, Klonierung oder DNA-Präparation und Susanne Schütz für die erstklassige Versuchstierpflege.

Ich bedanke mich ebenfalls herzlich bei Dr. Salim A. Seyfried für die Möglichkeit, Experimente am Zebrafisch durchführen zu können. Bei allen Mitarbeitern seiner Arbeitsgruppe möchte ich mich für die Einarbeitung in die Zebrafisch-Arbeitstechniken bedanken.

Für die Hilfe bei den P-Smad- und TuJ1-Antikörperfärbungen möchte ich mich bei Dietmar Zechner bedanken.

Ein besonderer Dank geht an Carsten Klages für das Korrekturlesen und die vielen Anregungen zur Gestaltung der Arbeit. Dass die SSomitenëin exotischer Volksstamm, die Älleleëin Musikinstrument und die "littermatesSSpielgefährten von der Mülldeponie sein könnten, wäre mir ohne ihn nicht in den Sinn gekommen.

Meiner Familie möchte ich für ihre andauernde Unterstützung während meines Stu-

diums, meines Auslandsaufenthaltes und meiner Doktoranden-Zeit danken. Ohne sie würde ich diese Zeilen nicht schreiben können.

Für die Finanzierung dieser Arbeit bedanke ich mich bei der Deutschen Forschungsgemeinschaft.

7.3 Selbstständigkeitserklärung

Hiermit erkläre ich, dass ich die vorliegende Arbeit mit dem Titel "A new role for LRP2 in forebrain development" selbstständig und ohne Hilfe Dritter angefertigt habe. Sämtliche Hilfsmittel, Hilfen sowie Literaturquellen sind als solche kenntlich gemacht.

Ausserdem erkläre ich hiermit, dass ich mich nicht anderweitig um einen entsprechenden Doktorgrad beworben habe.

Die Promotionsordnung der Mathematisch-Naturwissenschaftlichen Fakultät I der Humboldt-Universität zu Berlin habe ich gelesen und akzeptiert.

Uwe Anzenberger

Berlin, Juni 2006